Aus dem Institut für Klinische Neuroimmunologie
Institut der Ludwig-Maximilians-Universität München
Vorstand: Prof. Dr. Martin Kerschensteiner

Visualization and Functional Characterization of $CD4^+$ T Cell Stimulation in the Ileal Lamina Propria

Dissertation
zum Erwerb des Doktorgrades der Naturwissenschaften
an der Medizinischen Fakultät der
Ludwig-Maximilians-Universität zu München

vorgelegt von

Isabel Julia Bauer

aus

Ebersberg

Jahr

2020

Mit Genehmigung der Medizinischen Fakultät

der Universität München

Betreuer(in): PD Dr. Naoto Kawakami

Zweitgutachter(in): Prof. Dr. Anne Krug

Dekan: Prof. Dr. med. dent. Reinhard Hickel

Tag der mündlichen Prüfung : 17. September 2021

TABLE OF CONTENTS

ABSTRACT

Multiple sclerosis (MS) is characterized is by immune cell infiltration into the central nervous system (CNS) causing inflammation and subsequent demyelination associated with neuronal degeneration. According to the leading paradigm of the etiology of MS, pre-existing autoreactive T cells are primed in the periphery before invading the CNS. Combined with the increasingly important role of microbiota as potential triggers of autoimmune diseases, the gut possibly constitutes the site of action. The main aim of this study was to investigate whether encephalitogenic T cells get stimulated in gut-associated lymphoid tissues prior to experimental autoimmune encephalomyelitis (EAE), a rodent model for MS.

Given that intracellular calcium signaling is a prerequisite for effective activation of T cells, cytosolic calcium levels constitute a useful indicator of stimulation. By combining the Förster resonance energy transfer (FRET)-based calcium sensor Twitch-2B with intravital two-photon microscopy, this study demonstrates that T cells specific for the CNS antigen myelin oligodendrocyte glycoprotein (MOG) as well as T cells specific for the control antigen ovalbumin (OVA) but not polyclonal T cells get stimulated in the ileal lamina propria. To investigate whether the ileal stimulation lead to activation-induced gene expression, transcriptome analysis of $CD4^+$ T cells from the efferent mesenteric lymph, i.e. downstream of the stimulation in the small intestine, was performed. The RNA sequencing of MOG-specific $CD4^+$ T cells from mice housed under specific pathogen-free (SPF) conditions indicated that stimulation in the small intestine induces Th17 cells with a pathogenic phenotype. In contrast, neither in germ-free mice, i.e. in the absence of microbiota, nor in polyclonal T cells, i.e. in the absence of extended calcium signaling in the ileal lamina propria, the upregulation of Th17 markers was observed. Furthermore, the transfer of gut-stimulated antigen-specific T cells to immunized recipient mice and subsequent analysis of the T cells' migration capacities demonstrated that the ileal stimulation does not only alter gene expression but also influences T cell behavior. $CD4^+$ T cells that had previously been stimulated by microbiota migrated more efficiently to lymphoid organs than T cells devoid of this stimulation.

The second part of this study focused on another crucial event in the pathogenesis of MS/EAE, i.e. the infiltration of encephalitogenic T cells into the CNS. The requirement of specific adhesion molecules for T cell extravasation was examined by intravital two-photon imaging of encephalitogenic T cells at the blood-brain barrier in a transfer EAE model in the Lewis rat. This enabled visualization of the mode of action of antibodies blocking the entry of encephalitogenic T cells into the CNS. Furthermore, this study confirmed that the blocking antibody against integrin $\alpha 4$, which is already in use as treatment for MS, has the most pronounced therapeutic effect.

The findings of the present study add to the mechanistic understanding of two critical steps in the pathogenesis of EAE, i.e., the peripheral stimulation by microbiota and the subsequent infiltration of encephalitogenic T cells into the CNS. Especially the priming process of autoreactive T cells in the periphery preceding CNS inflammation remains one of the least deciphered processes in the pathogenesis of CNS autoimmunity affecting millions of people worldwide.

ZUSAMMENFASSUNG

Multiple Sklerose (MS) wird durch die Infiltration von Immunzellen ins zentrale Nervensystem (ZNS) und dadurch ausgelöste Entzündungen gefolgt von Demyelinisierung und neuronaler Degeneration gekennzeichnet. Das vorherrschende Paradigma für die Ätiologie der MS ist die Präexistenz von autoreaktiven T-Zellen, die in der Peripherie stimuliert werden, um das ZNS infiltrieren zu können. Zusammen mit der immer größer werdenden Rolle, die der Darmflora als Auslöser von Autoimmunkrankheiten zugeschrieben wird, ist der Darm möglicherweise der Ort des Geschehens. Das Hauptaugenmerk der vorliegenden Arbeit lag darin, zu untersuchen, ob vor dem Ausbruch der experimentellen Autoimmunenzephalomyelitis (EAE), einem Nagetiermodell für MS, eine Stimulation enzephalitogener T-Zellen im darmassoziierten lymphatischen Gewebe stattfindet.

Da eine Erhöhung der intrazellulären Calciumspiegel als Voraussetzung für die Aktivierung von T-Zellen gilt, stellen zytosolische Calciumkonzentrationen einen nützlichen Indikator für T-Zell-Stimulierung dar. Mithilfe der Kombination aus dem Förster-Resonanzenergietransfer-(FRET)-basierten Calciumsensor Twitch-2B und der intravitalen Zweiphotonenmikroskopie zeigt diese Arbeit, dass sowohl T-Zellen spezifisch für das ZNS-Antigen Myelin-Oligodendrozyten-Glykoprotein (MOG) als auch T-Zellen spezifisch für das Kontrollantigen Ovalbumin (OVA) im Gegensatz zu polyklonalen T-Zellen in der Lamina propria des Ileums stimuliert werden. Um herauszufinden, ob diese Stimulation im Ileum zu einer durch Aktivierung induzierten Änderung der Genexpression führt, wurde eine Transkriptomanalyse an $CD4^+$ T-Zellen aus der efferenten mesenterialen Lymphe, also nach der Aktivierung im Dünndarm, durchgeführt. Die RNA-Sequenzierung der MOG-spezifischen $CD4^+$ T-Zellen aus der Lymphe von Mäusen, die unter spezifisch pathogenfreien (SPF) Bedingungen gehalten wurden, zeigen, dass die Stimulation im Dünndarm zur Induktion von Th17-Zellen mit einem pathogenen Phänotyp führt. Im Gegensatz dazu wurde weder in T-Zellen aus der Lymphe von keimfreien Mäusen noch in polyklonalen T-Zellen, die keine kontinuierliche Calcium-Signalgebung in der Lamina propria des Ileums aufweisen, eine Hochregulierung der Th17-Marker beobachtet. Durch den Transfer von Darm-stimulierten T-Zellen in immunisierte Empfängermäuse und die anschließende Analyse

der migratorischen Kapazitäten der transferierten Zellen konnte gezeigt werden, dass die Stimulation im Darm neben der Genexpression auch das Verhalten der antigen-spezifischen $CD4^+$ T-Zellen beeinflusst. $CD4^+$ T-Zellen, die zuvor durch intestinale Mikrobiota stimuliert worden waren, migrierten effizienter in die Lymphorgane des Empfängertiers als T-Zellen, die nicht im Darm stimuliert worden waren.

Der zweite Teil der vorliegenden Arbeit befasste sich mit einem weiteren wesentlichen Schritt in der Pathogenese von MS/EAE, nämlich mit der Infiltration von enzephalitogenen T-Zellen in das ZNS. Die Notwendigkeit spezifischer Adhäsions-molekule und Integrine für die T-Zell-Extravasation wurde mithilfe der intravitalen Zweiphotonenmikroskopie an der Bluthirnschranke in einem Transfer-EAE Modell in der Lewis-Ratte evaluiert. Diese Technik ermöglichte die Visualisierung der Wirkungsweise von Antikörpern die gegen verschiedene Integrine und deren Liganden gerichtet sind und die den Eintritt von enzephalitogenen T-Zellen in das ZNS blockieren. Diese Untersuchungen bestätigen, dass die Antikörper, die eine Blockade von Integrin α4 verursachen und bereits in der Behandlung von MS angewendet werden, den ausgeprägtesten therapeutischen Effekt haben.

Die Erkenntnisse aus der vorliegenden Arbeit tragen zum mechanistischen Verständnis von zwei Schritten in der Pathogenese von EAE bei, nämlich der peripheren Stimulation durch Mikrobiota und der darauffolgenden Infiltration der autoreaktiven T-Zellen in das ZNS. Besonders die Stimulation enzephalitogener T-Zellen in der Peripherie ist einer der am wenigsten entschlüsselten Prozesse in der Pathogenese der Autoimmunerkrankungen des ZNS, unter denen weltweit Millionen von Menschen leiden.

List of Figures

LIST OF TABLES

List of Abbreviations

aEAE	Active EAE
APC	Antigen-presenting cell
BBB	Blood-brain barrier
bw	Body weight
CAM	Cell adhesion molecule
CaMK	Calmodulin-dependent kinase
CFA	Complete Freund's adjuvant
CFP	Cyan fluorescent protein
CNS	Central Nervous System
CRAC	Calcium-release-activated calcium
CREB	Cyclic-AMP-responsive-element-binding protein
CSF	Cerebrospinal fluid
CTR	CellTrace^{TM} FarRed
CTV	CellTrace^{TM} Violet
DC	Dendritic cell
DEG	Differentially expressed gene
DMSO	Dimethylsulfoxide
DMT	Disease-modifying therapy
EAE	Experimental autoimmune encephalomyelitis
EBV	Epstein-Barr virus
ER	Endoplasmic reticulum
FBS	Fetal bovine serum
FC	Fold change
FP	Fluorescent protein
FRET	Förster resonance energy transfer
GALT	Gut-associated lymphoid tissues
GECI	Genetically encoded calcium indicators
GF	Germ-free
GM-CSF	Granulocyte-macrophage colony-stimulating factor
HBSS	Hank's balanced salt solution
HLA	Human leukocyte antigen
HyD	Hybrid photo detector
IEC	Intestinal epithelial cell
IEL	Intraepithelial lymphocyte
IFN	Interferon
IL	Interleukin
ILF	Isolated lymphoid follicles
iLN	Inguinal LN
i.p.	Intraperitoneal

IP_3	Inositol-1,4,5-trisphosphate
ITG	integrin
i.v.	Intravenous
KO	Knockout
LB	Luria Bertani medium
LCMV	Lymphocytic choriomeningitis virus
LN	Lymph node
LP	Lamina propria
MAG	Myelin-associated glycoprotein
MAIT	Mucosal associated invariant T cells
MBP	Myelin basic protein
MHC	Major histocompatibility complex
mLN	Mesenteric LN
MMF	Midazolam/medetomidine/fentanyl
MOBP	Myelin-associated oligodendrocytic basic protein
MOG	Myelin oligodendrocyte glycoprotein
MS	Multiple Sclerosis
MWCO	Molecular weight cut-off
NGS	Next-generation sequencing
NF-κB	Nuclear factor-κB
NFAT	Nuclear factor of activated T cells
NO	Nitric oxide
OCB	Oligoclonal bands
ON	Optic neuritis
OSE	Opticospinal EAE
OVA	Ovalbumin
Padj	Adjusted p-value
PBS	Phosphate buffered saline
PEI	Polyethylenimine
p.i.	Post immunization
PLP	Proteolipid protein
PP	Peyer's patch
p.t.	Post transfer
PTX	Pertussis toxin
RIN	RNA integrity number
RM	Restimulation medium
RR	Relapsing-remitting
RT	Room temperature
s.c.	subcutaneously
SFB	Segmented filamentous bacteria
SFM	Serum-free medium

SNP	Single nucleotide polymorphism
SPF	Specific pathogen-free
STIM1	Stromal interaction molecule 1
TCM	T cell medium
TCR	T cell receptor
tEAE	Transfer EAE
TF	Transcription factor
Th	Helper T cell
TH mice	IgH^{MOG} mice
TMEV	Theiler's murine encephalomyelitis virus
TNF	Tumor necrosis factor
Treg	Regulatory T cell
TnC	Troponin C
wt	Wild-type

1 INTRODUCTION

1.1 Multiple Sclerosis

Multiple sclerosis (MS) is the most common inflammatory demyelinating disease of the central nervous system (CNS) affecting more than two million people worldwide (GBD, 2017). It is characterized by immune infiltrates into the CNS causing inflammation and subsequent demyelination associated with axonal and neuronal degeneration (Lassmann et al., 2007; Reich et al., 2018). Patients present with a variety of symptoms such as fatigue, pain, muscle weakness, sensory or cognitive deficits, optic neuritis, bladder and bowel dysfunctions (Wiesel et al., 2001; Pau et al., 2011; Dobson and Giovannoni, 2019). The diversity of the disease is not restricted to the variety of occurring impairments but is also reflected in different lesion patterns and the types of symptom onset: the majority of patients (about 85 %) experiences an initial relapsing-remitting phase that very often converts to a secondary progressive form over time and leads to profound disability. For the minor proportion of patients (15 %), the disease directly sets in with a primary progressive form (Weinshenker et al., 1989; Lublin and Reingold, 1996; Lublin et al., 2014).

Diagnostic criteria for MS have constantly evolved over time from Charcot's first description of MS in 1868. He reported various neurological symptoms of a single disease with distinct pathological features such as nystagmus, ataxia and dysarthria (Charcot et al., 1868). The most recent diagnostic recommendations are the 2017 revised McDonald criteria from the International Panel on Diagnosis of Multiple Sclerosis. The key requirement for MS diagnosis is the presence of CNS lesions that are disseminated in time and space, whereby these revised criteria provide further avenues for obtaining supporting evidence of dissemination, such as the presence of oligoclonal bands (OCB) in the cerebrospinal fluid (CSF) and the consideration of asymptomatic and cortical lesions (Thompson et al., 2018).

The CNS lesions found in MS patients arise from the immune system reacting with tissue-specific self-antigens by mechanisms that are still poorly understood. Despite a pronounced role of inflammation in MS, the traditional view of inflammation being the cause of axonal and neuronal degeneration has been challenged recently (Stys et al., 2012). There is increasing evidence that neurodegeneration is not only a consequence

of inflammation but can also occur independently of inflammatory processes. This perception emerges from the findings that anti-inflammatory or immunomodulatory treatments have only little or no effect on the development of neurodegeneration and clinical disability in the progressive phase of disease and especially in patients with primary progressive disease. (Coles et al., 1999; Filippi et al., 2000; Molyneux et al., 2000; Filippi et al., 2004).

Albeit decades of research, the definite etiology of MS remains elusive, yet seems to be a complex interplay of both genetic and environmental factors. The genetic contribution appears in a concordance rate of 25 % in monozygotic twins, which is decreased to 5 % in their dizygotic counterparts (Willer et al., 2003). A very prominent genetic risk factor is human leukocyte antigen (HLA) class II, in particular the HLA-DR15 haplotype among the Caucasian population that strengthens the perception of MS as both an inflammatory and at least in part hereditary condition (Sospedra and Martin, 2005; Sawcer et al., 2011). Furthermore, genome-wide association studies have identified more than 100 common genetic variants (single nucleotide polymorphisms, SNPs) associated with MS susceptibility (Beecham et al., 2013). Many of these SNPs lie close to gene loci related to immune function, typically rather in regulatory than in coding regions. Identified functional variants comprise e.g. those within interleukin (IL)-2RA (Maier et al., 2009), IL-7R (Lundmark et al., 2007) and TNFR1 (Gregory et al., 2012).

The significant environmental influence on the susceptibility of MS becomes evident with its geographical variations. MS occurrence is higher in temperate climates such as Northern Europe and Northern America as compared to (sub-)tropical regions. The best-established risk factor associated to these differences is vitamin D deficiency due to diminished sun exposure (Smolders et al., 2008). Many other environmental influences have been associated with the socioeconomic status of the population, e.g. exposure to pathogens such as Epstein-Barr virus (EBV) (Munch et al., 1998), cigarette smoking, obesity in early life and high salt intake (Baecher-Allan et al., 2018). Increasing importance is assigned to the gut microbiome in the development of autoimmunity and specifically to MS via either molecular mimicry and/or bystander immune activation (Croxford and Miyake, 2015).

1.2 Experimental Autoimmune Encephalomyelitis

To date, there is no curative treatment available for MS but a variety of disease-modifying therapies (DMTs). Many of these DMTs have been developed based on findings in animal models (Teitelbaum et al., 1971; Yednock et al., 1992). Due to the complex interplay of immune and neuropathological processes in MS, there is not one single animal model that perfectly embodies all aspects. Hence, there is a broad spectrum of models representing different features of MS. The most common family of MS-mimicking models is encompassed in the spectrum of experimental autoimmune encephalomyelitis (EAE) (Krishnamoorthy and Wekerle, 2009). The first description of EAE was published in 1925 by Schweinburg and Koritschoner, who inoculated rabbits with human spinal cord and induced paralysis and spinal cord inflammation (Koritschoner and Schweinburg, 1925). In 1933, CNS inflammation and demyelination were induced in rhesus monkeys to investigate the encephalitic complications of rabies vaccines. The monkeys were repeatedly immunized with CNS homogenate (Rivers et al., 1933). Later, the invention of a mineral oil based adjuvant (Freund and McDermott, 1942) facilitated EAE induction with only a single injection of CNS tissue (Kabat et al., 1947). This response was further enhanced by supplementing the adjuvant with high amounts of heat-inactivated *Mycobacterium tuberculosis* (complete Freund's adjuvant, CFA). Since then, EAE has been shown in various species, e.g. in guinea pigs, marmosets, rats and mice. Although EAE in mice has been introduced in the 1950s, they have not been the model of choice due to their low disease incidence and high heterogeneity until 20 years later (Gold et al., 2006). With the development of more susceptible mouse strains (Levine and Sowinski, 1973; Bernard and Carnegie, 1975) and the application of pertussis toxin (PTX) to increase EAE incidence (Munoz et al., 1984), mouse EAE became more popular. With the ability to generate transgenic mouse lines enabling the investigation of the influence of single genes, the mouse became the gold standard in the EAE field (Capecchi, 1989; Croxford et al., 2011).

Typical clinical signs of EAE constitute paralysis in increasing intensity. The first symptoms are loss of body weight as well as weakness and subsequent loss of tail tonicity. Paresis and paralysis progress from caudal to rostral: after the tail, the hind limbs and ultimately the fore limbs become limp and then paralyzed (Stromnes and Goverman, 2006; Bittner et al., 2014). EAE may result in death of the animal but may

also subside spontaneously, continue in a chronic manner or establish a fluctuating disease course. These classical symptoms reflect the common localization of inflammation in the spinal cord as it is observed in most rodent EAE models. This constitutes a major limitation in mimicking human disease, where lesions are likewise found in the brain. There are EAE models where immune cell infiltration and thus lesion formation occurs in brain areas which is mirrored in symptoms like head tilting, axial rotation or ataxia. These so-called atypical EAE symptoms can be found e.g. in Interferon (IFN)-γ knockout BALB/c mice immunized with myelin basic protein (MBP) exon 2 peptide (Abromson-Leeman et al., 2004) or in an adoptive transfer EAE model in the Lewis rat, where T cells specific for β-synuclein are transferred (Lodygin et al., 2019). Also in a spontaneous EAE model, the so-called relapsing-remitting (RR) mice, that harbor a transgenic T cell receptor (TCR) specific for myelin oligodendrocyte glycoprotein (MOG) peptide 92-106 and recruit MOG-specific B cells from the endogenous repertoire, a substantial number of animals develops ataxia rather than classical EAE symptoms (Pöllinger et al., 2009).

As reported, the first immunizations were conducted with whole CNS homogenate. Over time, scientists managed to refine the immunogenic components of crude brain tissue and identified several myelin antigens, among them proteolipid protein (PLP), MBP, MOG, myelin-associated glycoprotein (MAG) and myelin-associated oligodendrocytic basic protein (MOBP) (Sospedra and Martin, 2005). Based on these findings, various EAE models have been established in different mouse or rat strains that embody distinct MS features. MBP was one of the first myelin proteins that has been purified and shown to induce EAE in SJL/J mice (Bernard and Carnegie, 1975). Various autoantigens have strikingly different potentials to elicit disease among rodent strains. C57BL/6 mice, for example, are highly susceptible to immunization with MOG (Lando et al., 1979; Mendel et al., 1995) but are almost resistant to immunization with MBP, while the reactivity of Lewis rats to these antigens is the exact opposite (Kibler et al., 1977; Wekerle et al., 1994; Weissert et al., 1998).

1.2.1 Adoptive transfer EAE in the Lewis rat

Ben-Nun and colleagues showed that EAE cannot only be induced by immunization with the autoantigen (termed active EAE, aEAE) but also by transfer of T cells with the respective specificity, the so-called adoptive transfer EAE (tEAE) (Ben-Nun et al., 1981). Until today, MBP is the antigen of choice to induce active as well as adoptive transfer EAE in the Lewis rat. The major advantage of EAE induction by transfer of encephalitogenic T cells is its unrivalled reproducibility: The time kinetics of EAE development follow a highly stable pattern. Hence, it is a suitable model to study preclinical events such as initiating T cell infiltration into the CNS. With onset of clinical symptoms on day three after transfer, rat tEAE starts at least one week earlier than aEAE. In the latter case, endogenous T cells are recruited *in vivo* by immunization with the autoantigen whereby in tEAE, encephalitogenic T cells are activated *in vitro* before transfer. However, it is known that also the previously activated T cells require stimulation in peripheral environments such as the spleen to upregulate migration-related genes such as chemokine receptors that enable them to arrive at the blood-brain barrier (BBB) and cross it (Flügel et al., 2001; Kyratsous et al., 2017). T cell infiltration happens in two waves: some pioneer T cell blasts manage to invade the CNS directly, whereas the second and much bigger wave of infiltrating T cells requires peripheral stimulation and will arrive at the BBB on day two to three after transfer. Once in the CNS, the T cells encounter endogenous antigen presented by antigen-presenting cells (APCs) and get re-activated. This time point coincides with the first clinical symptoms, which are loss of tail tonicity and hind limb weakness. Until day five or six, the disease will worsen and the rat will experience ascending paralysis before EAE goes to remission and the animals recover completely within two weeks after onset (Flügel et al., 2007; Kyratsous et al., 2017). To sum up, the rat tEAE model is highly suitable to study prodromal or early EAE as the time kinetics are highly stable. In contrast, one of its major limitations is that the transfer of *in vitro* activated T cells skips the peripheral priming step. Furthermore, the rat model offers very limited abundance of transgenic strains.

1.2.2 MOG-induced EAE

Despite their initial and remaining popularity as a model for MS, rats were gradually replaced by mice. Given that mice are smaller and of lower price, therefore allowing for more repetitions or experiments, their abundance in labs increased and the availability of modern reagents and antibodies shifted accordingly (Croxford et al., 2011). Scientists have shown that MOG peptide 35-55 is the most potent antigen to induce EAE in C57BL/6 mice (Mendel et al., 1995), although MOG constitutes a minor component of myelin, as it accounts for 0.01-0.05 % of membrane protein (Linnington et al., 1984). However, in contrast to MBP and PLP, MOG is displayed on the surface of the myelin sheath. Also in MS, MOG seems to be an important CNS antigen as MOG-reactive T cells have been detected in patients to a greater extent as T cells specific for PLP or MBP (Sun et al., 1991a; Sun et al., 1991b; Kerlero de Rosbo et al., 1997; Raddassi et al., 2011). Some MS patients harbor MOG-specific autoantibodies, too, and recent findings assigned a pathological function to them (Karni et al., 1999; Berger et al., 2003; Pittock et al., 2007; Spadaro et al., 2018). In C57BL/6 mice, MOG-induced EAE follows a chronic course with ascending paralysis and neuropathology (Mendel et al., 1995). The generation of the MOG_{35-55}-induced EAE C57BL/6 model entailed an emerging synergy between this model system and the increasing abundance of gene knockout (KO) strains. This allowed for extensive investigations on the impact of individual immune factors in governing autoimmune responses against CNS myelin, including T cell surface receptors (Malipiero et al., 1997; Eugster et al., 1999), cytokines (Körner et al., 1997; Tran et al., 2000), transcription factors (Bettelli et al., 2004) and signaling molecules (Du and Sriram, 2002).

1.2.3 Transgenic models of MOG-driven EAE

Bettelli and colleagues aimed at developing a transgenic mouse line that harbors a class II restricted TCR specific for the MOG peptide 35-55. Therefore, they isolated an epitope-reactive T cell clone (2D2) from MOG_{35-55}-immunized C57BL/6 mice and knocked its α- and β-chains into the C57BL/6 germline by transgenesis. The resulting 2D2 T cells are $V\alpha3.2^+$ and $V\beta11^+$, and react specifically to MOG_{35-55}. T_{MOG} cells from these mice do not undergo central or peripheral tolerance and develop normally. Peptide-immunization induced EAE in these so-called 2D2 mice is stronger as

compared to non-transgenic littermates and, more surprisingly, around 4 % of these mice develop spontaneous EAE. (Bettelli et al., 2003) Interestingly, more than 30 % of 2D2 mice develop spontaneous optic neuritis (ON), an inflammatory disease of the optic nerve. This high incidence of ON in 2D2 animals compared to their low incidence of spontaneous EAE was associated with an easier T cell infiltration into the optic nerve and the enhanced abundance of the autoantigen MOG as compared to brain and spinal cord (Bettelli, 2007). Isolated ON also occurs as early symptom in MS (Pau et al., 2011).

Immunization or transfer of *ex vivo* stimulated T cells, respectively, constitute a major limitation of all induced EAE models, since disease-triggering factors are bypassed and thus cannot be examined. To overcome this issue, Krishnamoorthy and colleagues developed a double-transgenic mouse strain, the opticospinal EAE (OSE) mouse, which spontaneously develops EAE (Krishnamoorthy et al., 2006). This strain was created by crossing the previously described MOG-TCR bearing 2D2 mouse with a mouse strain expressing MOG-specific B cells (IgHMOG, also known as TH mouse). The TH mouse strain has a B cell heavy chain knock-in and thus harbors a high frequency of anti-MOG antibody secreting B cells in the periphery. The incidence of active EAE in TH mice is increased as compared to non-transgenic littermate controls, yet EAE never occurs spontaneously (Litzenburger et al., 1998). Crossing of 2D2 and TH mouse lines, that both hardly develop spontaneous EAE, resulted in a strain with a spontaneous EAE incidence of more than 60 %. The disease sets in between four and eight weeks of age and is characterized by inflammatory lesions in the spinal cord and optic nerve as well as ectopic follicle-like structures in the CNS resulting from pathogenic T_{MOG}- and B_{MOG} cell interactions (Bettelli et al., 2006; Krishnamoorthy et al., 2006).

1.3 Pathogenesis of CNS autoimmunity in MS and EAE

1.3.1 Pathogenic role of $CD4^+$ T cells

Both MS and EAE are considered T-cell mediated pathologies (Wekerle et al., 1994; Weiner, 2004). As stated above, Ben-Nun and colleagues have shown in the 1980s that the adoptive transfer of CNS-specific $CD4^+$ T cells into naïve animals is sufficient to induce disease (Ben-Nun et al., 1981). In most active EAE models, myelin-specific $CD4^+$ rather than $CD8^+$ T cells constitute the central factor of autoimmune pathogenesis as

the immunization protocol favors activation via major histocompatibility complex (MHC) class II due to the use of CFA. Also in MS, $CD4^+$ T cells are considered to initiate and coordinate immune responses leading to tissue damage as evidenced by the application of immunomodulatory treatments that impede lymphocyte trafficking to the CNS (e.g. natalizumab) or deplete lymphocytes from the periphery (e.g. alemtuzumab) (Polman et al., 2006; Coles et al., 2012). Interestingly, myelin-specific T cells were detected in similar or increased proportions in blood and CSF of MS patients as compared to healthy controls (Ota et al., 1990; Pette et al., 1990; Liblau et al., 1991). However, there are crucial differences between these autoreactive T cells in MS patients and healthy controls: Many of the patients' T cells exhibit an elevated frequency of high-avidity T cells, an activated phenotype (Pette et al., 1990; Vandevyver et al., 1995; Bielekova et al., 2004) and an increased production of proinflammatory cytokines (Sharief and Thompson, 1993; Zhang et al., 1994; Strunk et al., 2000). Thus, the suspicion is obvious that these naïve autoreactive $CD4^+$ T cells might be activated in the periphery by a trigger that remains elusive.

1.3.2 T cell priming in the periphery

One major limitation of induced EAE models is that they bypass the naturally occurring priming or add an artificial priming process of encephalitogenic T cells. The situation in MS is likewise complicated, as its pathological process is already ongoing for a long time before clinical onset, and autoimmunity is probably not directed against one but against multiple unknown antigens. Therefore, the mechanism of MS induction remains to be deciphered. As mentioned above, it is known that autoreactive CNS-specific T cells exist in the periphery of both healthy people and MS patients. This indicates that central tolerance is not completely efficient and cells with intermediate affinity can escape it (Walker and Abbas, 2002). However, the myelin-specific T cells of healthy controls and MS patients exhibit one major difference: T cells of patients display an activated phenotype as described above (chapter 1.3.1). The trigger of these autoreactive T cells to be activated and thus to initiate disease is the big missing link in the etiology of MS. Several concepts have been postulated to explain the induction of autoimmunity to myelin antigens.

Infections unhide autoantigen

One of them is termed bystander activation and refers to non-specific activation of autoreactive T cells due to an infection causing a strong immune response. Infectious microbes may induce tissue damage and thus trigger the unveiling of self-antigens that are unseen by the immune system under homeostatic conditions. Along with the adjuvant effects of the infectious agent, the presentation of these host antigens may result in the activation of self-reactive T cells and induce CNS-directed autoimmunity (Yasukawa et al., 1993; Fujinami et al., 2006). With the persistence of the infection and continued tissue damage, epitope spreading can occur: novel antigens are released from damaged cells e.g. in the CNS and lead to *de novo* activation of further encephalitogenic T cells (Vanderlugt and Miller, 1996). Both bystander activation and epitope spreading have been shown to exist in infection with Theiler's murine encephalomyelitis virus (TMEV) in a murine model for MS, where an initial virus-specific T cell response spreads to myelin antigens in the course of continuous infection of the CNS (Miller et al., 1997). This expansion of the repertoire of T cells targeting different CNS antigens has been found to be crucial in chronic EAE models and is very likely but hard to prove in human disease (Lehmann et al., 1993; Vanderlugt and Miller, 2002).

Molecular mimicry

Another proposed mechanism for T cell priming in the periphery is molecular mimicry, which refers to the cross-recognition of a self- and a non-self-antigen by the same lymphocyte due to sequence homologies and/or structural similarities (Fujinami et al., 1983). When T cells recognize self-antigens at low or intermediate levels of affinity during thymic selection, they can escape the central tolerance and egress into the periphery. Encounter of the foreign peptide that mimics the self-antigen can lead to T cell activation enabling infiltration into the CNS and self-antigen recognition. Molecular mimicry of CNS antigens in MS has been demonstrated for several viral components. For instance, Fujinami and colleagues detected that hepatitis B virus polymerase shares an immunologic epitope with MBP and can induce an EAE-like disease in rabbits (Fujinami and Oldstone, 1985). Subsequent studies revealed several viral peptides that can activate MBP-specific T cells, such as determinants from EBV or

human papillomavirus (Wucherpfennig and Strominger, 1995). These findings indicate that cross-reactive immune responses of host and virus constitute an abundant phenomenon. Besides viral components, also gut microbiota share sequence similarities with myelin peptides, suggesting that gut bacteria may contribute to MS via molecular mimicry (Westall, 2006). Peptides from *Escherichia coli*, a common gut commensal, exhibit structural similarities to MBP and induced EAE in a transgenic mouse expressing a humanized TCR (Harkiolaki et al., 2009). Furthermore, also epitopes of *Pseudomonas*, an enriched genus in the gut of MS patients (Chen et al., 2016), have been shown to activate MBP-specific T cells (Wucherpfennig and Strominger, 1995). Horai and colleagues have successfully demonstrated that priming of autoreactive T cells by commensal microbes induced an autoimmune attack in the immune privileged target organ, which was the eye in a respective spontaneous mouse model of uveitis in this study (Horai et al., 2015).

To date, the biological relevance of these findings to patients with MS remains unclear as experimental evidence is missing and many questions are still unanswered, like the identity of the foreign antigen. It is probable that there are several cross-reactive antigens and a combination of all proposed mechanisms underlying the pathogenesis of MS (McCoy et al., 2006).

1.3.3 Infiltration of T lymphocytes into the CNS

Encephalitogenic $CD4^+$ T cells are activated in a remote peripheral site, for instance in the intestine (Berer et al., 2011) (refer to chapter 1.4). Peripheral activation induces the upregulation of migration-related genes and the expression of adhesion molecules and thus enables the T cells to reach and attach to the BBB (Wekerle et al., 1986; Kuchroo et al., 1993; Flügel et al., 2001; Kebir et al., 2007; Kawakami et al., 2012). The application of intravital two-photon microscopy revealed that the T cells first roll and then crawl along the intraluminal surface of CNS blood vessels before they infiltrate the spinal cord in tEAE in the Lewis rat (Bartholomäus et al., 2009). Rolling T cells move along the blood stream with high velocity, whereby transiently interacting with endothelial cells via selectins (Piccio et al., 2002). Upon crawling, T cells significantly reduce their motility, preferentially moving against the blood stream. This process is mainly mediated by surface expression of α4β1 integrins on encephalitogenic T cells.

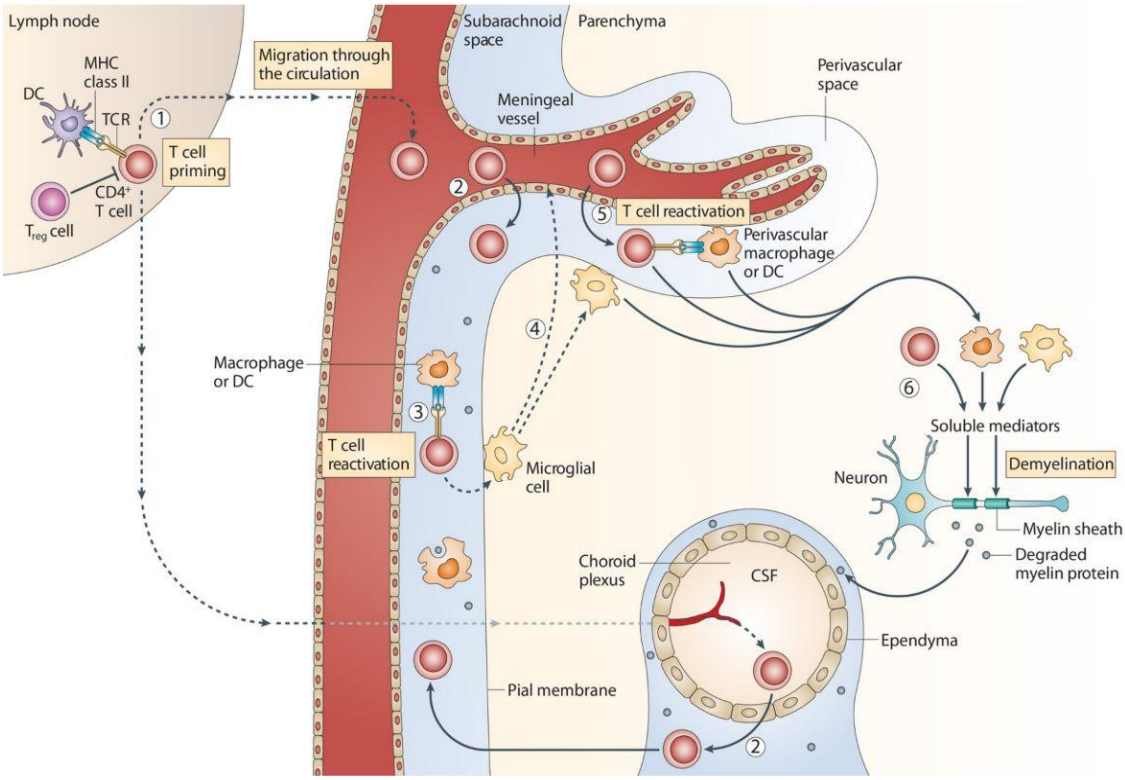

Figure 1.1: T cell infiltration into the CNS. *1* APCs prime T cells via presentation of CNS-derived epitopes or antigens that cross-react with CNS-specific epitopes in peripheral lymph nodes (LNs). *2* Those peripherally activated T cells are able to cross the BBB into the perivascular space, *3* where they interact with local APCs to be reactivated by antigen presentation. *4* Activated T cells in the CNS stimulate microglia which in turn induce the activation of distal microglia and endothelial cells. *5* The emerging inflammatory milieu triggers the infiltration of vast amounts of peripheral immune cells like macrophages and further encephalitogenic T cells. *6* The activated immune cells release soluble mediators that induce inflammation and subsequent demyelination. Adapted with permission from Goverman, 2009.

Blocking of integrin α4 (ITGA4) significantly reduces the number of crawling T cells and dramatically ameliorates EAE (Yednock et al., 1992; Bartholomäus et al., 2009). The successful application of natalizumab, a blocking antibody against Integrin α4 (ITGA4), in the therapy of MS patients proves the great importance of this integrin also in the pathogenesis of MS (Lanzillo et al., 2013). T cells mainly extravasate at the level of post-capillary venules into the perivascular space (Engelhardt and Ransohoff, 2005). Here, MHCII-expressing phagocytes, e.g. perivascular macrophages or infiltrating dendritic cells (DCs), present foreign or local antigens (Fabriek et al., 2005; Greter et al., 2005; Kivisäkk et al., 2009) and thus activate T cells (Pesic et al., 2013; Kyratsous et al., 2017). Upon reactivation, T cells are directed deeper into the CNS parenchyma and spread in the tissue (Kawakami et al., 2004). These activated T cells release proinflammatory cytokines such as IFNγ, IL-17, granulocyte-macrophage colony-

stimulating factor (GM-CSF), or tumor necrosis factor α (TNFα). The emerging inflammatory milieu in turn activates macrophages and microglia and makes the BBB even more leaky. This allows for the massive infiltration of further immune cells and perpetuates the inflammatory cascade resulting in an aggressive immune attack against the axon-wrapping myelin sheath. This inflammatory milieu can also mediate direct neuronal toxicity by cytokines and effector molecules such as nitric oxide (NO) and reactive oxygen species (ROS). Autoantibodies against myelin proteins also contribute to myelin sheath destruction. In summary, CNS inflammation induces demyelination and axonal degeneration resulting in the clinical symptoms observed in MS and EAE. (Goverman, 2009; Herz et al., 2010; Constantinescu et al., 2011) (Figure 1.1).

1.4 The gut microbiome as modulator of CNS autoimmunity

Besides their known impact on bowel-related disorders, there is mounting evidence that the gut microbiota play a crucial role in the development of autoimmune diseases of remote organs such as the CNS via the above-mentioned mechanisms of molecular mimicry, bystander activation, epitope spreading and beyond.

Under physiological conditions, the gut bacteria establish a symbiotic relationship with the host and support the maintenance of homeostasis. The composition of the gut microbiome is highly variable and influenced by diverse factors such as diet, antibiotics, infections and other events in life. An unfavorable modification of the gut microbiome is called dysbiosis and may include an increment of pathobionts and a reduced abundance of beneficial microbes (Round and Mazmanian, 2009; Hill and Artis, 2010). The association of dysbiosis with neurodegenerative and autoimmune disorders has been shown for several pathologies, e.g. Alzheimer's disease (Vogt et al., 2017), Parkinson's disease (Scheperjans et al., 2015), Ischemic Stroke (Benakis et al., 2016) Autism spectrum disorders (Finegold, 2011; Hsiao et al., 2013) and also for MS as described in the following chapters.

1.4.1 Gut microbiota in EAE

Major findings in this field came from animal models with manipulated microbiomes. Germ-free (GF) facilities constitute a powerful tool to study the influence of gut microbiota and have had a substantial impact on our understanding. The use of

gnotobiotic animals as well as pro- and antibiotics further allows investigating the influence of specific microbes. Almost 30 years ago, Goverman and colleagues already described that transgenic mice with a high frequency of MBP-specific T cells exhibited a higher incidence of spontaneous EAE in conventional dirty facilities compared to clean housing conditions (Goverman et al., 1993). Furthermore, there is empirical evidence from many labs suggesting that incidence and severity of spontaneous EAE vary among facilities, which is most likely depending on their microbiota status (Berer et al., 2011).

Berer and colleagues elegantly demonstrated that gut microbiota are crucial to activate autoreactive T cells in a spontaneous EAE model, the so-called relapsing-remitting (RR) mouse. RR mice harbor a transgenic TCR specific for MOG peptide 92-106 and develop spontaneous EAE with an incidence of 80 % in specific pathogen-free (SPF) facilities. When housed under GF conditions, these mice were almost entirely protected from the spontaneously developing disease. However, when re-colonizing the mice with conventional commensal microbiota from SPF mice, their susceptibility for spontaneous EAE was completely restored. This provides evidence for a crucial role of microbiota in the peripheral priming of CNS-specific T cells (Berer et al., 2011). The observation that EAE was significantly less severe under GF conditions has also been made in a previous study (Lee et al., 2011). In line with this, the oral application of antibiotics significantly impaired the development of active EAE in wild-type (wt) mice by reducing bacterial populations (Yokote et al., 2008; Ochoa-Repáraz et al., 2009). The protective effect induced by eradicating the gut microbiota has been associated with different mechanisms, such as a reduction of proinflammatory cytokines and increased production of IL-10 and IL-13 (Ochoa-Repáraz et al., 2009). Others found an increased number of $FoxP3^+$ regulatory T (Treg) cells, reduced populations of helper T (Th)1 and Th17 cells, and impaired ability of dendritic cells to generate Th1 and Th17 responses in the mice housed in GF facilities (Ochoa-Reparaz et al. 2009; Berer et al. 2011; Lee et al. 2011). Lee and colleagues were able to pin down the microbes required for induction of EAE to segmented filamentous bacteria (SFB) by showing that originally GF animals became more susceptible to EAE when colonized with these gut commensals (Lee et al., 2011). The role of SFB in autoimmunity has not been entirely new as they had already been identified as potent inducers of Th17 cells in the gut in 2009 (Ivanov

et al., 2009). Intriguingly, Bradley and colleagues recently elucidated the new conception that SFB as example for gut commensals could specifically expand Th17 cells that express dual TCRs recognizing both SFB and self-antigens. In their study, these T cells were then recruited to the lung where they induce pathology (Bradley et al., 2017). This dual TCR mechanism might add another possibility on how microbiota modulate autoimmunity beyond molecular mimicry or bystander activation. Horai et al have set one impressive example of how T cells educated in the gut-associated lymphoid tissues (GALT) influence distant organs. They were able to show that autoreactive T cells require activation by microbiota to induce autoimmunity in the immune-privileged eye in a uveitis model (Horai et al., 2015). However, still little is known about the interconnections and underlying mechanisms of action of T cells stimulated in the GALT.

Accordingly, probiotic bacterial strains and commensal isolates have been shown to ameliorate disease in active EAE models, e.g. *Bacteroides fragilis* (Ochoa-Repáraz et al., 2010), *Lactobacillus helveticus* (Yamashita et al., 2017), *Prevotella histicola* (Mangalam et al., 2017) or the commensal strain *E. coli* Nissle 1917 (Secher et al., 2017).

1.4.2 Dysbiosis in MS patients

Encouraged by these successful studies in the EAE model, rising attention was drawn to the role of microbiota in MS. To disentangle this complex interrelationship of host and microbiota in humans is challenging because the available samples constitute snapshots of the microbiome at a time point long after the disease has developed. Another major limitation of studying microbiota constitutes the fact that most samples derive from feces that do not reflect the diversity and composition of microbiota along the intestinal tube (Sartor, 2015). This leaves the question unanswered whether the microbiome status is cause or consequence to the disease. Several groups used modern 16S rRNA sequencing techniques for the analysis of microbes without culturing, comparing microbiota of MS patients with healthy donors. No dramatic change, but rather a subtle dysbiosis has been reported in these studies. A study examining 60 MS patients from the US found an increase of *Methanobrevibacter* and *Akkermansia* and a decreased frequency of *Butyricimonas* in individuals with MS. Further analysis showed that MS patients under DMTs (IFN-β and glatiramer acetate)

had increased numbers of *Prevotella* and *Sutterella* and decreased *Sarcina* compared to untreated patients (Jangi et al., 2016). In a Japanese cohort of 20 patients, *Clostridia* and *Baceroidetes* species were found to be diminished (Miyake et al., 2015). And, to name another example, Chen and colleagues reported an increased abundance of *Mycoplana*, *Pseudomonas*, *Blautia*, *Dorea* and *Haemophilus* species with lowered numbers of *Prevotella*, *Adlercreutzia* and *Parabacteroides* genera in MS patients (Chen et al., 2016). These studies provide evidence for a subtle dysbiosis of the microbiota in MS patients, yet they all are different and none of them was able to assign a role in disease pathogenesis to those alterations in the microbiome.

Intriguingly, two independent studies recently added to our understanding of the causal link by elucidating potential mechanisms of T cell autoimmunity induced by commensal microbiota. Both groups reported that isolated fecal content from MS patients increased EAE incidence and severity, respectively, when transplanted into GF mice. In line with the previous studies, the gut microbiota profiles of MS patients in the studies did not display overt differences, but both groups found an increase in the abundance of *Akkermansia* (Berer et al., 2017; Cekanaviciute et al., 2017). Berer and colleagues reported that, upon transplanting the feces of monozygotic twins discordant for MS into GF RR mice, the gut microbiota retrieved from the MS twin exacerbated the EAE course as compared to the healthy twin derived microbiota (Berer et al., 2017). Correspondingly, microbiota transplants from MS patients into GF C57BL/6 mice and subsequent immunization with MOG_{35-55} peptide resulted in a more severe EAE as compared to transfer of feces from healthy controls. Furthermore, by monocolonizing mice with specific microbe species, they showed that MS-associated bacteria induced a proinflammatory profile in T cells. For example, *Akkermansia*, which is enriched in MS patients, amplified Th1 cell differentiation. Additionally, both studies demonstrated a compromised IL-10 expression by T cells in mice that had received MS patient's gut microbiota. These studies corroborate the perception that MS patient derived gut microbiota comprise factors that coordinate adaptive autoimmune responses and trigger an MS-like autoimmune disease in mouse models.(Berer et al., 2017; Cekanaviciute et al., 2017)

In summary, maintenance of the correct balance of gut microbiota occurs to be crucial for homeostasis between proinflammatory Th1 and Th17 cells and anti-inflammatory

Treg cells. MS patients appear to have a tendency to harbor more proinflammatory bacteria and may feature a failure of commensal tolerance, respectively. However, the underlying molecular pathways and microbiota-derived factors, which contribute to the protective or enhancing effect for autoimmune diseases, remain elusive.

1.5 Gut-associated lymphoid tissues

The small and large intestines are luminally lined by a single-layered columnar epithelium. The small intestine begins at the pylorus and is subdivided into three segments, namely the duodenum, the jejunum and the ileum. The large intestine consists of caecum, colon, and rectum (Fig. 1.2). The intestinal mucosa of the small intestine consists of finger-like processes, termed villi, and their surface is made up of a single layer of intestinal epithelial cells (IECs) providing an extensive surface area for the digestion and absorption of metabolites from the diet. Besides IECs, the epithelium of the small intestine contains Paneth cells, which produce antimicrobial peptides and maintain homeostasis and stem cell activity via growth factor production. Furthermore, mucus-producing goblet cells make up for 10-25 % of all epithelial cells with increasing frequency down the gastrointestinal tract. Accordingly, the mucus layer coating the mucosa is the thickest in the colon, thereby acting as a physical barrier between epithelium and microbes. The layer of connective tissue beneath the epithelium is called lamina propria (LP). Many immune cells are found scattered throughout these tissues and also in organized lymphoid tissues of the intestine such as the Peyer's patches (PP) and isolated lymphoid follicles (ILFs) forming the so-called the gut-associated lymphoid tissues (GALT). The epithelium primarily contains T cells whereas in the LP, plenty of immune cell types can be detected such as T and B cells as well as macrophages, DCs, mast cells and eosinophils. In sum, the intestinal LP and epithelium harbor the biggest population of T cells in the body and constitute the effector sites of the intestinal immune system. (Murphy et al., 2012; Mowat and Agace, 2014)

The LP contains approximately twice as many $CD4^+$ T cells as $CD8^+$ T cells but also innate lymphocyte types such as invariant natural killer (iNK) cells and mucosal associated invariant T (MAIT) cells. The $CD4^+$ T cells are highly diverse and contain different kinds of subsets (e.g. Th1, Th17 and Tregs) with varying numbers along the

intestinal tube. For instance, Th17 cell numbers are higher in ileum and colon as compared to the jejunum (Sathaliyawala et al., 2013) and Tregs are the most abundant in the colon (Maynard et al., 2007). This distribution can be at least partly explained by the various luminal content, i.e. the discrepancies in gut microbiota and processes taking place in the different gut segments. T cells in the LP are thymus-derived conventional T cells that express TCRαβ along with CD4 or CD8αβ as co-receptors, in contrast to intraepithelial lymphocytes (IELs), which also comprise unconventional T cells expressing either TCRαβ or TCRγδ and typically CD8αα homodimers (Zeitz et al., 1991).

1.6 Lymphatic drainage in the intestine

The lymphatic system constitutes a blind-ended one-way transport network collecting immune cells, interstitial fluid and dietary lipids from the interstitial space in peripheral tissues and returning them to the blood circulation via lymphatic vessels. All afferent vessels pervade LNs delivering antigen and leukocytes from peripheral tissues and efferent vessels take the lymph from the LNs back to the blood circulation. Hence, the lymphatic system plays a crucial role for the induction of adaptive immunity and general immune-surveillance (Mowat and Agace, 2014; Cifarelli and Eichmann, 2019). In the small intestine, so-called lacteals (lymph capillaries) inside the villi constitute the initial lymphatics comprising a specialized structure with intercellular junctions that act as microscopic valves. Via these primary valves, fluids and cells are able to enter the lymphatic lumen (Schmid-Schönbein, 1990; Murfee et al., 2007). The lacteals then merge into larger collecting vessels consisting of both endothelial and smooth muscle layers that are organized into lymphangions, i.e. segments with unidirectional valves to prevent backflow of lymphatic fluid. In concert with the valves, smooth-muscle contractions facilitate the collecting lymphatics to work as pumps pushing lymph forward to the next segments and further to the draining LNs (Benoit et al., 1989).

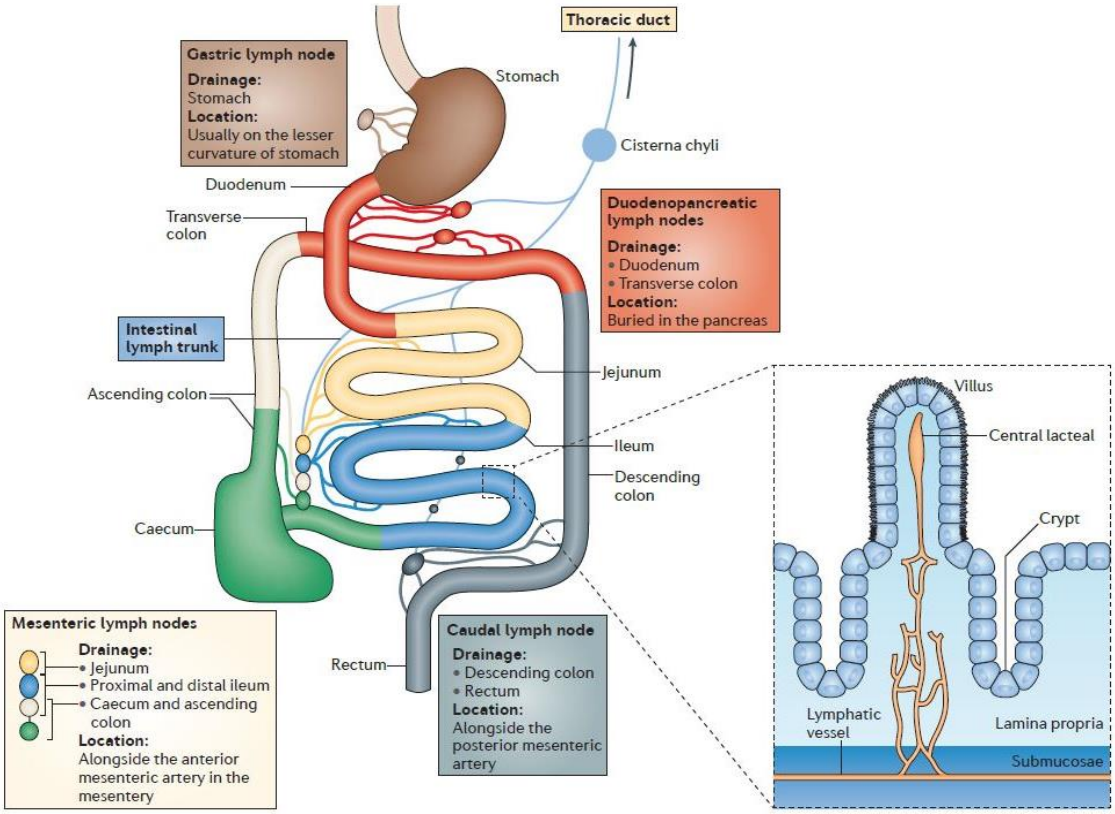

Figure 1.2: The mesenteric lymphatic system and draining lymph nodes. The formation of the mesenteric lymphatic fluid commences in central lacteals residing in the intestinal villi. Central lacteals are relatively permeable to immune cells, interstitial fluids and macromolecules and deliver the lymph to a capillary network that then converges into lymphatic vessels. Via those lymphatic vessels, the mesenteric lymph percolates the tissue-draining lymph nodes and finally the lymphatic vessels of the small intestine coalesce into the efferent superior mesenteric lymph duct. Adapted with permission from Mowat and Agace, 2014.

The LNs draining the intestine are the largest of the body corresponding to the constant exposure to environmental stimuli. These LNs are substantially differing from each other as they drain distinct intestinal segments (Figure 1.2), whereby neighboring LNs often drain overlapping areas (Tilney, 1971; Van den Broeck et al., 2006). A single postnodal vessel exits from each LN, eventually percolating through another LN and finally several lymphatic vessels converge to a larger lymph trunk. For instance, all lymph flowing from the small intestine coalesces into the efferent superior mesenteric lymph duct and finally enters directly into a sac-like structure at the distal end of the thoracic duct, namely the cisterna chyli. In the cisterna chyli, the lymph from the small intestine is merged with lymph draining the caudal peripheral tissues, other intestinal as well as hepatic and lumbar regions. Upon leaving the cisterna chyli, the lymph enters the thoracic duct together with lymph from the thorax and cranial parts of the

body and finally empties into the left subclavian vein. (Schmid-Schönbein, 1990; Breslin, 2014; Mowat and Agace, 2014)

1.7 Calcium Signaling in T cells

In T cells, elevation of intracellular calcium levels is an essential second messenger for external stimuli that crosslink TCRs or chemokine receptors and may trigger a variety of functions such as activation, differentiation, proliferation, homeostasis and cell death via complex signaling cascades (Crabtree and Clipstone, 1994; Trebak and Kinet, 2019). At a resting state, the cytoplasmic calcium concentration ranges between 50 and 100 nM but can increase to 1 µM upon TCR engagement. The endoplasmic reticulum (ER) with an elevated calcium concentration of ~500 nM and the extracellular space featuring Ca^{2+} concentrations of ~ 1 mM constitute the main sources of calcium influx upon T cell stimulation (Lewis, 2001). For instance, antigen recognition via TCRs as well as chemokine receptor ligation may lead to T cell activation via the generation of the second messenger inositol-1,4,5-trisphosphate (IP_3). Intracellular calcium signaling divides into two main stages: the first involves the second messenger IP_3 binding its receptor in the ER membrane and induces rapid but transient Ca^{2+} release from the ER stores. Incorporated in the ER membrane, stromal interaction molecule 1 (STIM1) is able to detect the decrease of Ca^{2+} in the ER and to activate calcium-release-activated calcium (CRAC) channels in the plasma membrane (Hogan et al., 2010). This second stage is characterized by a sustained calcium influx across the cell membrane via CRAC channels. Ca^{2+} influx via CRAC channels accounts for the largest increase in intracellular calcium concentration (Lewis and Cahalan, 1988) setting off a signaling cascade via calcium-dependent enzymes like calcineurin or calmodulin-dependent kinase (CaMK). These enzymes dephosphorylate transcription factors such as nuclear factor of activated T cells (NFAT), nuclear factor-κB (NF-κB) and cyclic-AMP-responsive-element-binding protein (CREB) and initiate their translocation into the nucleus. These transcription factors (TF) induce activation-dependent gene expression. (Macian, 2005; Feske, 2007; Fracchia et al., 2013; Joseph et al., 2014; Trebak and Kinet, 2019)

Fluctuations of cytoplasmic calcium levels exhibit a variety of signaling patterns, e.g. irregular transient spikes, repetitive oscillations or sustained plateaus that also differ in

frequency and amplitude. These distinct patterns affiliate with different signaling pathways and induce various cellular responses. For example, NFAT translocation requires higher frequency and amplitude of calcium signaling, whereas NF-κB translocates into the nucleus upon less frequent high-calcium spikes (Dolmetsch et al., 1998; Quintana et al., 2005). Besides affecting the differential activation of transcription factors, oscillations in Ca^{2+} signaling also seem to increase the efficacy of detecting rather weak stimuli and thus enhance the sensitivity to low doses of antigen (Dolmetsch et al., 1998; Li et al., 1998). Calcium can also induce negative effects, e.g. low and sustained calcium levels in turn prevent NFAT translocation to the nucleus (Dolmetsch et al., 1997) and persistent calcium signaling in the absence of co-stimulation may even lead to anergy in T cells (Heissmeyer and Rao, 2004). Furthermore, calcium signals may support the establishment of contacts between APCs and T cells by altering their motility and cytoskeletal organization (Delon et al., 1998).

1.7.1 Visualizing calcium signaling *in vivo*

As mentioned above, intracellular calcium is an essential trigger to signaling cascades downstream of both chemokine receptors and TCRs. Hence, measuring intracellular calcium levels allows for conclusions on the activation status of T cells. Genetically encoded calcium indicators (GECI) constitute a powerful tool to visualize the fluctuations of calcium levels in living lymphocytes that was introduced more than 20 years ago (Miyawaki et al., 1997). GECI are stably expressed in living cells allowing for long-term observations.

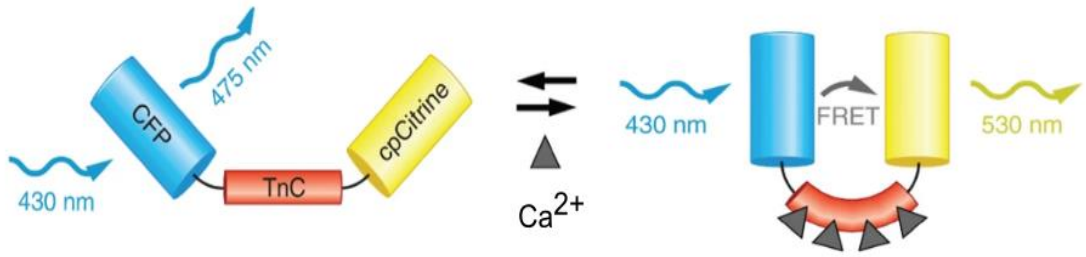

Figure 1.3: Schematic of the calcium indicator TN-XXL. TN-XXL is a GECI that uses the fluorophore CFP as a FRET donor and cpCitrine as acceptor. The two fluorophores are linked by the calcium-sensitive domain troponin C that changes its conformation upon binding of calcium. Adapted with permission from Mues et al., 2013

They consist of one or two fluorescent proteins (FP) and a calcium sensitive moiety that, upon reversibly binding calcium ions, change their conformation. GECI are distinguished into two modes of action: single-wavelength sensors and Förster resonance energy transfer (FRET)-based ratiometric sensors. The latter ones bear several advantages over the single fluorophore sensors for the application in functional imaging studies, e.g. they are significantly brighter at rest, indicate basal calcium levels and are less influenced by physical conditions such as changes in optical path length or excitation light intensity (Thestrup et al., 2014). One widely used FRET indicator is Twitch-2B. It is an enhanced version of TN-XXL that underwent several changes to enable and optimize its expression and function in mouse T cells. For example, Twitch-2B contains a codon-diversified cpVenus^{CD} and mCerulean3 as a FRET pair instead of cpCitrine and cyan fluorescent protein (CFP), respectively, in TN-XXL. Furthermore, the calcium-sensitive domain of Troponin C (TnC) was replaced with a higher affinity calcium-binding moiety, as it has already been applied in Twitch-1 (Mues et al., 2013). To create FRET signals, the excitation wavelength is tuned to (mainly) excite mCerulean3. In a low calcium situation, the calcium indicator emits cyan fluorescence. Upon rising intracellular calcium levels, free calcium ions bind to the TnC domain and induce a conformational change that leads to approximation of both fluorophores, allowing for fluorescence energy transfer from the excited mCerulean3 to cpVenus^{CD} in the case of Twitch-2B. This results in a drop in blue fluorescence and an increase in yellow fluorescence (Figure 1.3). The ratio of emitted fluorescence in the two channels (cpVenus^{CD}/mCerulean3) indicates direct changes of intracellular calcium levels in real time. (Mues et al., 2013; Thestrup et al., 2014)

2 OBJECTIVES

According to the leading paradigm of the etiology of MS, pre-existing autoreactive T cells are primed in the periphery before they infiltrate the CNS. Combined with the increasingly important role of microbiota as potential triggers of autoimmune diseases, the gut constitutes a probable site of action. The main goal of this study was to investigate whether encephalitogenic T cells get stimulated in gut-associated lymphoid tissues prior to EAE, a rodent model for MS.

The first aim of this work was to visualize T cell stimulation in the ileal lamina propria of mice by combining intravital two-photon microscopy with a calcium-sensitive fluorophore. Given that intracellular calcium signaling is a prerequisite for effective activation of T cells, cytosolic calcium levels constitute a useful indicator of stimulation. The second question was whether these calcium signals translate into activation-induced gene expression, which was assessed by transcriptome analysis. Third, to assign a functional role to T cell stimulation in the gut, T cells that had been stimulated in the small intestine were transferred to recipient mice and their behavior was assessed and compared to non-gut-stimulated T cells *ex vivo*.

Another crucial event in the pathogenesis of MS/EAE following the peripheral priming is infiltration of encephalitogenic T cells into the CNS. This process requires the availability of certain integrins and adhesion molecules. In the last part of the project, the involvement of specific adhesion molecules in T cell infiltration was examined by intravital imaging of encephalitogenic T cells at the blood-brain barrier in a transfer EAE model in the Lewis rat.

3 Material and Methods

3.1 Material

3.1.1 Plasmids

Table 3.1 Plasmids used in this study

Name	Provider
pMSCV-Δneo-Twitch-2B	Thestrup et al., 2014
pCL-Eco	Mues et al., 2013

3.1.2 Media, Reagents and Buffers

Table 3.2 Media, reagents and buffers used in this study

Medium	Amount	Constituent	Company
ACK buffer	8.024 mg/l	NH_4Cl	Merck KGaA
	1.001 mg/l	$KHCO_3$	Merck KGaA
	3.722 mg/l	$EDTA.Na_2{\cdot}2H_2O$	Merck KGaA
EH	97.5 % Vol.	DMEM	Sigma-Aldrich
	2.5 % Vol.	HEPES solution, 1 M	Sigma-Aldrich
FACS buffer	99 % Vol.	PBS	-
	1 % Vol.	Rat serum	-
	0.05 % Vol.	NaN_3	Carl Roth GmbH
Freezing medium	50 % Vol.	Horse serum	Gibco
	40 % Vol.	EH	-
	10 % Vol.	Dimethylsulfoxide (DMSO)	Sigma-Aldrich
Hank's balanced salt solution (HBSS) [10x]	80 g/l	NaCl	VWR
	4 g/l	KCl	VWR
	0.6 g/l	KH_2PO_4	Merck KGaA
	10 g/l	Glucose	Merck KGaA
	0.478 g/l	Na_2HPO_4	Sigma-Aldrich
HBSS + Hepes	50 ml	10x HBSS	-
	7.5 ml	HEPES solution, 1 M	Sigma-Aldrich
	Ad 500 ml	MilliQ water	Merck MilliPore
HBSS + HEPES+EDTA	50 ml	10x HBSS	-
	7.5 ml	HEPES solution, 1 M	Sigma-Aldrich
	50 ml	Fetal bovine serum (FBS)	Merck KGaA
	5ml	EDTA [0.5 M]	Merck KGaA
	Ad 500 ml	MilliQ water	Merck MilliPore
Isolation buffer	500 ml	Ca^{2+} and Mg^{2+} free PBS, pH 7.4	Sigma-Aldrich
	0.1 % Vol.	BSA	Sigma-Aldrich
	2 mM	EDTA	Merck KGaA
Luria Bertani (LB)	10 g/l	Tryptone	Merck KGaA

Medium	5g/l	Yeast Extract	Merck KGaA
	5 g/l	NaCl	Carl Roth GmbH
LB Agar	Ad 1 l	LB Medium	-
	15 g/l	Bacto Agar	BD
PBS, adjusted to pH 7.4 [10x]	100 mM	Na_2HPO_4	Carl Roth GmbH
	18 mM	KH_2PO_4	Merck KGaA
	1.4 M	NaCl	Carl Roth GmbH
	27 mM	KCl	Merck KGaA
Isotonic Percoll	90 % Vol.	Percoll	GE Healthcare
	10 % Vol.	10x PBS	-
Restimulation medium (RM)	99 % Vol.	TCM	-
	1 % Vol.	Rat serum	-
RPMI + Hepes + FBS	7.5 ml	HEPES solution, 1 M	Sigma-Aldrich
	50 ml	FBS	Merck KGaA
	Ad 500 ml	RPMI	Sigma-Aldrich
Sorting buffer	99 % Vol.	PBS	-
	1 % Vol.	Rat serum	-
	2mM	EDTA	Merck KGaA
T cell medium (TCM)	Ad 1 l	DMEM	Sigma-Aldrich
	2 mM	L-Glutamine	Sigma-Aldrich
	100 µg/ml	Penicillin/Streptomycin	Sigma-Aldrich
	36 mg/l	Asparagine	Sigma-Aldrich
	1 mM	Sodium-Pyruvate	Sigma-Aldrich
	10 ml/l	Non-essential amino acids	Sigma-Aldrich
	4 µl/l	β-Mercaptoethanol	Merck KGaA
TCM + FBS	90 % Vol.	TCM	-
	10 %	FBS	Merck KGaA
TCGF	88 % Vol.	TCM	-
	10 % Vol.	Horse serum	Gibco
	2 % Vol.	Supernatant of ConA stimulated EL4.Il-2 cells	-

3.1.3 Antibodies

Table 3.3 Antibodies used in this study

Specificity Clone, Isotype	**Host and conjugation**	**Source**	**Application**
CD3 17A2, IgG2β,κ	Rat anti mouse APC	Biolegend	Flow Cytometry
CD3e 500A2, IgG	Golden Syrian Hamster anti mouse unconjugated	Invitrogen	Cell culture
CD3e 500A2, IgG	Golden Syrian Hamster anti mouse V450	eBioscience	Flow Cytometry

CD4 **RM4-5, IgG2a,κ**	Rat anti mouse FITC	Biolegend	Flow Cytometry
CD4 **RM4-5, IgG2a,κ**	Rat anti mouse PE-Cy7	eBioscience	Flow Cytometry
CD8 **53-6.7, IgG2a,κ**	Rat anti mouse PE	Biolegend	Flow Cytometry
CD11a **WT.1, IgG2a**	Mouse anti rat unconjugated	Produced by hybridoma culture	Intravital application, Flow Cytometry
CD18 **WT.3, IgG1**	Mouse anti rat unconjugated	Thermo Fisher	Intravital application, Flow Cytometry
CD19 **1D3, IgG2a,κ**	Rat anti mouse V450	BD Pharmingen	Flow Cytometry
CD19 **6D5, IgG2a,κ**	Rat anti mouse PerCP/Cy5.5	Biolegend	Flow Cytometry
CD28 **37.51, IgG**	Armenian Hamster anti mouse unconjugated	Invitrogen	Cell culture
CD29 **Ha2/5, IgM, κ**	Armenian hamster anti rat unconjugated	BD Pharmingen	Intravital application, Flow Cytometry
CD45 **30-F11, IgG2β,κ**	Rat anti mouse BV785	Biolegend	Flow Cytometry
CD49d **MRα4-1, IgG2a**	Mouse anti rat unconjugated	Kindly provided by Dr. Yagita, Juntendo University, Japan	Intravital application, Flow Cytometry
FoxP3 **FJK-16s, IgG2a, κ**	Rat anti mouse V450	eBioscience	Flow Cytometry
ICAM-1 **1A29, IgG1**	Mouse anti rat unconjugated	Produced by hybridoma culture	Intravital application, Flow Cytometry
IgG2a,κ Isotype **control, eBR2a**	Rat anti mouse V450	eBioscience	Flow Cytometry
OX40L **ATM-2, IgG1, κ**	Mouse anti rat unconjugated	Kindly provided by Dr. Yagita, Juntendo University, Japan	Intravital application, Flow Cytometry
Vα3.2 TCR **RR3-16, IgG2β,κ**	Rat anti mouse PerCP	Thermo Fisher	Flow Cytometry
Vα3.2 TCR **RR3-16, IgG2β,κ**	Rat anti mouse FITC	Biolegend	Flow Cytometry
Vβ5.1/5.2 TCR **MR9-4, IgG1, κ**	Mouse anti mouse PE	Invitrogen	Flow Cytometry
Vβ11 TCR **RR3-15, IgG2b,κ**	Rat anti mouse APC	Biolegend	Flow cytometry

VCAM-1 MR106, IgG1	Mouse anti rat unconjugated	Kindly provided by Dr. Yagita, Juntendo University, Japan	Intravital application, Flow Cytometry
VE-Cadherin C-19, IgG	Goat anti rat unconjugated	Santa Cruz	Flow Cytometry
Armenian Hamster IgG (H+L), secondary AB, IgG	Goat anti Armenian hamster APC	Jackson ImmunoResearch	Flow Cytometry
Mouse IgG (H+L), secondary AB, F(ab')$_2$ fragment	Rabbit anti mouse PerCP	Jackson ImmunoResearch	Flow Cytometry
Mouse IgG (H+L), secondary AB, F(ab')$_2$ fragment	Donkey anti mouse APC	Jackson ImmunoResearch	Flow Cytometry
Goat IgG (H+L) Secondary AB, IgG	Donkey anti goat Alexa Fluor 647	Jackson ImmunoResearch	Flow Cytometry

3.1.4 Antigens

MBP was prepared from guinea pig brain homogenates as reported (Campbell et al., 1973). Ovalbumin (OVA) and MOG peptides were purchased from BioTrend (Köln, Germany). OVA protein was purchased from Sigma-Aldrich (Taufkirchen, Germany).

3.2 Methods

3.2.1 DNA techniques

DNA transformation. 5-alpha Competent *E.coli* (NEB, Ipswich, MA) were thawed on ice. 50 ng of plasmid DNA were transferred to the competent cells and the mixture was placed on ice for 30 minutes. Afterwards, the vial was heated to 42°C for exactly 30 seconds. The volume of the mixture was increased by 500 µl SOC medium (Sigma-Aldrich) and the sample was shaken with 250 rpm at 37 °C for one hour. Serial dilutions in SOC medium were spread on LB plates containing 100 µg/ml ampicillin and incubated at 37 °C o/n. On the next day, single colonies were picked to inoculate LB medium for an overnight culture. The next day, plasmid DNA was isolated and the correct sequences were validated before downstream applications.

Plasmid isolation from E.coli. Plasmid DNA was isolated using the NucleoBond Xtra Midi EF kits (Macherey-Nagel, Düren) according to the manufacturer's instructions.

E.coli glycerol stock. An overnight culture of transformed *E.coli* was mixed in a ratio of 1:1 with 50 % glycerol and stored at -80 °C.

3.2.2 RNA techniques

Total RNA isolation. Cells were lysed in RLT plus buffer (provided by RNeasy Plus Micro kit, Qiagen, Hilden) and subsequently loaded onto QiaShredder spin columns (Qiagen) prior to RNA isolation. RNA isolation was performed using the Qiagen RNeasy Plus Micro kit (Qiagen) according to manufacturer's instructions.

Agilent bioanalyzer. RNA quality and concentration were measured using the Agilent RNA 6000 Pico Kit on an Agilent 2100 bioanalyzer machine (Agilent Technologies, Inc., Santa Clara, CA) according to the manufacturer's instructions

RNA storage. RNA was eluted in nuclease-free water and stored at -80°C until further use.

Next generation sequencing (NGS) and data analysis. Transcriptome analysis and subsequent bioinformatics were performed by BGI Group (Shenzhen, China) using their DNBseq™ platform. The sequence alignment to the reference genome was performed using HISAT2 (Hierarchical Indexing for Spliced Alignment of Transcripts 2) (Kim et al., 2019). Differentially expressed genes (DEGs) were detected using DEseq2 (Love et al., 2014).

3.2.3 Cell culture

HEK293T cells.

Cell Culture. HEK293T cells were kept in 10 cm culture dishes TCM + 10 % FBS in an incubator with culture conditions of 37 °C with 10 % CO_2. In general, cells were passaged when reaching around 90 % confluency.

Freezing and thawing. HEK293T cells were frozen at -80 °C in cryotubes at a concentration of 1 x 10^6/ml in freezing medium. For thawing, cell stocks were incubated in a 37 °C water bath and then washed with 10 ml EH to remove DMSO.

Transfection with polyethylenimine (PEI). 1.2-1.5 x 10^6 cells were seeded per 10 cm culture dish in 10 ml TCM + 10 % FBS and incubated o/n. For each dish to transfect, 6 µg pMSCV-Δneo-Twitch-2B and 3.5 µg pCL-Eco were added to 500 µl TCM and 20 µl

PEI MAX [2 mg/ml] (Polysciences, Warrington, PA) were added to another 500 µl TCM. Both solutions were incubated for 5 min and then pooled and vortexed. After 20 min incubation at room temperature (RT), the mixture was added dropwise onto the plated HEK293T cells. The cells were incubated at 5 % CO_2 o/n. The next day, the supernatant was discarded and exchanged to 8 ml TCM+10 % FBS and the culture was continued in 10 % CO_2. 48 h and 72 h after transfection, the HEK293T cell supernatant containing viral particles were collected and stored at 4 °C until further use.

Concentration of retroviral supernatant. The retroviral supernatant was placed at RT 30 min prior to concentration. To get rid of cellular debris, the supernatant was centrifuged at 2000 g for 5 min at RT and the pellet was discarded. Subsequently, the supernatant was filtered with a 0.45 µm sterile filter (Merck Millipore, Burlington, MA) prior to concentration of viral particles. Afterwards, the supernatant was concentrated by centrifugation at 4000 g for 20 min at RT using Amicon® Ultra Filters (Merck KGaA) with a molecular weight cut-off (MWCO) of 100 KDa. The viral concentrate was stored in cryotubes at -80 °C for up to three months.

Antibody production. Antibody-producing hybridoma lines were kindly provided by Prof. Masayuki Miyasaka from Osaka University. Cells were cultured in serum-free medium (SFM) (Gibco, Thermo Fisher, Waltham, MA). The supernatant was harvested from overgrown cell culture plates. The antibodies in the supernatant were concentrated by using a Centricon Plus-70 (Merck Millipore) according to manufacturer's protocol. Antibody concentration was measured using a NanoDrop spectrophotometer (NanoDrop, Wilmington, DE) and the samples were stored at a concentration of 0.5 mg/ml at -20 °C.

Primary mouse T cell culture. Primary cells were cultured in standard tissue-culture-treated 12-well culture plates (Corning, New York, NY) at a concentration of 4 x 10^6 cells/ml TCM + 10 % FBS in the presence of 0.5 µg/ml anti-CD3e and anti-CD28 stimulating antibodies.

Isolation of mouse $CD4^+$ T cells. For comparisons of $CD4^+$ T cells from different organs, this T cell subset was isolated from either splenocytes or lymphocytes from the mesenteric lymphatic fluid using the EasySep Mouse $CD4^+$ T cell isolation kit from StemCell Technologies. Therefore, the cells were resuspended in RoboSep buffer

(StemCell Technologies, Vancouver, Canada) at a concentration of up to 1 x 10^8 cells/ml in a 5 ml FACS tube. After adding 50 µl/ml Rat serum, the same amount of $CD4^+$ T cell isolation cocktail was added and cells were incubated for 10 min at RT. EasySep beads were vortexed extensively and then added at a concentration of 75 µl/ml cell suspension and incubated for 2.5 min at RT. Subsequently, the volume was increased to 2.5 ml by adding a respective amount of RoboSep buffer and the sample was put into the StemCell magnet for another 2.5 min. Then, the liquid was poured into a new 15 ml tube and the cells were counted immediately.

Depletion of B cells. For culturing primary T cells, B cells were depleted from lymphocyte populations of different organs using the Dynabeads B220 depletion kit (Thermo Fisher). The cells were resuspended in B220 Isolation buffer at a concentration of 1 x 10^7/ml in 15 ml tubes. For each ml of cell suspension, 25 µl of B220 depletion beads were taken into a 5 ml FACS tube containing 1 ml isolation buffer. The FACS tube containing the beads was put into a magnet for 2 min before the liquid was taken out and substituted with an equal amount of isolation buffer. Then, 25 µl beads were added per ml of cell suspension. This mixture was incubated on a tube rotator (IKA, Staufen im Breisgau, Germany) with 10 rpm at 4 °C for 40 minutes. Afterwards, the tubes were put onto a magnet to take out the bead-bound cells and the liquid was transferred to new tubes.

Depletion of $CD8^+$ T cells. For culturing primary $CD4^+$ T cells, $CD8^+$ T cells were depleted from lymphocyte populations of different organs in C57BL/6J mice using the Dynabeads $CD8^+$ (Lyc6) depletion kit (Thermo Fisher) according to manufacturer's instructions. For the detailed procedure, refer to "*Depletion of B cells".*

Retroviral transduction. After 48 h of stimulation with anti-CD3e and anti-CD28 stimulating antibodies, the primary $CD4^+$ T cells were blasting and thus ready for retroviral transduction. The cells were harvested from the dishes and centrifuged at 400 g for 5 min 4 °C. Afterwards, the cells were resuspended at a concentration of 4 x 10^6/ml in RPMI+ 10 % FBS containing 10 ng/ml IL-2 (PeproTech, Cranbury, NJ) and 8 µg/ml polybrene (Sigma-Aldrich). The cells were seeded in non-tissue-culture-treated 12-well plates with 500 µl/well (Corning). 50 µl of the concentrated retroviral supernatant were added to each well and the plates were centrifuged at 2000 g for

90 min at RT. Afterwards, 1 ml TCGF was added to each well and the cells were resuspended briefly.

Cell labeling with tracking dyes. In order to follow and retrieve transferred T cells *ex vivo* from recipient mice, T cells were stained with either CellTrace™ Violet (CTV) (Thermo Fisher Inc.) or CellTrace™ FarRed (CTR) (Thermo Fisher Inc.). Both dyes were diluted in PBS to a working concentration of 1 µM. 1 x 10^6 cells/ml were resuspended in 1 ml staining solution and incubated for 20 min at RT under protection from light. Subsequently, the reaction was stopped by adding 10 ml TCM+10 % FBS and the samples were kept on ice for at least 5 min. After centrifugation at 400 g for 5 min at 4 °C, the cells were resuspended either in culture medium or in PBS for direct injection.

Restimulation of rat T cell lines. $T_{MBP\text{-}GFP}$ cell lines have been previously generated in our lab as described before (Kawakami et al., 2004). T cells were cultivated at a concentration of 0.6-0.7 x 10^6/ml in 5 ml RM in 6 cm cell culture dishes (BD, Franklin Lakes, NJ) in a humidified incubator at 37 °C and 10 % CO_2. To restimulate T cells, irradiated (50 Gy) syngeneic thymocytes at a concentration of 14-20 x 10^6/ml and 10 µg/ml MBP were added. After 48 h, the restimulated T cells were either injected into recipient animals or expanded in TCGF.

Freezing and thawing of T cell stocks. 20-30 x 10^6 T cells were harvested and resuspended in 1.5 ml freezing medium. Stocks were slowly frozen in a freezing container at -80 °C and afterwards transferred to liquid nitrogen for long-term storage. For thawing, the T cell vials were put into a 37 °C water bath and washed once with 10 ml EH to dispose of DMSO.

3.2.4 Flow Cytometry

Surface staining. The cells to be stained were transferred into V-shaped 96-well plates and washed once with 150 µl PBS and once with 150 µl FACS buffer. Each washing step was followed by a centrifugation step with 400 g for 3 min at 4 °C. Primary or directly conjugated surface marker binding antibodies were used in a 1:100 dilution in FACS buffer unless stated differently by the manufacturer. Cells were incubated in 100 µl of the staining solution for 30 min on ice under protection from light. Afterwards, the cells were washed twice in 150 µl FACS buffer. If needed, the samples were incubated with secondary antibody at a dilution of 1:500 in FACS buffer for 30 minutes on ice

under protection from light. After two washing steps with FACS buffer, the cells were resuspended in 150 µl sorting buffer for the analysis on a FACS Verse (BD) or analysis and sorting at a FACS Aria IIIu (BD).

Intracellular staining. As for the surface staining, the cells were transferred to V-shaped 96-well plates and washed with PBS before resuspension in 100 µl 2 % PFA for 15 min on ice. After fixation, the cells were washed with PBS and permeabilization buffer (eBioscience) and then incubated in permeabilization buffer for 15 minutes on ice. After permeabilization, cells could be stained for intracellular antigens in a 1:100 dilution of antibody in permeabilization buffer. The cells stayed in the staining solution for 30 min on ice under protection from light. Afterwards, additional dye was washed away in two washing steps with first permeabilization buffer and then PBS. For the FACS analysis, the cells were resuspended in 150 µl PBS and acquired on a FACS Verse.

Cell sorting. Antibody-stained splenocytes, blood lymphocytes or cells from mesenteric lymph were resuspended in PBS and sorted on a FACS Aria IIIu (BD) using a 70 µm nozzle. Cell sorting was performed at the Core Facility Flow Cytometry of the Biomedical Center, LMU Munich.

Data analysis. FACS data was analyzed using FlowJo (Tree Star Inc., Ashland, OR).

3.2.5 Mouse routine

License. The SPF mice used in this study were bread and kept in the Core Facility Animal Models of the Biomedical Center, LMU Munich. SMARTA-1 mice were kindly provided by Prof. Dr. Dirk Baumjohann from the Institute of Immunology (LMU Munich, Biomedical Center). The GF mice were bred in the animal facilities of the Technical University of Munich (School of Life Sciences Weihenstephan) and were kindly provided by Prof. Dr. Dirk Haller. The local authority (Regierung von Oberbayern) approved all mouse experiments.

Lymphocyte preparation from isolated organs. Mice were sacrificed and spleens and lymph nodes were dissected and transferred to EH. Single-cell suspensions were obtained by forcing the organs through 40 µm cell strainers (Greiner Bio-One GmbH, Kremsmünster, Austria) using a syringe plunger. Strainers and plates were washed with 5 ml EH each and cells were centrifuged 400 g for 5 min at 4 °C. Splenocytes were

subjected to erythrocyte lysis by incubating the cell suspension in 2 ml ACK buffer for 3 min at RT. To stop the reaction, 5 ml EH + 10 % HS were added and the tube was filled with PBS. After spinning down, the cells were resuspended in suitable medium for culture or downstream processing.

Lymphocyte preparation from blood. Directly after sacrifice with CO_2 or overdose of anesthesia, blood was withdrawn from the heart into a syringe that had been flushed with heparin (5000 U/ml) (Sigma-Aldrich) in PBS. Erythrocytes were lysed by incubation in 1 ml ACK buffer for 10 minutes and finally resuspended in PBS.

Lymphocyte isolation from the small intestine LP. Mice were sacrificed and a piece of the small intestine was cut, approximately 10 cm starting from the caecum, and the fat tissue was removed carefully. Peyer's patches (PP) were excised and the intestinal content was removed by sliding blunt forceps along the tube. Subsequently, the intestine was cut open and intersected into pieces of ~ 5 mm in a 10 cm dish containing HBSS + Hepes medium. The dish was swirled and the content poured onto a 70 µm nylon mesh (Greiner Bio One) to wash it. The intestinal pieces were put into 13 ml of fresh HBSS + Hepes solution, swirled and poured onto another mesh to remove the liquid. This washing step was repeated three times. Afterwards, the gut samples were added to an Erlenmeyer flask containing 25 ml HBSS + Hepes + 5 mM EDTA + 10 % FBS and stirred on a magnet for 15 min at 350 rpm before removing the liquid by pouring the samples on a new 70 µm mesh. Then, the pieces were put back into the Erlenmeyer flask with 25 ml of fresh medium and stirred as previously. This step was repeated twice before replacing the medium to RPMI+Hepes+10 % FBS and stirring for 5 min to remove residual EDTA. Subsequently, liquid was exchanged to 25 ml RPMI+Hepes+10 % FBS supplemented with 1.25 mg/ml Collagenase D (Sigma-Aldrich). The plate was heated to 37 °C and the gut pieces were stirred for 1 h at 550 rpm. Afterwards, the tissue was forced through a new 70 µm mesh and washed two times with RPMI. The cells were subjected to a Percoll gradient in order reduce the amount of debris and undesired cells. To do so, the cells were resuspended in 5 ml 40 % Isotonic Percoll (GE Healthcare) and overlaid onto 2.5 ml 80 % Isotonic Percoll. The tube was centrifuged at 380 g for 20 min at RT with mild acceleration and deceleration. The phase containing the lymphocytes was taken out and cells were washed before subjected to surface stainings for flow cytometry.

Oral gavage. To either apply antigen orally or to render the lymphatic fluid milky and thus visible, 30 min prior to surgery, mice were gavaged with 200 µl antigen (4 mg) or olive oil, respectively, using 20G oral gavage needles while being anesthetized with isoflurane.

Immunization. To induce active EAE, mice were subcutaneously (s.c.) injected into the flanks with an emulsion containing 200 µg MOG_{35-55} peptide (MEVGWYRSPFSRVVHLYRNGK) (BioTrend) and 500 µg *M. tuberculosis* (Difco Laboratories Inc., Franklin Lakes, NJ) in CFA (Difco). Furthermore, the mice received intraperitoneal (i.p.) injections of 200 ng Pertussis toxin (List Biological Laboratories, Campbell, CA) on day 0 and 2 after immunization. Body weight and EAE scores were evaluated daily according to the following criteria:

score 0 – no disease; score 0.5 – reduced tail tonus; score 1: limp tail; score 1.5 – limp tail and ataxia; score 2 – limp tail and hind limb weakness; score 2.5 – at least one hind limb paralyzed/weakness; score 3 – both hind limbs paralyzed; score 3.5 –complete paralysis of hind limbs and weakness of front limbs; score 4 – paralysis of hind and front limbs; score 5 – moribund or dead.

To control for the effect of CFA alone, mice were immunized with an emulsion containing PBS instead of antigen.

In order to deliver antigen to the skin-draining lymph nodes, mice were immunized with a similar emulsion as for active EAE, but containing 200 µg OVA_{1-125} protein (Sigma-Aldrich) instead of MOG_{35-55}. Furthermore, the Pertussis toxin injection was spared.

Cell transfer for migration studies and for imaging. For injection, T cells were resuspended in 200 µl PBS and injected i.p..

Lymphatic cannulation. In order to obtain mesenteric lymph and thus the totality of lymphocytes exiting the gut, the efferent mesenteric lymph duct was cannulated. The technique was modified from Druzd and colleagues (Druzd et al., 2017). 30 minutes prior to cannulation, the animals were orally gavaged with 200 µl olive oil.

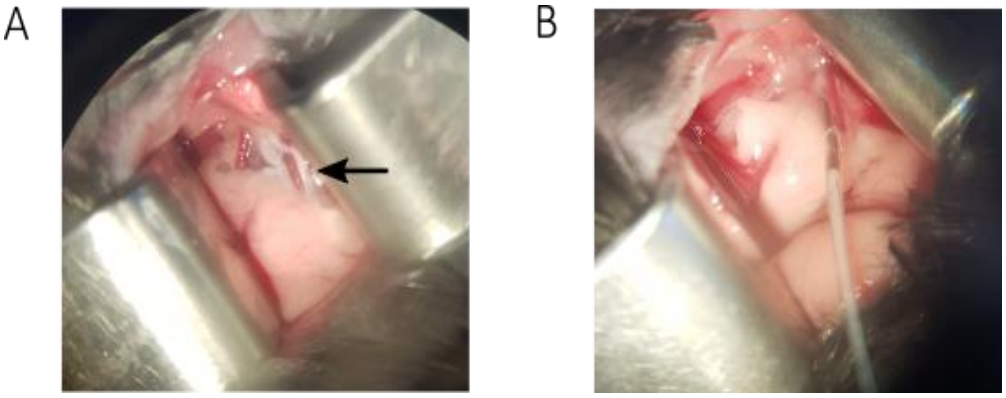

Figure 3.1: Cannulation of mesenteric lymph. (A) The mesenteric lymph duct containing milky lymph surrounding a big artery indicated by black arrow. (B) Lymphatic fluid flowing into the tube after inserting the cannulation needle into the vessel.

15 min before cannulation, the mice were anesthetized with midazolam/ medetomidine/fentanyl (MMF) (5, 0.5 and 0.05 mg per kg body weight (bw), respectively). The skin was incised along the left costal arch and the abdomen was opened. The mesenteric lymphatic duct locates below the left kidney (Figure 3.1A). The cannulation tube consists of the tip of a 29G needle inserted on one side of a 0.61 mm polyethylene tube, whereby the other and is connected to a 29G syringe (BD). The system was flushed with 15 µl heparin (5000 U/ml) and the needle tip was carefully inserted into the lymph duct in a very flat angle. By pulling the syringe plunger very slowly, negative pressure was created to draw the milky liquid into the tube (Figure 3.1B).

3.2.6 Rat routine

License. Lewis rats were obtained from Charles River (Sulzfeld, Germany) and kept in the animal facility of the Max Planck Institute of Neurobiology. All animal experiments have been conducted under approval of the local authority (Regierung von Oberbayern).

Adoptive transfer EAE. tEAE was induced by intravenous (i.v.) injection of 3-5 x 10^6 *in vitro* stimulated $T_{MBP\text{-}GFP}$ cells into the tail vein of 8-12 week old rats. Weight loss and clinical scores were monitored daily according to the following criteria:

Score 0 - no disease; Score 0.5 - loss of tail tonus; Score 1 - tail paralysis; Score 2 - gait disturbance; Score 3 - complete hind limb paralysis; Score 4- tetraparesis; Score 5 - death.

Isolation of cells after imaging. In order to analyze T cells and endothelial cells for their antibody saturation after imaging, the spleen was isolated after euthanasia. Single-cell suspensions were obtained by forcing the organs through 40 µm cell strainers (Greiner Bio-One GmbH) using a syringe plunger. Strainers and plates were washed with 5 ml EH each and cells were centrifuged 400 g for 5 min at 4 °C. Splenocytes were subjected to erythrocyte lysis by incubating the cell suspension in 3 ml ACK buffer for 5 min at RT. To stop the reaction, 5 ml EH + 10 % HS were added and the tube was filled with PBS. After spinning down, the cells were resuspended in suitable medium for downstream processing.

3.2.7 Intravital two-photon microscopy

Image acquisition. Time-lapse two-photon laser-scanning microscopy was performed using an SP2 or SP8 MP microscope (Leica, Wetzlar, Germany).

The SP2 system was equipped with a 10 W Millenia/Tsunami laser (Spectra Physics, Darmstadt, Germany). Excitation wavelength was tuned to 835 nm and routed through a water immersion objective (25x, NA 0.95, Leica). With a zoom factor of 2, areas of 240 x 240 µm size were scanned, and 30-50 µm z-stacks were acquired with 3-4 µm z-step size. Acquisition rate was 25 s interval time with images line-averaged twice. Fluorescent signals were detected using non-descanned photomultiplier tube detectors (Hamamatsu, Herrsching, Germany) equipped with 475/50 nm, 537/26 nm, 630/69 nm, and 685/40 nm bandpass filters (Semrock, Rochester, NY, USA).

Multi-photon microscopy using the SP8 MP microscope was performed at the Core Facility Bioimaging of the Biomedical Center, LMU Munich. The SP8 system featured a pulsed InSight DS+ laser (Spectra Physics) and emission was tuned to 841 nm and routed through a water immersion objective (25x, NA 1, Leica). Using a 2x zoom, areas of 221x 221 µm were scanned and acquired in 30-50 µm z-stacks with 3-4 µm step size and an acquisition rate of 25 s per z stack. Images were recorded with external, non-descanned hybrid photo detectors (HyDs) equipped with 483/32 nm, 535/30 nm, 585/40 nm and 650/50 nm bandpass filters.

Animal preparation. Prior to surgery, the animals were anesthetized with MMF (table 3.4):

Table 3.4: MMF anesthesia concentrations for mice and rats

Species	Midazolam [mg/kg bw]	Medetomidine [µg/kg bw]	Fentanyl [µg/kg bw]
Mouse	5	500	50
Rat	2	150	5

Then, they were tracheotomized and ventilated with 1.5-2 % isoflurane throughout the surgery and imaging procedure. The animals were placed on a custom-made heated microscope stage and their body temperature was regulated to stay at 37.5 °C. Electrocardiograms and breathing parameters such as concentrations of inspiratory and expiratory gases and ventilation pressure were constantly monitored during imaging. When needed, mice and rats were i.v. injected with 10 µg of fluorescently labelled dextran (70 kDa, Thermo Fisher) to render the blood vessels visible. In the rat study, antibodies were also injected i.v. at a concentration of 0.5 mg/ml.

Mouse gut imaging ileal LP: For imaging the ileal LP, the mouse abdomen was opened by midline incision. The mouse was facing left and the small intestine was pulled out as little as necessary and placed on a custom-made stage padded by dampened tissues. The intestinal tube was opened with a longitudinal incision of approximately 1 cm using a cautery pen (Bovie, Clearwater, FL). Both sides were folded back onto the dampened tissues on the stage to have a flat layer exposing the ileal LP. The intestinal content was carefully removed before fixing the gut with a cover slip and tissue adhesive (3M Animal Care Products, Saint Paul, MN). The cover slip was pressed down so that peristaltic movements could not disturb image acquisition.

Mouse mesenteric lymph node imaging. As previously described, the abdomen was incised with the mouse facing left. The caecum was pulled out so the mesenteric lymph nodes are exposed. The front most lymph node was fixed between a layer of dampened tissues and a glass cover slip for imaging.

Mouse inguinal lymph node imaging. To expose the inguinal lymph nodes (iLN), the mouse was placed on its back and the skin was cut open along the ventral surface of the abdomen and to the knee of the mouse. Then the skin was retracted towards the

mouse's back until the iLN is visible. The skin was fixed with a needle to expose the LN laying on dampened tissue. Connective and adipose tissue were cleared from the LN. A cover slip was fixed on the skin using tissue adhesive surrounding the LN.

Rat spinal cord imaging. Spinal cord imaging was performed at level Th12/L1 as previously described by our lab (Bartholomäus et al., 2009). The skin was opened with a midline incision of 3 cm and subsequently, the paravertebral musculature was detached. Three spines were fixed using a custom-made stage in order to facilitate stable imaging and reduce artifacts such as breathing. A dental drill (Foredom, Bethel, USA) was used to perform a laminectomy on the central spine disc. In order to keep the tissue hydrated and to allow use of the water immersion objective, a ring-shape surrounding was built from low-melting agarose to keep PBS in the opened spine.

3.2.8 Image processing and analysis

Time-lapse images were acquired with Leica LCS software (Leica) for the SP2 system and with LAS X software (Leica) for the SP8 setup, respectively, and processed and analyzed using ImageJ (NIH, Bethesda, MD, USA).

A Gaussian blur filter was used before Z-projecting the stacks with maximum intensity to generate two-dimensional movies. For Twitch-2B transduced cells, ratiometric pseudocolor images were obtained by dividing the cpVenus^{CD} (FRET) by the mCerulean3 (CFP) channel and changing to a fire lookup table. To analyze the calcium ratios, the cell shapes were manually outlined in each time frame in the 2D maximum projection to create a region of interest (ROI) for every cell to be tracked. The bleed-through of CFP into the YFP channel was determined to be 44 %, hence the FRET signal was corrected as YFP = FRET – 0.44 x CFP. The average signal intensities of all pixels in each ROI were defined to calculate the calcium ratio at every given time point. When analyzing cells that expressed GFP, T cells were tracked using the manual tracking plugin in ImageJ. Motility parameters were calculated from the cell coordinates over time using ImageJ.

3.2.9 Statistical analysis

The statistical evaluation was performed using Prism software (GraphPad, San Diego, CA) as described in the figure legends. Significance was indicated by p-value as follows: *p<0.05, **p<0.01, ***p<0.001.

4 RESULTS

4.1 Calcium Imaging in CD4$^+$ T cells in the ileal lamina propria of mice

4.1.1 Transduction of mouse CD4$^+$ T cells with Twitch-2B

In order to visualize calcium signaling in T cells, they were stably transduced using a retrovirus harboring the sequence of the GECI Twitch-2B. Viral particles were produced by HEK293T cells that have been transfected with the retroviral vector, pMSCV-Δneo-Twitch-2B as well as with the viral packaging vector pCL-Eco (Figure 4.1).

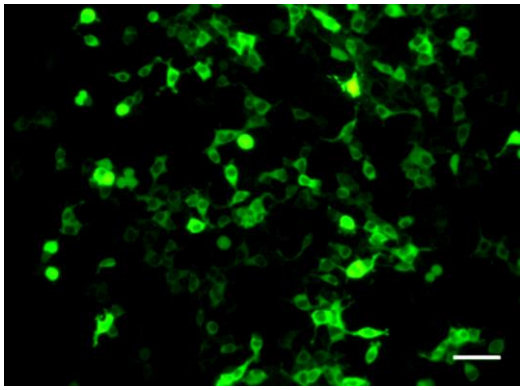

Figure 4.1: HEK293T cells expressing Twitch-2B visualized by fluorescence microscopy. Scale bar 50 µm.

The HEK293T cells released the virus into the extracellular space. After harvesting and concentrating the HEK293T supernatant, the density of viral particles was high enough to transduce CD4$^+$ T cells. As retroviruses only enter dividing cells, the T cells needed to be activated with stimulating anti-CD3 and anti-CD28 antibodies beforehand. Prior to culture and subsequent transduction, CD4$^+$ T cells were enriched from spleens and lymph nodes of donor mice by depleting other lymphocyte subsets. Figure 4.2A shows Twitch-2B expressing T cells on day 1 after transduction under a fluorescence microscope. The transduction efficiency usually ranged between 30 and 70 % and was assessed by flow cytometry on the day of injection, i.e. one or two days after transduction. Figure 4.2B, C). To validate that the fluorescent cells are positive for CD4, the cells were subjected to flow cytometric analysis before injection.

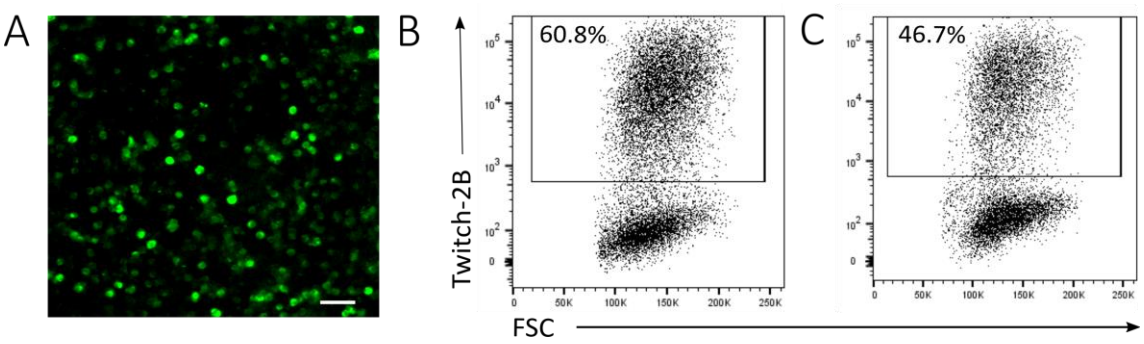

Figure 4.2: Transduction of T cells with Twitch-2B. (A) Fluorescence image of transduced T cells. Representative FACS plots for (B) MOG-specific and (C) polyclonal T cells analyzed for their Twitch-2B expression by FACS. Scale bar 50 µm.

Figure 4.3 depicts a representative FACS analysis indicating that 92.5 % of Twitch-2B$^+$ cells in the culture are CD4$^+$ T cells, whereas CD8$^+$ T cells (2.2 %) and CD19$^+$ B cells (4.9 %) account for minor populations. Furthermore, the culture contains hardly any FoxP3$^+$ regulatory T cells (1.3 %).

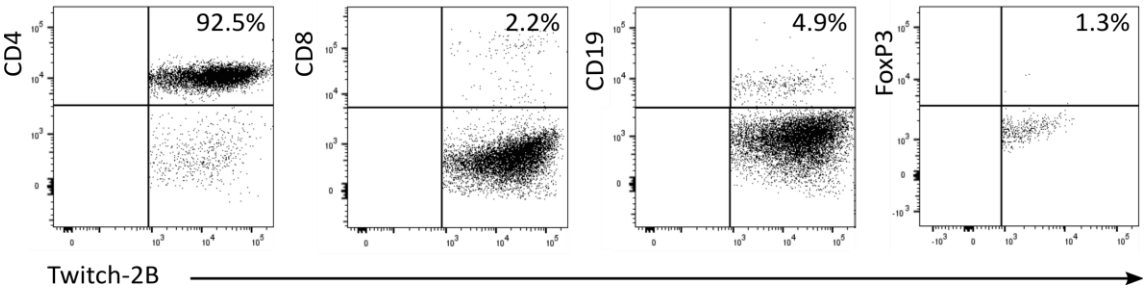

Figure 4.3: Characterization of cultured lymphocytes. Representative FACS plots showing staining with different lymphocyte subset markers. Cells were pre-gated on Twitch-2B$^+$ living lymphocytes.

4.1.2 Threshold determination based on calcium ratios in polyclonal T cells

In order to detect calcium signaling in the intestine, the Twitch-2B labelled T cells were i.p. injected into C57BL/6J wt recipient mice. From two days post transfer (p.t.) on, the Twitch-2B-transduced T cells could be detected in the LP of the ileum. The threshold to identify intracellular calcium concentrations as calcium signaling has been previously defined by our lab as being above the maximal level reached spontaneously by 95 % of Twitch-positive cells in the absence of antigen (Kyratsous et al., 2017). In the present study, we regarded polyclonal T cells as corresponding condition and found 95 % of calcium ratios to be below a value of 0.63. Values exceeding this threshold were considered as calcium signaling (Figure 4.4A). As seen in other organs in previous

studies, calcium signaling is associated with lowered motility (Mues et al., 2013; Kyratsous et al., 2017).

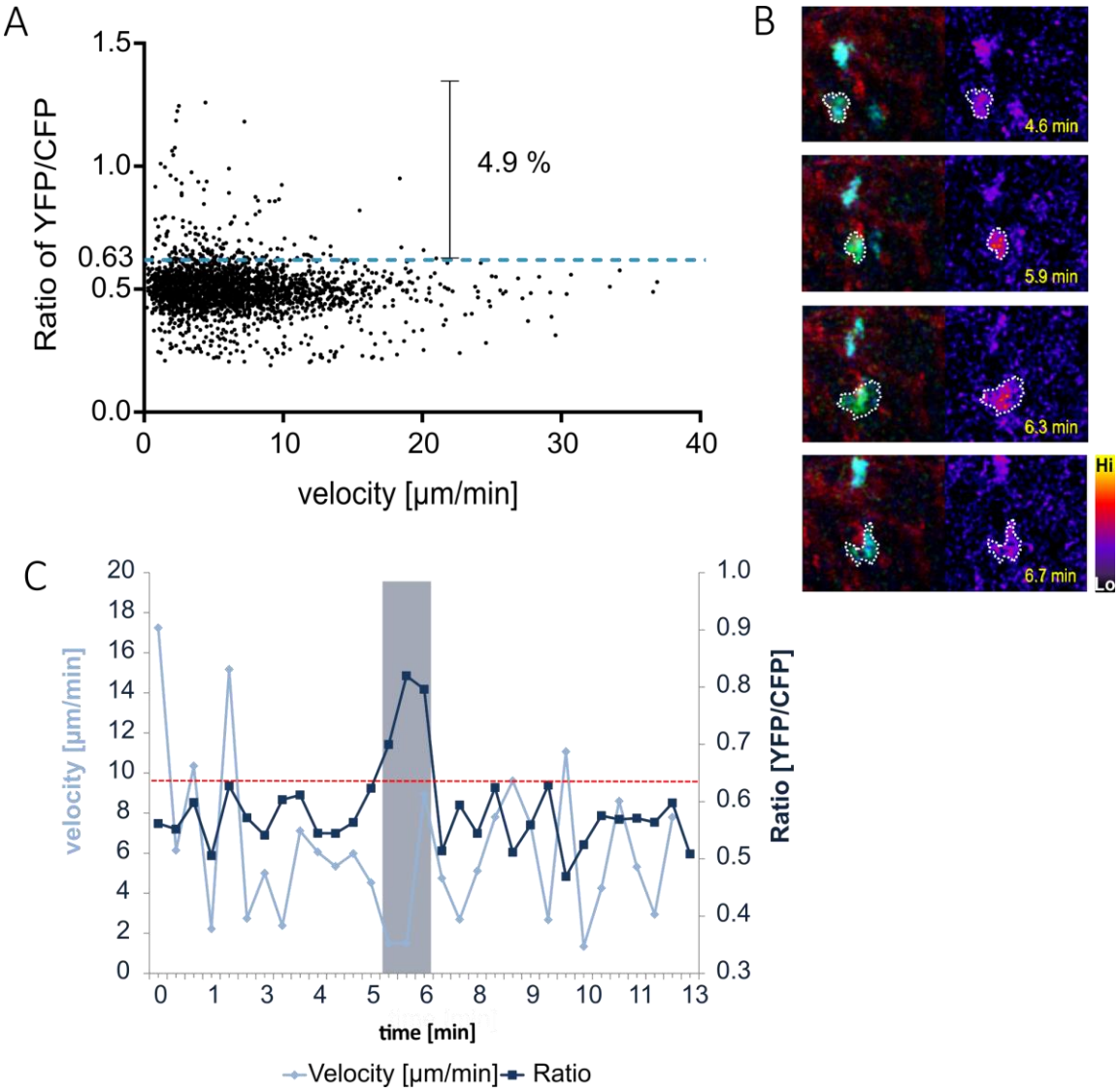

Figure 4.4: Analysis of calcium ratios and velocities of polyclonal T cells in the ileal LP of a wt mouse. (A) Scatterplots showing polyclonal Twitch-2B$^+$ T cells' velocity versus calcium-indicator ratio change. The dotted line indicates the ratio threshold of YFP/CFP=0.63. Each dot represents a single time point in a particular cell. Cumulative results encompass 2943 FRET values of 96 cells from three independent experiments. (B) A fluorescence overlay of Twitch-2B$^+$ T cells (left) and a pseudocolor calcium ratio image (right) are shown. Blood vessels were rendered visible by i.v. injection of 10 µg Texas red-conjugated dextran (70 kDa). Images were acquired by two-photon microscopy. (C) A representative track of a polyclonal T cell (depicted in (B) indicated with white dotted line) shows velocity [µm/min] and ratio [YFP/CFP] in each time frame. The red dotted line indicates the ratio threshold and the gray background indicates the time points where the T cell showed calcium signaling.

This became more evident when looking at single cell tracks as shown in Figure 4.4C. In this representative T cell track (visualized in Figure 4.4B), there was a short calcium spike whereby the T cell simultaneously reduced its speed.

4.1.3 Intravital imaging of MOG-specific T cells in the ileal LP

Preliminary data from our lab indicated that encephalitogenic T cells get increased stimulation in the GALT. To prove and intensify these findings, Twitch-2B transduced MOG-specific T cells in the ileal LP of C57BL/6J mice were imaged in this study.

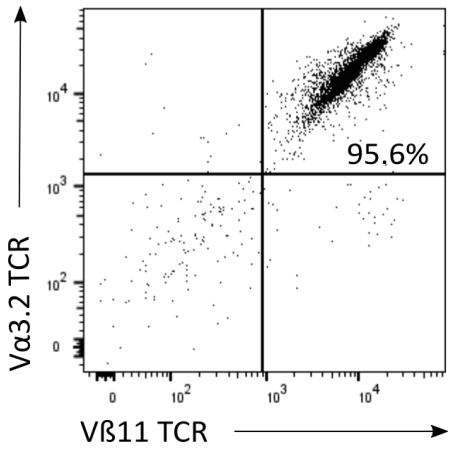

Figure 4.5: Representative FACS analysis of isolated CD4$^+$ T cells from a 2D2 donor mouse. After three days of culture, cells were stained with antibodies specific for α- and β- chains of the MOG-specific TCR in 2D2 mice.

Therefore, T cells from a 2D2 mouse with a MOG-specific TCR transgene were isolated and stained for the alpha and beta chains of the MOG-specific TCR, i.e. the TCR Vα3.2 and Vβ11 chains to see how many T cells were MOG-specific and to confirm the transgenic background of the donor mouse. FACS analysis showed that more than 95 % of the lymphocytes in the culture were CD4$^+$ T cells specific for MOG (Figure 4.5). After transduction with Twitch-2B and transfer into a C57BL/6J wt recipient mouse, the T cells were imaged in the ileal LP on days 3-6 p.t. In line with preliminary findings, MOG-specific T (T_{MOG}) cells exhibited more pronounced calcium signaling as compared to polyclonal T cells: in T_{MOG} cells, 18.5 % of all calcium ratios exceeded the threshold of YFP/CFP=0.63 (Figure 4.6A). Figure 4.6B depicts snapshots of a representative MOG-specific T cell in the ileal LP showing calcium signaling. Figure 4.6C shows the respective calcium ratios and velocities of this T cell track in every time frame. The cell exhibited long-term calcium signaling that lasted for more than 4 minutes.

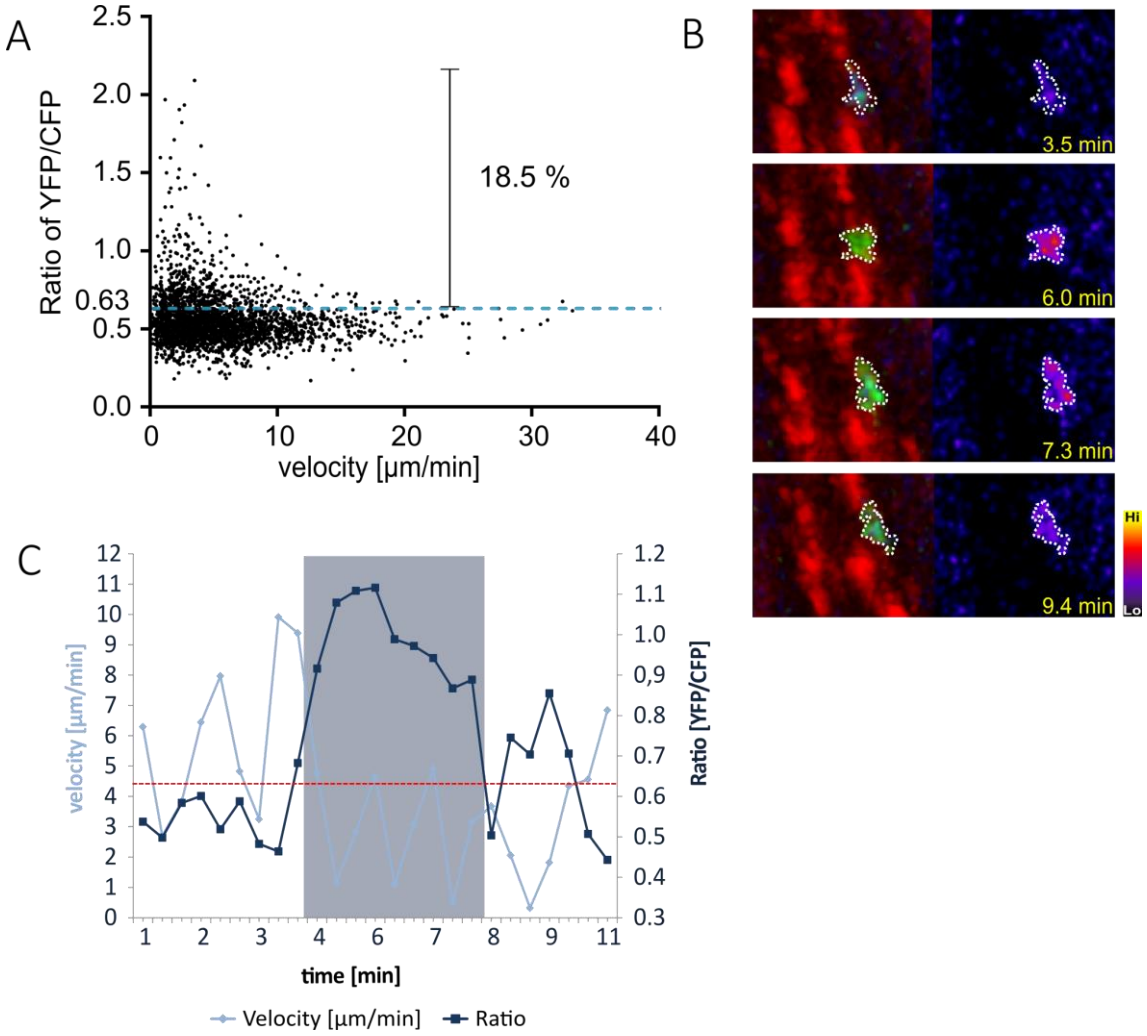

Figure 4.6: Analysis of calcium ratios and velocities of MOG-specific T cells in the ileal LP of a wt C57BL/6J mouse. (A) Scatterplots showing MOG-specific Twitch-2B$^+$ T cells' velocity vs. calcium-indicator ratio change. The dotted line indicates the ratio threshold of YFP/CFP=0.63. Each dot represents a single time point in a particular cell. Cumulative results show 3184 FRET values of 93 cells from five independent experiments. (B) A fluorescence overlay of Twitch-2B$^+$ T cells (left) and a pseudocolor calcium ratio image (right) are shown. Blood vessels were rendered visible by i.v. injection of 10 µg Texas red-conjugated dextran (70 kDa). Images were acquired by two-photon microscopy. (C) A representative track of a MOG-specific T cell (depicted in (B)) shows velocity [µm/min] and ratio [YFP/CFP] in each time frame. The dotted line indicates the ratio threshold and the gray background indicates the time points where the T cell showed calcium signaling.

Generally, when calcium signaling lasts longer than two minutes, it is being referred to as long-term signaling. The duration of high calcium signals in T_{MOG} vs. polyclonal T cells were more frequent and longer in the MOG-specific T cells, as 138 high-calcium signals were identified in the transgenic T cells of which 23 exceeded the threshold of 2 min lasting up to 20 min. In contrast, in polyclonal T cells, only 6 out of 73 high calcium

signals lasted longer than two minutes with a maximum duration of 5 minutes (Figure 4.7A).

In the MOG TCR transgenic cells, 46 % of all T cells showed short-lasting calcium signaling and 20.4 % exhibited calcium signals lasting longer than two minutes. In contrast, in polyclonal cells both the proportion of short lasting calcium spikes and long-lasting calcium signal were much less: 33.3 % of polyclonal T cells showed at least one calcium ratio above threshold, and only 5 % of cells spiked longer than two minutes. In absolute numbers, out of 96 polyclonal T cells measured, five showed long-term calcium signaling. No calcium value above threshold was detected in 46.2 % of MOG-specific T cells and in 64.6 % of polyclonal cells (Figure 4.7B).

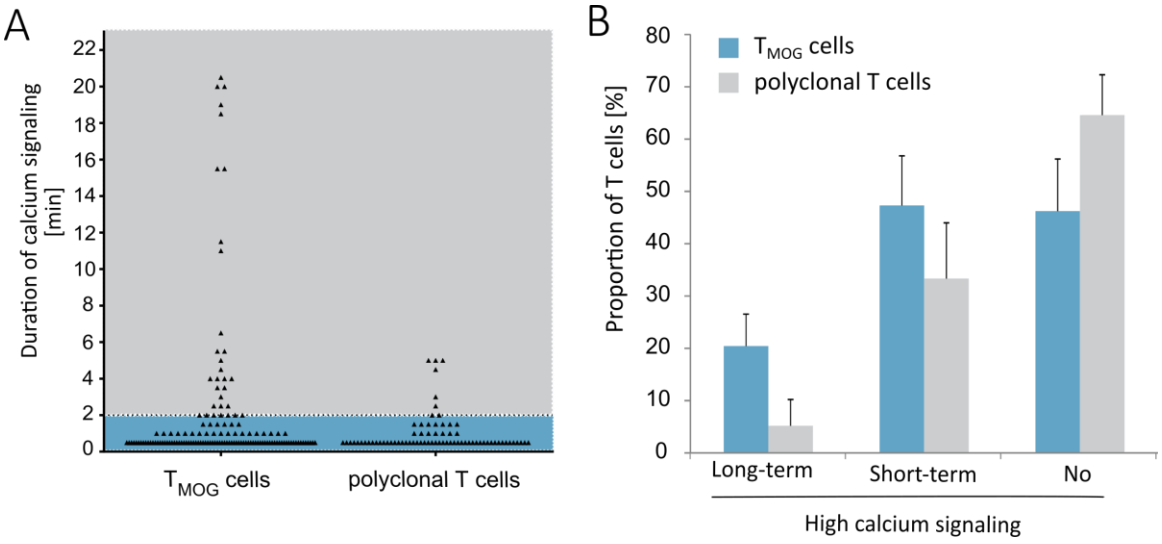

Figure 4.7: Duration of calcium signaling in MOG-specific and polyclonal T cells. (A) Calcium spikes and their duration in minutes. Cumulative results of 93 cells from five independent experiments (T_{MOG} cells) or of 96 cells from three independent experiments (polyclonal) are shown. (B) Proportions of MOG-specific vs. polyclonal T cells that present short- and long-term or no calcium signaling. Data is shown as mean + SEM from five (T_{MOG} cells) or three (polyclonal) independent experiments.

4.1.4 Intravital imaging of OVA-specific T cells in the ileal LP

To understand whether the increased stimulation was a unique feature of T_{MOG} cells or also occurred in other antigen-specific T cells, the intravital imaging setup was applied to investigate the calcium levels of T cells specific for OVA, a chicken egg white protein.

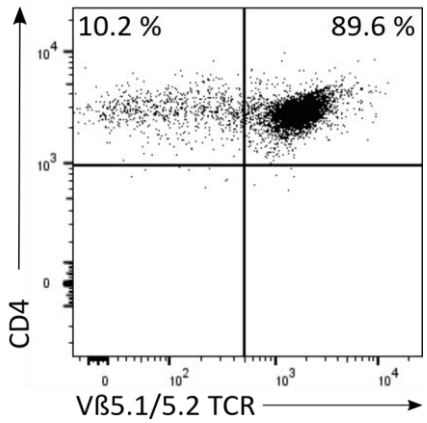

Figure 4.8: Representative FACS staining for expression of OVA-specific TCRs. Cells were pre-gated on living $CD4^+$ T lymphocytes.

OVA-specific T cells were isolated from OTII-mice, which express the α/β TCR (Vα2/Vβ5) recognizing ovalbumin 323-339 peptide in the context of $I\text{-}A^b$ on a C57BL/6J background (Barnden et al., 1998). To identify OVA-specific (T_{OVA}) T cells, they were routinely stained with an antibody anti-mouse TCR Vβ5.1/5.2. Figure 4.8 shows that 89.6 % of lymphocytes expressed the transgenic TCR specific for the OVA peptide. After transduction with Twitch-2B and transfer to a wt recipient, T_{OVA} cells were imaged under the same conditions as polyclonal and MOG-specific T cells in the ileal LP. The imaging data indicated that ileal stimulation was not unique to encephalitogenic T cells but also occurred in other transgenic T cells, as 12.1 % of calcium levels exceeded the threshold in the OVA-specific T cells (Figure 4.9A). The proportion of high-calcium concentrations was not as pronounced as in the single time points of MOG-specific T cells (18.5 %, Figure 4.6A) but significantly increased as compared to polyclonal T cells (4.9 %, Figure 4.4A).

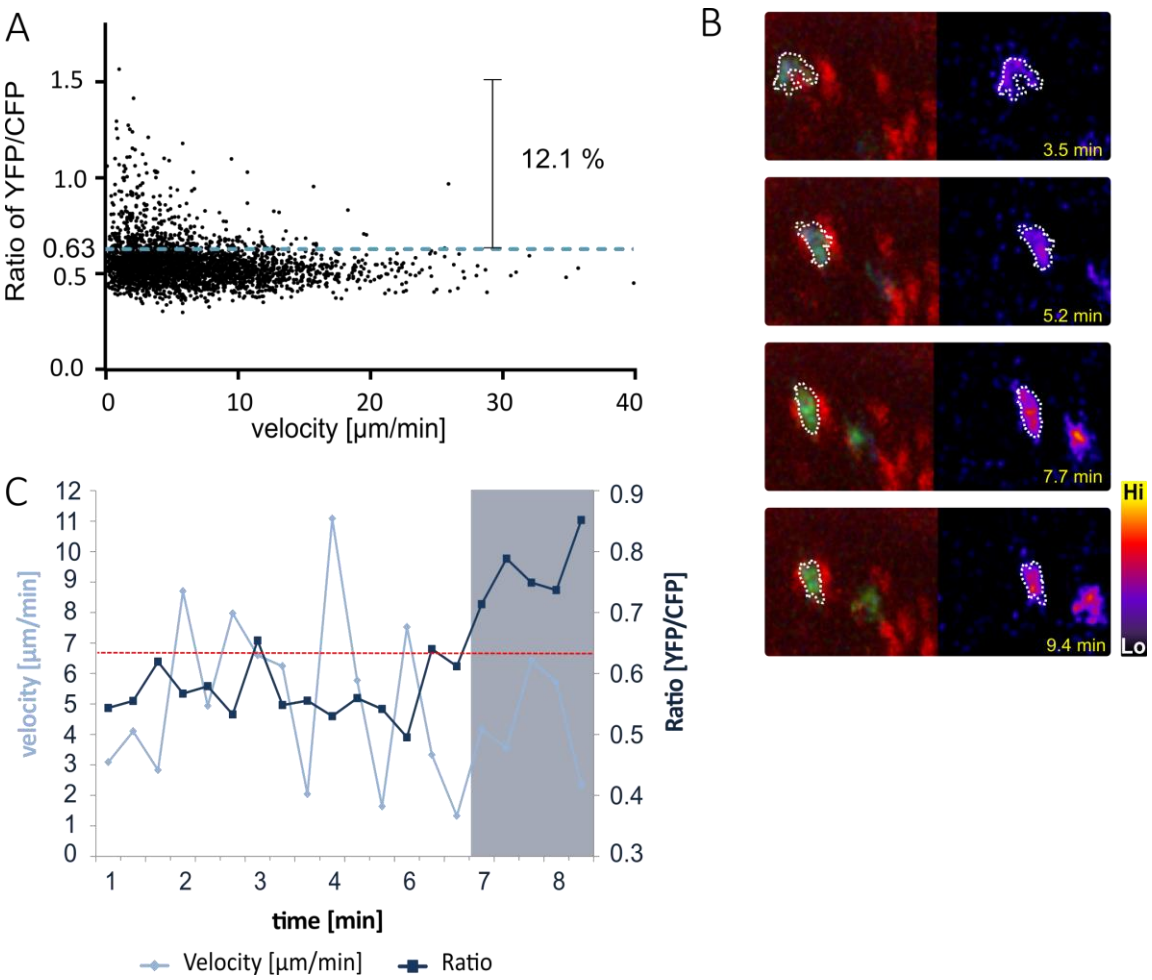

Figure 4.9: Analysis of calcium ratios and velocities of OVA-specific T cells in the ileal LP of a C57BL/6J mouse. (A) Scatterplots showing OVA-specific Twitch-2B$^+$ T cells' velocity versus calcium-indicator ratio change. The dotted line indicates the ratio threshold of 0.63. Each dot represents a single time point in a particular cell. Cumulative results show 4229 calcium levels of 104 T_{OVA} cells from four independent experiments. (B) A fluorescence overlay of Twitch-2B$^+$ T cells (left) and a pseudocolor calcium ratio image (right) are shown. Blood vessels were rendered visible by i.v. injection of 10 µg Texas red-conjugated dextran (70 kDa). Images were acquired by two-photon microscopy. (C) A representative track of an OVA-specific T cell (depicted in (B), indicated by white dotted line) shows velocity [µm/min] and ratio [YFP/CFP] in each time frame. The red dotted line indicates the ratio threshold of 0.63 and the gray background indicates the time points where the T cell showed calcium signaling.

4.1.5 Intravital imaging of LCMV-specific T cells in the ileal LP

In the attempt of deciphering whether the stimulation was antigen-specific or induced by the increased affinity of the engineered TCRs, T cells from another TCR transgenic mouse were tested: the SMARTA-1 TCR transgenic mouse line harbors $CD4^+$ T cells specific for the H2-I-A^b-restricted lymphocytic choriomeningitis virus (LCMV) glycoprotein residues 61-80 (Oxenius et al., 1998).

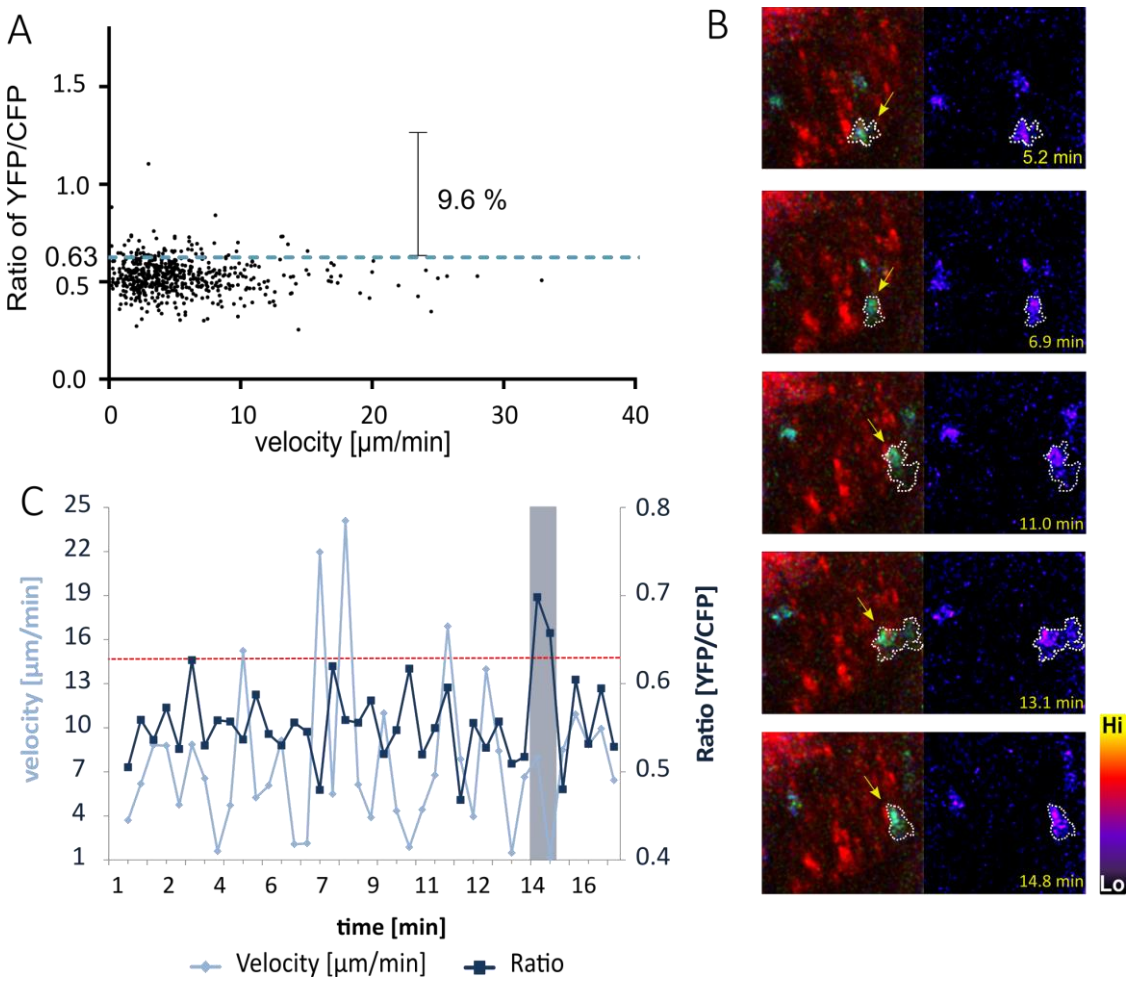

Figure 4.10: LCMV-specific T cells in the ileal LP of a wt mouse. (A) Scatterplots showing LCMV-specific Twitch-$2B^+$ T cells' velocity versus calcium-indicator ratio change. The dotted line indicates the ratio threshold. Each dot represents a single time point in a particular cell. Cumulative results depict 616 calcium ratios of 20 T_{LCMV} cells from two independent experiments. (B) A fluorescence overlay of Twitch-$2B^+$ T cells (left) and a pseudocolor calcium ratio image (right) are shown. Blood vessels were rendered visible by i.v. injection of 10 µg Texas red-conjugated dextran (70 kDa). Images were acquired by two-photon microscopy. (C) A representative track of a LCMV-specific T cell (depicted in (B)) shows velocity [µm/min] and ratio [YFP/CFP] in each time frame. The dotted line indicates the ratio threshold of 0.63 and the gray background indicates the time points where the T cell showed calcium signaling.

Corresponding to the previous sets of experiments, the LCMV-specific T cells were isolated from the SMARTA-1 mice, cultured and transduced with Twitch-2B before being injected into wt recipient mice. On days 3 or 4 p.t., the labelled LCMV-specific T cells were imaged in the ileal LP and their calcium levels were analyzed. The data revealed that also T cells specific for LCMV exhibit elevated calcium levels as compared to polyclonal T cells (9.6 vs. 4.9 % above threshold)(Figure 4.10 A and 4.4A), but were a bit lower than in the OVA-specific T cells (12.1 %) (Figure 4.9). The calcium signals were pooled from two independent experiments with 616 calcium ratios/velocities from 20 different cells. As also seen in the previous sets of experiments, the calcium level was negatively correlated to the motility of the cells (Figure 4.10C).

4.1.6 Differential calcium signaling behavior in TCR-transgenic T cells

To get a better insight into the spiking behavior of antigen-specific T cells, durations of calcium spikes and proportions of spiking cells were compared among the three antigen-specific groups (T_{MOG}, T_{OVA} and T_{LCMV} cells) and polyclonal T cells. In line with the overall percentage of calcium ratios above threshold (18.5 % (MOG) vs. 12.1 % (OVA) vs. 9.6 % (LCMV) vs. 4.9 % (polyclonal)), also the maximum duration of calcium signaling was the highest in the MOG-specific T cells (20.5 minutes), second-highest in the OVA condition (11 minutes) and the lowest in the T_{LCMV} cells (10 minutes) (Figure 4.11A). In addition, more MOG- and OVA-specific T cells presented long-term calcium signaling (20 % in MOG and 15 % in OVA) as compared to LCMV-specific T cells, in which the proportion of long-term spikes equaled the proportion in polyclonal T cells (5 % in both). Short-term signals were frequent in all three antigen-specificities with being the least abundant in T_{MOG} cells as of 47 % of T_{MOG} cells exhibiting them, whereby 60 % and 67 % of T_{LCMV} and T_{OVA} cells, respectively, displayed short-term spikes (Figure 4.11B).

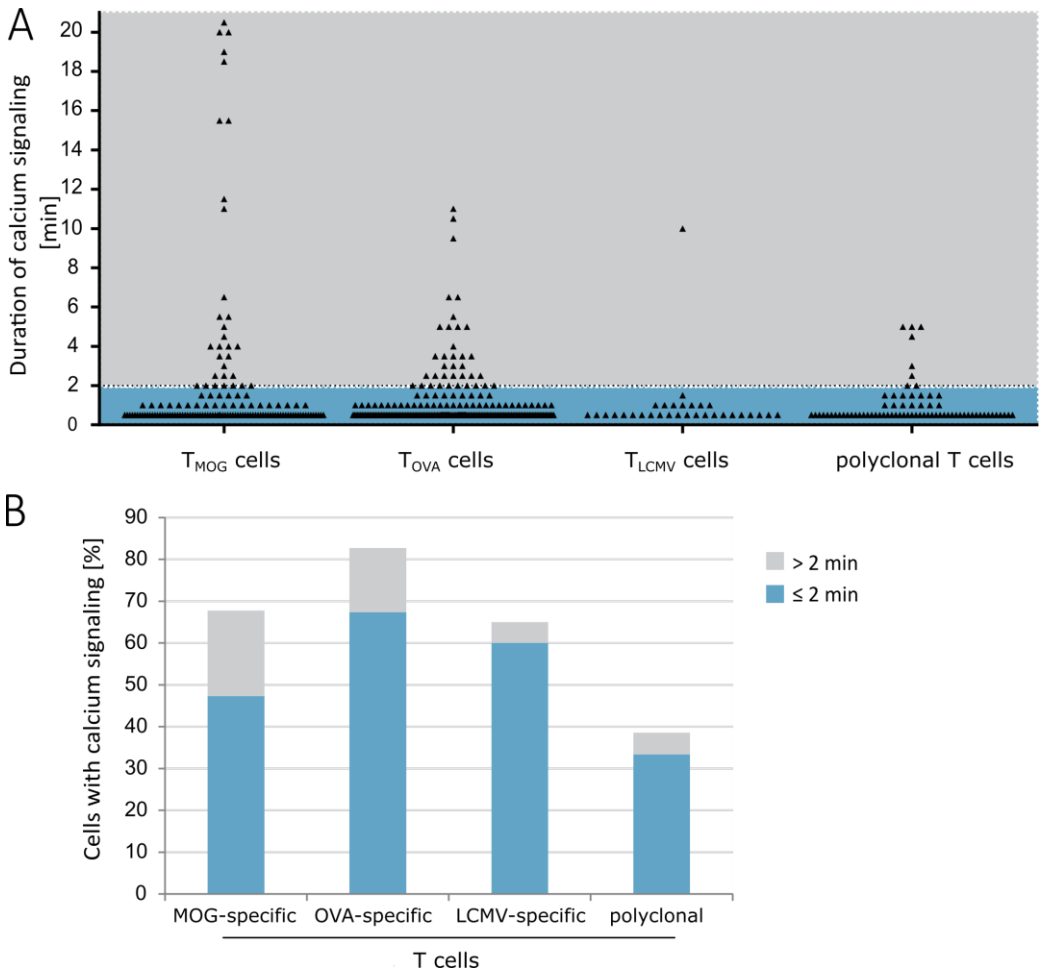

Figure 4.11: Duration and proportions of calcium signaling in MOG/OVA/LCMV-specific and polyclonal T cells. (A) Calcium spikes and their duration in minutes. Cumulative results show data from 93 (T_{MOG}), 104 (T_{OVA}), 20 (T_{LCMV}) and 96 (polyclonal T cells) from two to five independent experiments, respectively. (B) Proportions of MOG-specific vs. OVA-specific vs. LCMV-specific vs. polyclonal T cells that present short- and long-term calcium signaling. The graphs encompass cumulative data from two to five independent experiments. The data from MOG-specific and polyclonal T cells has been shown in Figure 4.7 already but is represented here again for a better comparison.

4.1.7 Impact of MOG-specific B cells in T_{MOG} cell stimulation in the ileal LP

In order to decipher whether B cells played a role in the stimulation of T cells in the gut, Twitch-2B transduced MOG-specific T cells were transferred to TH mice that harbor MOG-specific B cells and compared to the previously shown behavior of MOG-specific T cells in the ileal LP of wt mice. The relative abundance of calcium levels above threshold was similar in both conditions and differed by 1 % (18.5 % in the wt and 17.4 % in the TH recipients) (Figure 4.12). The proportion of cells that showed long-term calcium signaling was equal with or without MOG-specific B cells (20 % in both conditions), whereas short-term spikes occurred to a bigger extent in TH mice (76 %) as compared to wt recipients (47 %) (Figure 4.12B). The fact that the total

percentage of calcium ratios above threshold was still higher in the wt recipient condition could be explained by looking at the absolute durations of calcium signaling. The spikes in T_{MOG} cells that had been transferred to C57BL/6J mice lasted longer with a maximum of 20.5 minutes compared to a maximum of 7 minutes in the TH recipients (Figure 4.12C).

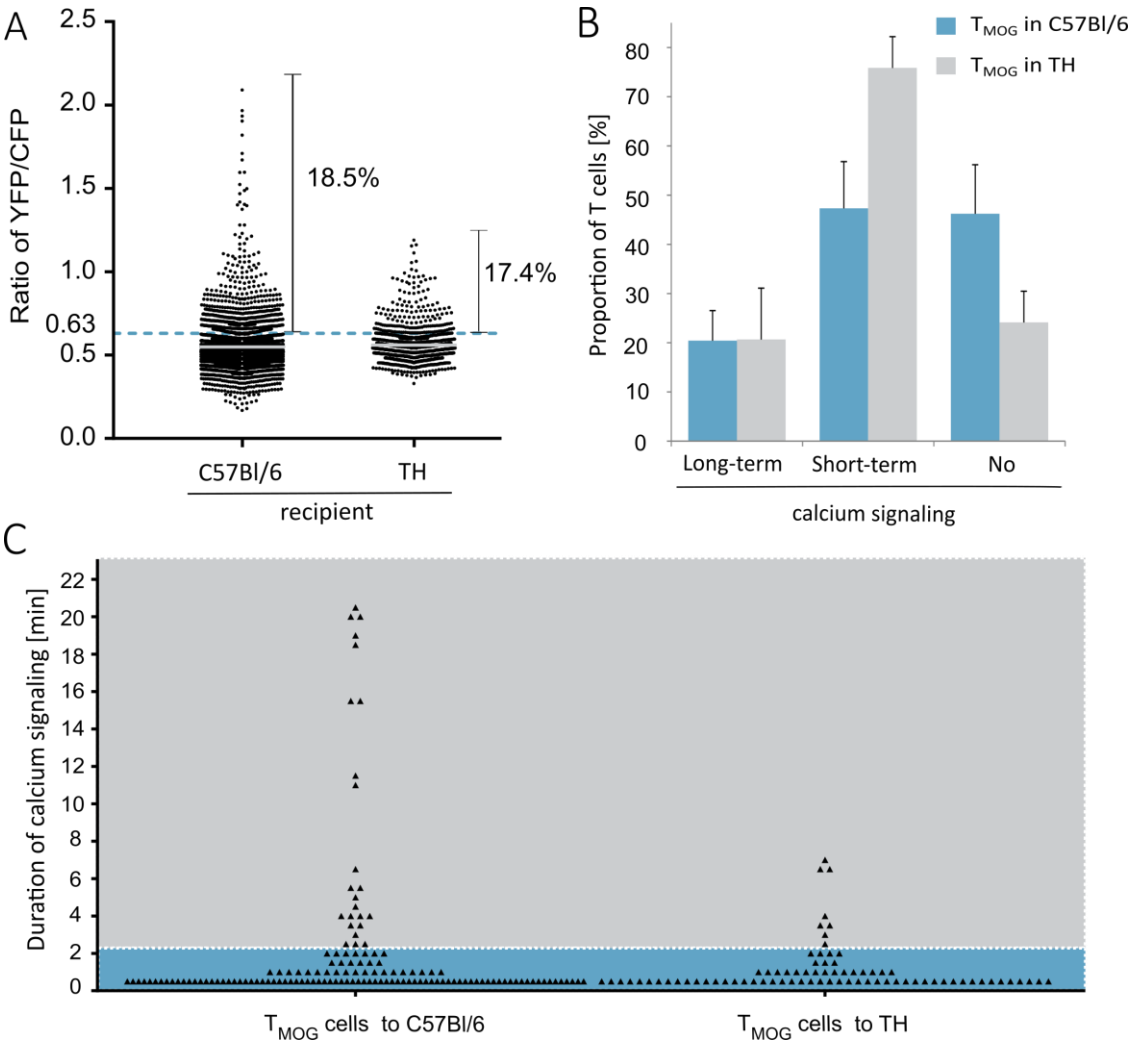

Figure 4.12: MOG-specific T cells in presence or absence of MOG-specific B cells. (A) Dot plots showing calcium-indicator ratios of MOG-specific Twitch-2B$^+$ T cells in the ileal LP of either C57BL/6J or TH mice. The dotted line indicates the ratio threshold of YFP/CFP=0.63. Each dot represents a single time point in a particular cell. Cumulative results show 3184 calcium ratios of 93 cells from five independent experiments (wt recipient) vs. 1026 calcium ratios of 29 cells from three independent experiments (TH recipient). (B) Proportions of MOG-specific T cells in either C57BL/6J or TH mice that present short- and long-term or no calcium signaling. (C) Calcium spikes and their durations in minutes. Cumulative results from five (C57BL/6J) or three (TH) independent experiments are shown. The data from C57BL/6J recipients has been shown in Figure 4.7 already but is represented here again for a better comparison.

4.1.8 T cell signaling in the ileal LP following oral administration of antigen

In the attempt of investigating whether oral application of exogenous antigen can activate OVA-specific T cells in the ileal LP, recipient mice were gavaged with 4 mg OVA protein prior to imaging of T_{OVA} cells on day three p.t. in the small intestine.

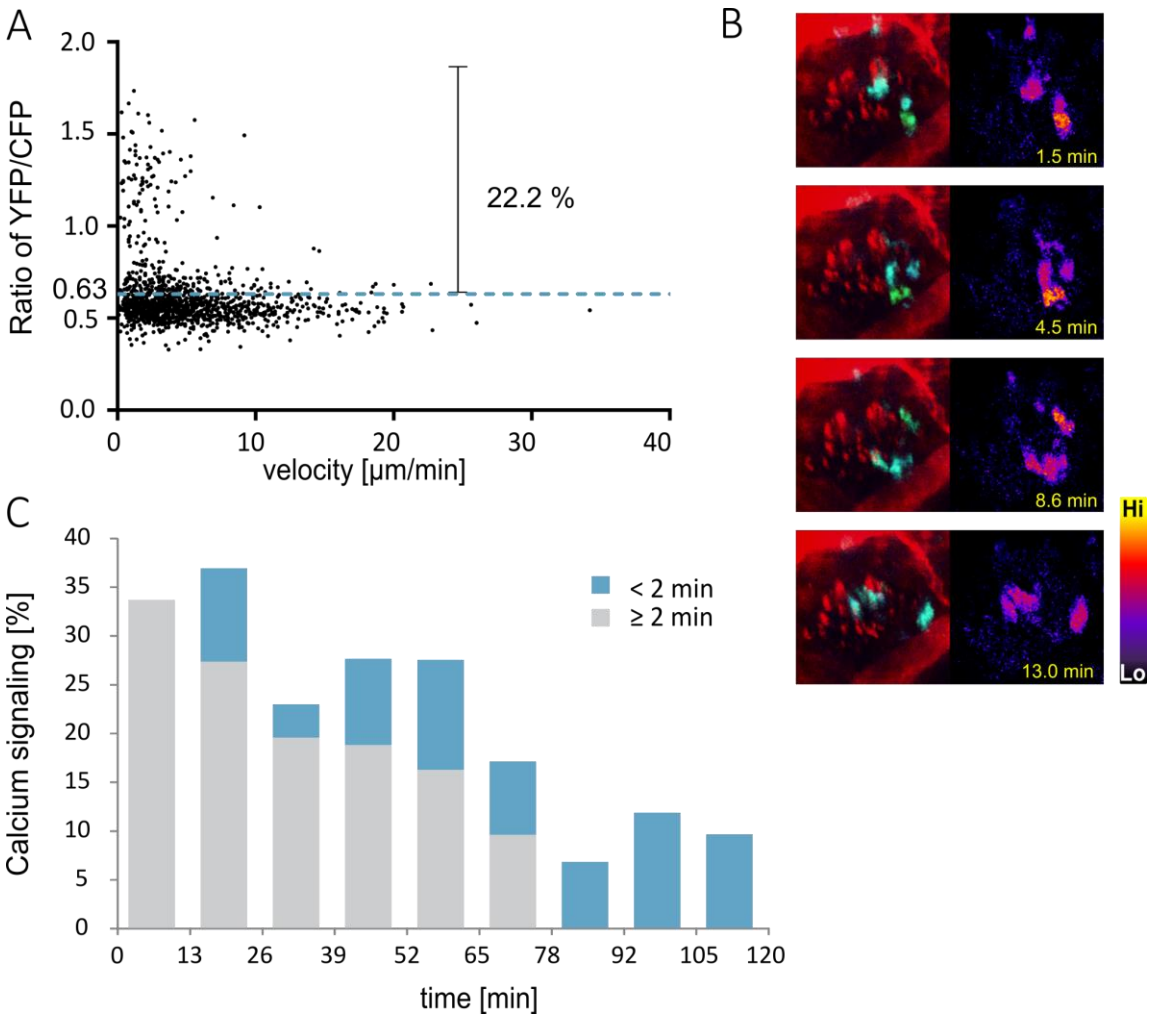

Figure 4.13: Imaging of T_{OVA} cells in the ileal LP after oral gavage with OVA protein. (A) Scatterplot showing OVA-specific Twitch-2B-T cells' velocity versus calcium-indicator ratio change. The dotted line indicates the ratio threshold of 0.63. Each dot represents a single time point in a particular cell. Cumulative results show 1448 calcium ratios from 36 T_{OVA} cells. (B) A fluorescence overlay of Twitch-2B T cells (left) and a pseudocolor calcium ratio image (right) are shown. Red fluorescence originates from intragastral application of 400 µg Texas red-conjugated dextran (70 kDa). Images were acquired by two-photon microscopy. (C) Percentage of calcium signals above threshold over time. Each bar represents cumulative data from one movie.

To visualize the successful administration of antigen, the OVA protein was pooled with 400 µg of Texas-red conjugated dextran (70 kDa) that could be detected as red fluorescence in the imaging setup. 40 min after oral gavage, the mouse was anesthetized and the ileal LP was exposed for imaging. 1448 calcium levels from

36 cells have been recorded with 321 ratios above threshold (22.2 %) (Figure 4.13A). To compare, this value was 10 % higher than in OVA-specific T cells imaged in recipients that have not been gavaged with OVA protein before (compare Figure 4.9). The high red fluorescence originates from the conjugated dextran that had been applied orally, indicating that the antigen/dye mixture was successfully delivered to the ileal LP (Figure 4.13B). The stimulating effect of the orally administered antigen became even more evident when the calcium signals were separated by time (Figure 4.13C). As the oral gavage had been conducted 40 minutes prior to surgery which took around 1 h, the first time point corresponds to approximately 100 min after antigen gavage. The movies consisted of 30 to 35 time frames each lasting 25 sec, i.e. the total time per movie was around 13 minutes. Three to eight cells were recorded simultaneously resulting in 90 to 231 calcium ratios (mean: 160 ± 50) per video. Impressively, in the beginning, the proportion of calcium ratios above threshold was very high (up to 36 %) whereby up to 100 % of signals constituted long-term signaling. This effect lasted for approximately one hour before the proportions of calcium signaling decreased down to the level of OVA-specific T cells without antigen gavage. Starting from 78 min, long-term spikes were not observed anymore.

4.2 T cell priming in mesenteric and inguinal lymph nodes in active EAE

In order to gain a better insight into T cell priming in the periphery, different lymph nodes were imaged in MOG-immunized mice in the early phase of EAE. As the MOG/CFA emulsion was s.c. injected into the lower back, the iLN constituted the draining lymph nodes and hence, the priming site for antigen-specific T cells in active EAE.

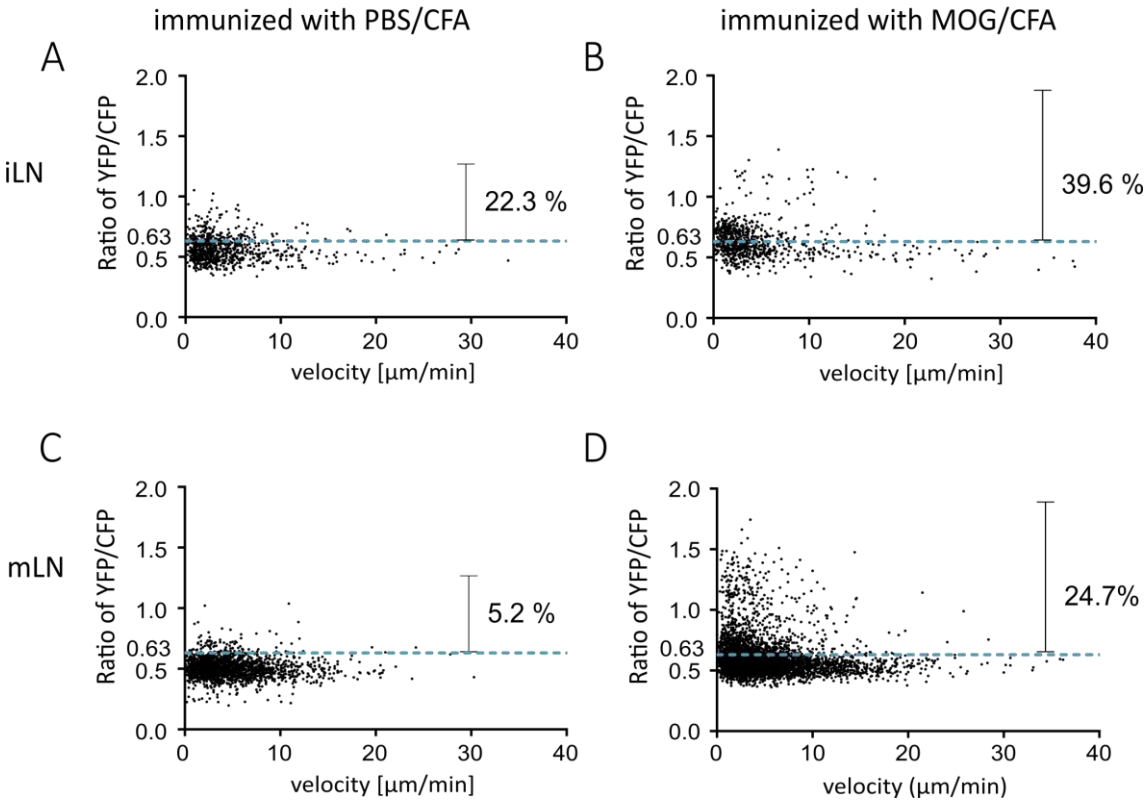

Figure 4.14: Calcium levels of MOG-specific T cells in the lymph nodes of immunized mice. Scatterplots depicting calcium ratios of Twitch-2B-tranduced MOG-specific T cells in the inguinal (A, B) or mesenteric LNs (C,D) of mice that have been immunized with MOG/CFA (B,D) or PBS/CFA (A,C), respectively. Each dot represents a single time point in a particular cell. Cumulative results depict 883 calcium ratios from 25 cells (A), 853 calcium ratios from 25 cells (B), 2352 calcium ratios from 67 cells (C) or 5971 calcium ratios from 167 cells (D) from two (A,C) or three (B,D) independent experiments are shown. The dashed line indicates the threshold ratio of YFP/CFP=0.63.

As described before, we used the calcium sensor Twitch-2B to visualize the priming of antigen-specific $CD4^+$ T cells on day 13 or 14 post immunization (p.i.) in the iLN of immunized mice. To investigate whether antigen also spreads to non-draining lymph nodes and primes T cells there, calcium levels of MOG-specific T cells were not only assessed in the iLNs but also in the mesenteric lymph nodes (mLNs) in the early phase

clinical of EAE. To control for the effect of CFA, a group of mice was immunized with PBS/CFA.

20-30 x 10^6 Twitch-2B-transduced MOG-specific T cells were transferred to immunized mice on day 10 p.i. and were imaged three to five days later. The results showed pronounced calcium signaling in the T cells when imaged in the iLN of mice immunized with MOG/CFA: 39.6 % of all calcium levels exceeded the threshold ratio of YFP/CFP of 0.63. In the control group immunized with PBS/CFA, i.e. without cognate antigen, 22.3 % of calcium levels were above threshold (Figure 4.14A,B).

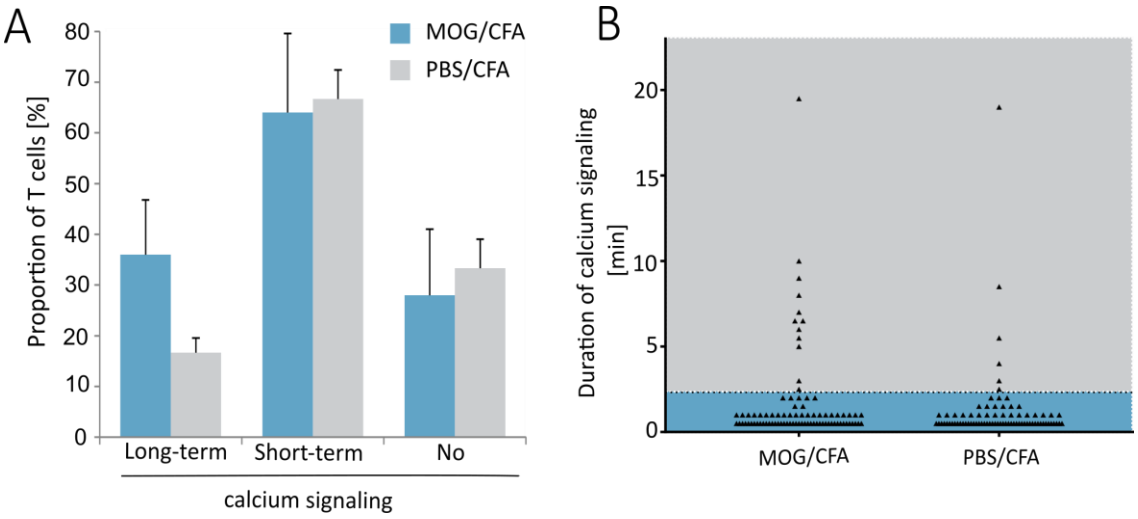

Figure 4.15: Frequency and duration of calcium signaling in the iLNs. (A) Proportions of MOG-specific T cells that present short- and long-term high-calcium signaling or no calcium spikes in the iLNs of mice immunized with either MOG/CFA or PBS/CFA. Data shown as mean+SEM. (B) Calcium spikes and their duration in minutes. Cumulative results of 25 cells each from three (MOG/CFA) or two (PBS/CFA) independent experiments are shown.

To get a deeper insight in the characteristics of the antigen-induced calcium signals, their amount and duration were analyzed. Figure 4.15 shows frequencies and durations of calcium signaling of the Twitch-2B transduced T cells in the iLNs. In total, 25 cells were analyzed in each condition. When comparing MOG-immunized and control (immunized with PBS) animals, the amounts of cells that exhibited short-term signaling (< 2 min) as well as cells without calcium signaling were very similar in the two conditions. 64 % in the MOG-immunized condition versus 67 % of cells in the control animal show display short-term calcium signaling and 28 % versus 33 % of cells do not spike at all, respectively. A major difference is observed in the numbers of cells with long-term spikes: in the mice that were immunized with antigen, 32 % of cells show calcium signaling lasting longer than two minutes in contrast to 17 % of cells in

control mice (Figure 4.15A). As in this set of experiments equal amounts of cells were imaged, absolute numbers can be taken into account. Figure 4.15B shows that the calcium spikes do not differ much between the two groups: both show very similar amounts of short-term spikes (72 (MOG/CFA) vs. 73 (PBS/CFA)) and a pronounced maximum duration of long-term signals (23.5 min (MOG/CFA) vs. 19 min (PBS/CFA)). However, in the control group, the amount of long-term spikes was reduced to less than half as compared to the MOG/CFA condition (13 (MOG/CFA) vs. 6 (PBS/CFA)).

In order to get an idea whether antigen spreads to and hence stimulates antigen-specific T cells in non-draining lymph nodes, the mLNs were imaged under the same conditions: mice were immunized with either MOG/CFA or PBS/CFA and Twitch-2B-transduced MOG-specific T cells were transferred on day 10 p.i. and imaged on days 13 to 15 p.i..

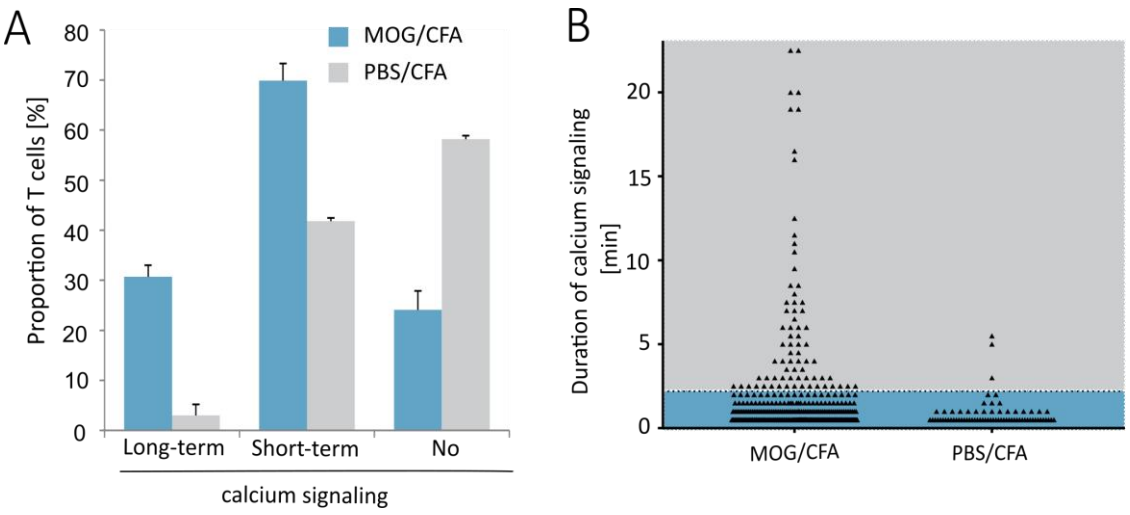

Figure 4.16: Frequency and duration of calcium signaling in the mLN. (A) Proportions of MOG-specific T cells that present short- and long-term calcium signaling or no calcium spikes in the mLNs of mice immunized either with MOG/CFA or PBS/CFA. Data is shown as mean + SEM. (B) Calcium spikes and their duration in minutes. Cumulative results of r of 167 cells from three (MOG/CFA) or 67 cells from two (PBS/CFA) independent experiments are shown.

The results show that also in the mLNs, the calcium signaling of MOG-specific T cells was enhanced in mice that were immunized with MOG (24.7 % above threshold) as compared to mice that received emulsions without antigen (5.2 %) (Figure 4.14C, D). As compared to the imaging in the iLNs, more pronounced differences were obtained from the imaging of Twitch-2B^{+} MOG-specific T cells in the mLNs of immunized vs. sham-immunized mice. Data were collected from 167 cells in the MOG/CFA group and 67 cells in mice immunized with PBS/CFA. In the control group, 58 % of cells do not

show any calcium signaling at all as compared to 24 % of the group immunized with antigen. Both the amount of cells exhibiting short-term and long-term calcium signaling were lower in the PBS-immunized group than in the MOG-immunized mice (short-term 42 % vs. 70 %, long-term 3 % vs. 31 %) (Figure 4.16A). With a maximum time of 22.5 min, the spikes in the antigen-immunized mice lasted more than four times longer than the longest spike in the sham-immunized control (5.5 min, Figure 4.16B). To sum up, in mice immunized with MOG/CFA, the T_{MOG} cells exhibited more short- and long-term calcium spikes and the maximum duration of calcium signaling was extended compared to control mice in both draining and non-draining LNs.

4.3 $CD4^+$ T cells in the efferent mesenteric lymph

4.3.1 Lymphatic cannulation

As the imaging data indicates, antigen-specific T cells showed long-term calcium signaling in the ileal LP in the presence of microbiota. To decipher whether these calcium spikes translate to transcriptional and/or functional changes in the cells, T cells were examined downstream of their stimulation in the small intestine. Therefore, the entirety of cells leaving the gut was collected by cannulating the mesenteric lymphatic fluid.

Table 4.1: Average amounts of fluid and lymphocytes in mesenteric lymph from different mouse lines kept under different hygiene conditions, n=2-7.

Mouse line	Hygiene condition	Average amount of lymphatic fluid (µl)	Average amount of lymphocytes /µl
C57BL/6J	SPF	134	926
C57BL/6J	GF	105	311
2D2	SPF	217	237
OSE	GF	90	146

Cannulation yielded in different volumes depending on the mouse line or hygiene condition, respectively (Table 4.1). Most liquid was isolated from 2D2 mice housed under SPF conditions, followed by SPF C57BL/6J mice. Both wt and OSE mice housed under GF conditions appeared to have a reduced lymph flow from the gut as cannulation of mesenteric lymph yielded in lower volumes. The different mouse lines also diverged in their lymphocyte concentrations whereby here the genetic background seemed to play a role: wt mice had the highest counts of lymphocytes/µl of mesenteric lymph, whereby their transgenic counterparts had lower lymphocytic concentrations in their lymph. The same effect was observed in the transgenic mice at a lower level: the transgenic mice housed under GF conditions harbored less lymphocytes in the lymphatic fluid as transgenic mice housed under SPF conditions. Overall, the number of lymphocytes in the efferent mesenteric lymph of 2D2 mice housed under SPF conditions was reduced to 25 % as compared to SPF wt mice.

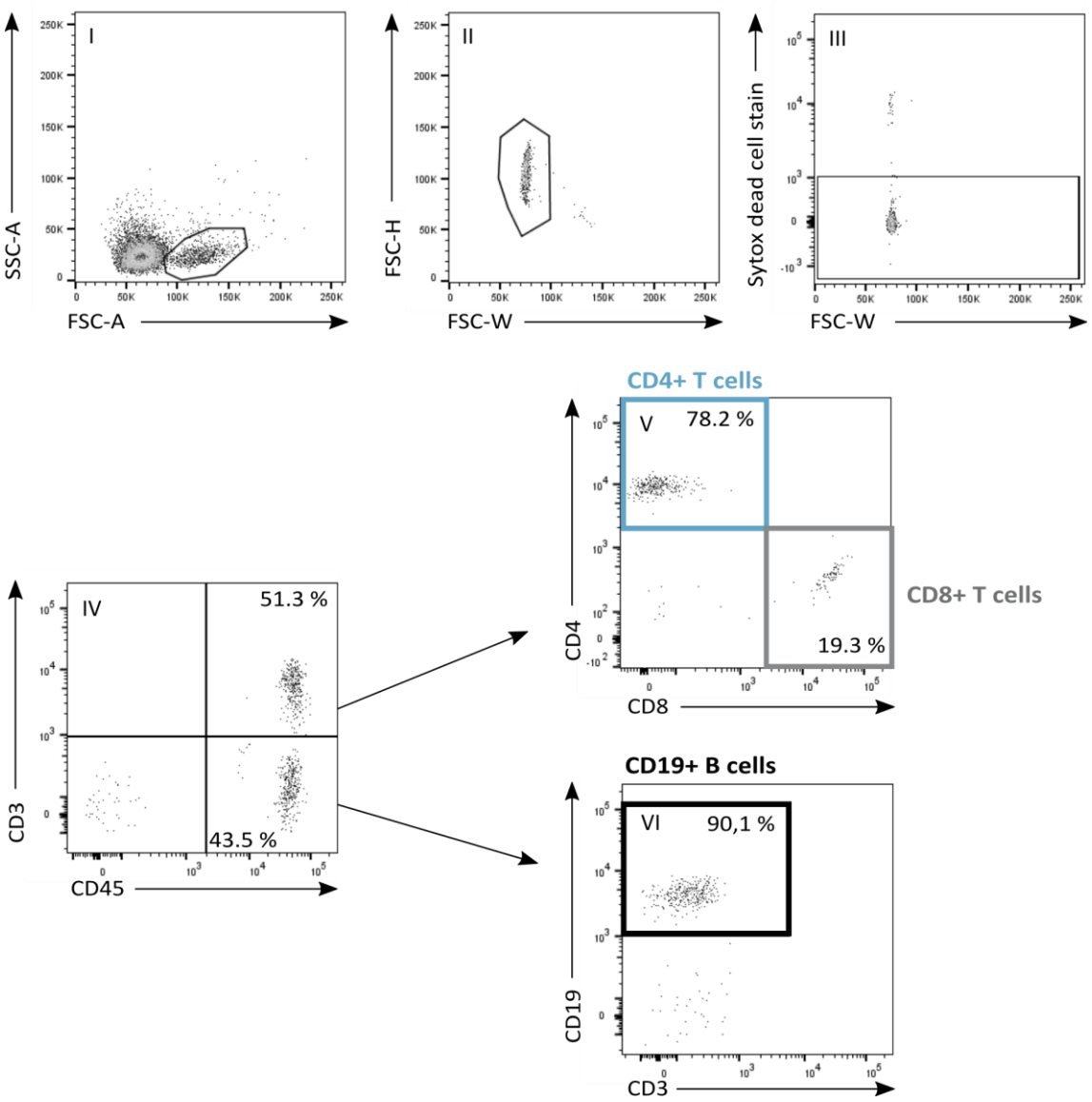

Figure 4.17: FACS gating strategy. Representative FACS plots showing that cells were gated on lymphocytes (plot I). Single cells were identified by plotting FSC area vs. height (plot II); dead cells were eliminated by gating on Sytox blue negative cells (plot III). $CD45^+$ T and B cells were distinguished by CD3 (plot IV) and then gated for CD4/CD8 (plot V) or CD19 (plot VI), respectively. $CD4^+$, $CD8^+$ and $CD19^+$ cells were sorted into pre-cooled cell lysis buffer.

After isolation, the lymphatic fluid was subjected to surface staining, FACS analysis and sorting of $CD4^+$, $CD8^+$ and $CD19^+$ lymphocytes. Figure 4.17 depicts the gating strategy and sort layout that were applied to isolate different lymphocyte subsets: Lymphocytes were gated for single, viable cells and then distinguished into $CD3^+$ and $CD3^-$ cells, whereby $CD3^+$ T cells were further subdivided into $CD4^+$ and $CD8^+$ T cells. Among the $CD3^-$ cells, the $CD19^+$ B cell population was identified and isolated. As controls, lymphocytes from blood and spleen were isolated as well and treated correspondingly.

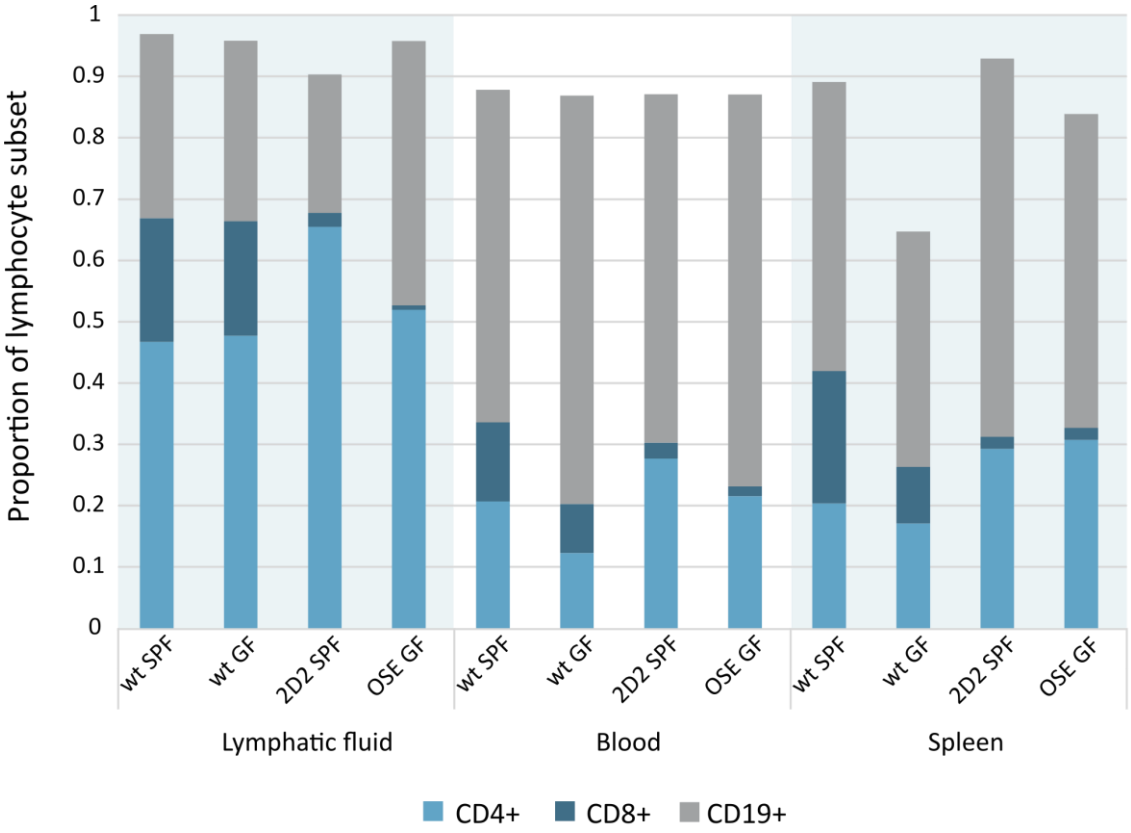

Figure 4.18: Proportions of lymphocyte subsets sorted from different compartments of the body and mouse lines. n=2-7

In the efferent mesenteric lymphatic fluid, $CD4^+$ T cells represented the predominant lymphocyte subset independent of the animals' hygiene condition (47 % (wt SPF), 48 % (wt GF)). In 2D2 mice, the $CD4^+$ population was increased (66 %), likely due to the genetic modification by TCR transgene. In OSE mice, this enriching effect was present in both $CD4^+$ (51 %) and $CD19^+$ (43 %) subsets as they were both genetically modified in this mouse line. In all mouse lines without genetic modification in the B cell compartment, $CD19^+$ cell abundance was lower (30 % (wt SPF), 29 % (wt GF), 23 % (2D2 SPF)) as compared to GF OSE mice (43 %). In both transgenic lines, those subsets were expanded on the expense of $CD8^+$ cells, which were almost entirely gone in the mesenteric lymph (2 % (2D2 SPF), 0.1 % (OSE GF)). In both blood and spleen, $CD19^+$ cells constituted the major population (blood: 54 % (wt SPF), 67 % (wt GF), 57 %(2D2 SPF) 64 % (OSE GF); spleen: 47 % (wt SPF), 38 % (wt GF), 62 % (2D2 SPF), 51 % (OSE GF)). The frequency pattern of $CD4^+$ T cells in blood and spleen was similar to the one in the lymph, i.e. enriched in both 2D2 mice (blood: 28 %, spleen: 29 %) and OSE mice (blood: 22 %, spleen:31 %) as compared to wt mice under SPF (blood: 21 %, spleen:

20 %) and GF conditions (blood: 12 %, spleen: 17 %). Likewise, the $CD8^+$ population is almost gone in both transgenic lines in blood (3 % (2D2 SPF), 2 % (OSE GF) as well as in spleen (2 % (both)) (Figure 4.18).

As this study focused on $CD4^+$ T cells, RNA was isolated from this subset in all samples (lymph, blood, spleen) from all animals. The lymph samples contained on average 4.4×10^4 cells and were processed when containing as little as 3000 cells. In the blood samples, the average number of sorted $CD4^+$ T cells was 3.5×10^4 whereas for the spleen samples, sorting was stopped when 2×10^5 $CD4^+$ cells had been collected. According to assessments using the Agilent Bioanalyzer, the isolated RNA was of very good quality with an average RNA integrity number (RIN) of 9.5 out of 10. The RNA yield was similar among the three origins, on average 1 pg/cell. As the RNA fulfilled the quality requirements, the samples were subjected to transcriptome analysis.

4.3.1 Transcriptome analysis of $CD4^+$ T cells from the mesenteric lymph

NGS and subsequent bioinformatics analysis were performed by BGI (Shenzen, China) using their DNBseq platform. In the first run, RNA samples from polyclonal $CD4^+$ T cells from the mesenteric lymph from C57BL/6J mice either housed under SPF or GF conditions were compared. Four samples were subjected to transcriptome analysis: $CD4^+$ T cells from the efferent mesenteric lymph of three wt mice housed under SPF conditions (sample ID 1, 4, 7) as well as lymphatic fluid from one wt mouse housed under GF conditions (sample ID 8).

Table 4.2: Quality assessment of polyclonal $CD4^+$ T cell samples subjected to NGS

Sample ID	Cell count	RNA [ng/µl]	Total RNA [ng]	RIN
1	111047	6.6	99	9.6
4	63000	2.5	69	10.0
7	69085	5.6	73	9.2
8	72844	2.3	30	9.8

Table 4.2 indicates that the four samples were of excellent quality with RIN values above 9. The sequencing yielded in more than 50 million clean reads per sample, of which on average 90 % could be mapped to the reference genome using HISAT2. The uniformity of the mapping result suggested that the samples were comparable.

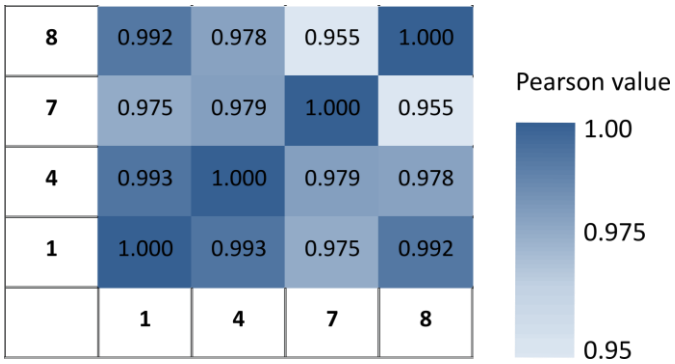

Figure 4.19: Heat map of Pearson correlation coefficients of polyclonal CD4+ T cell transcriptomes. CD4+ T cells were isolated from the efferent mesenteric lymph of wt mice housed under SPF (samples 1, 4, 7) of GF (sample 8) conditions.

The Pearson correlation coefficients between the individual samples revealed a high similarity among all lymph samples (Figure 4.19). The least similar samples were sample 8 (GF) and sample 7 (SPF) with a correlation coefficient of 0.955, whereas the most similar ones were samples 1 (SPF) and 4 (SPF) (Pearson value = 0.993).

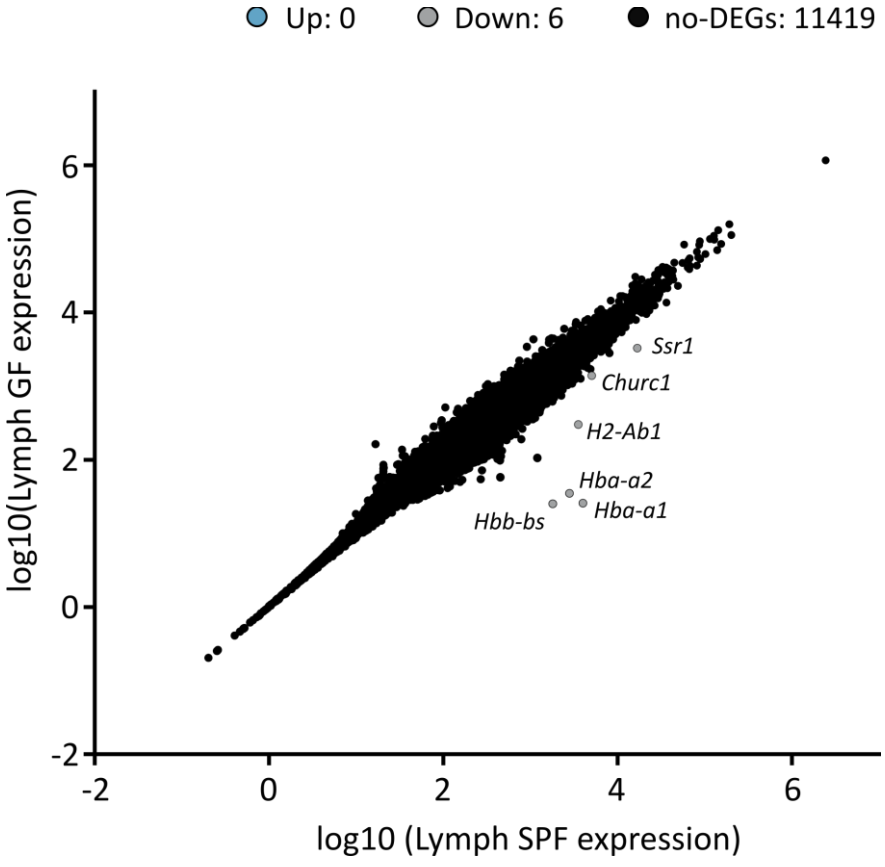

Figure 4.20: Scatterplot showing expression levels in polyclonal CD4$^+$ T cells from the lymph of SPF vs GF mice. Genes were considered as upregulated when the fold change was >2 and an adjusted p-value (Padj) ≤ 0.05; downregulated genes were identified with a fold change of < -2 and Padj ≤ 0.05.

Differential gene expression (DEG) was assessed using the DEseq2 algorithm and identified 11425 genes expressed in both groups. Of those, six were significantly upregulated in SPF mice as compared to GF mice (Figure 4.20, Supplementary Table 1). Those six genes were *Ssr1*, *Churc1*, *H2-Ab1*, *Hba-a1*, *Hba-a2* and *Hbb-bs*.

Table 4.3: Quality assessment of RNA samples from MOG-specific $CD4^+$ T cells isolated from the mesenteric lymph of mice housed under SPF vs. GF conditions.

Sample ID	Cell count	RNA [ng/µl]	Total RNA [ng]	RIN
11L (SPF)	55256	8.9	124.5	10.0
12L (SPF)	22890	2.6	36.4	10.0
13L (SPF)	20157	1.6	22.1	10.0
11B (SPF)	62795	10.2	142.2	10.0
12B (SPF)	100250	12	167.5	9.8
13B (SPF)	65966	6	83.4	10.0
14S (SPF)	200271	27.8	389.2	9.7
16S (SPF)	200435	20.6	267.8	10.0
25S (SPF)	200994	7.9	102.7	9.9
17L (GF)	3279	1.1	13.9	8.6
21L (GF)	19197	0.3	3.7	9.7
23L (GF)	7458	0.4	4.3	7.9
17B (GF)	11323	1.4	18.6	9.9
21B (GF)	5648	0.3	3.3	7.8
22B (GF)	25068	0.4	5.8	9.7
17S (GF)	200423	16.4	213.3	10.0
21S (GF)	200997	2.9	38.2	9.8
23S (GF)	200604	4.8	57.8	9.7

The latter three are associated with erythrocytes, H2-Ab1 is expressed on antigen-presenting cells and Ssr1 and Churc1 are also not involved in any immunological function but in translational and transcriptional processes, respectively. Apparently, the presence or absence of microbiota had no impact on the RNA expression profile of polyclonal $CD4^+$ T cells in the efferent mesenteric lymph. In a second and equally

conducted run, transcriptomes of MOG-specific CD4$^+$ T cells were analyzed to compare their gene expression in different tissues and under different hygiene conditions. In this run, 18 samples from 6 different groups (with 3 samples each) were submitted to the sequencing service: MOG-specific CD4$^+$ T cells from lymph (L), blood (B) and spleen (S) from each three SPF vs. GF housed MOG-TCR transgenic mice. Also those samples were of good quality according to their RINs, whereby they contained at least 3 ng of RNA isolated from as little as 3279 CD4$^+$ T cells (Table 4.3).

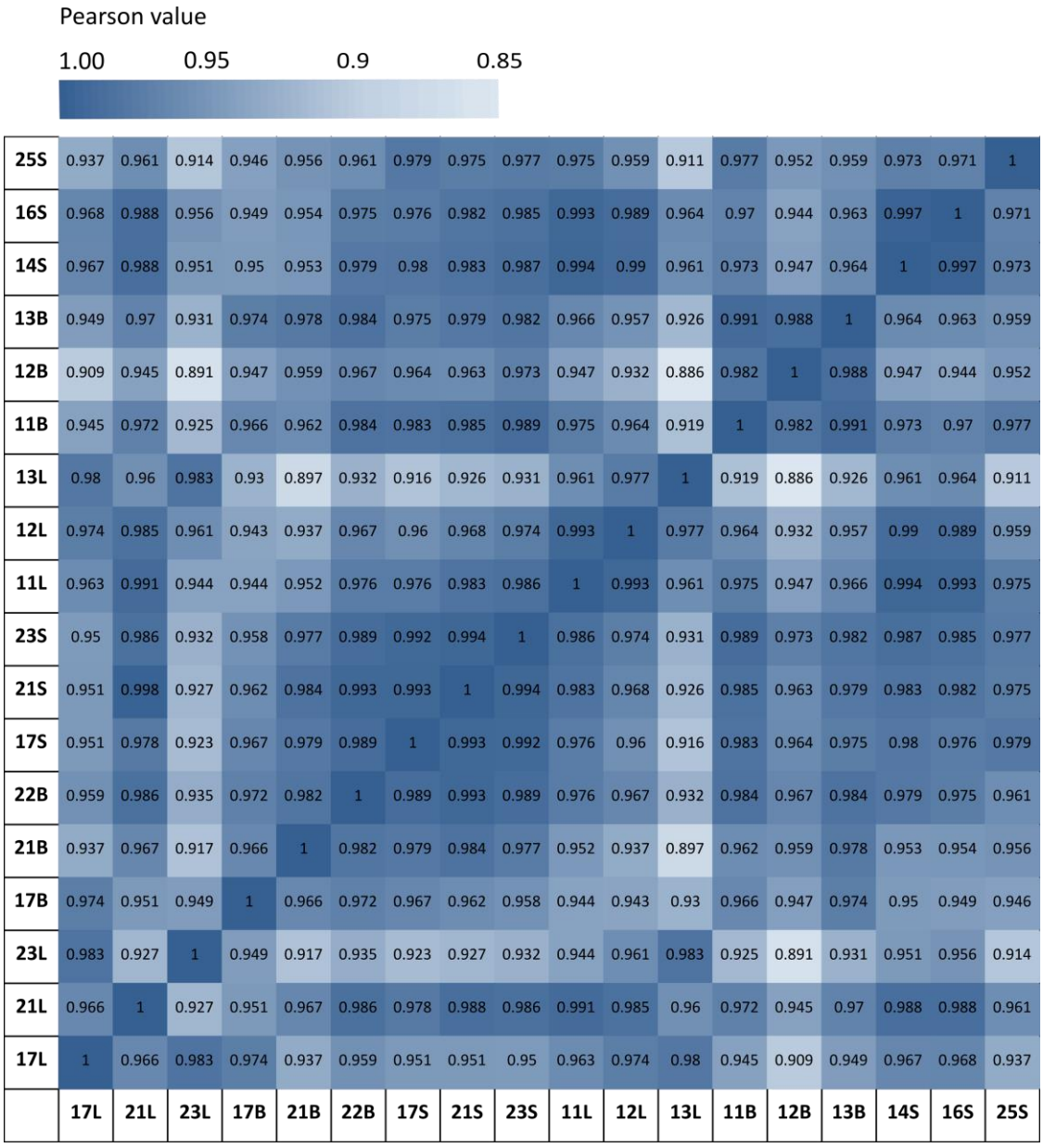

Figure 4.21: Heat map of Pearson correlation coefficients of MOG-specific CD4$^+$ T cell transcriptomes. CD4$^+$ T cells were isolated from the efferent mesenteric lymph (L), the spleen (S) or the blood (B) of mice housed under SPF of GF conditions.

As seen in the polyclonal $CD4^+$ T cells, also $CD4^+$ T_{MOG} cells from different mice and different organs harbored similar mRNA profiles: Pearson correlation coefficients of all 18 samples that were subjected to transcriptome analysis showed that the least similar samples were 12B (SPF) and 13L (SPF) with a coefficient of 0.886. The highest correlation was detected in animal 21 (GF) when comparing $CD4^+$ T cells from its spleen vs its lymph (p=0.998). As the overall correlation was very high and there were no major dissimilarities observed in one specific group (Figure 4.21).

However, for a better visualization of the similarity among samples, a cluster dendrogram indicating the hierarchical similarities of the 18 mRNA samples from six groups of MOG-specific $CD4^+$ T cells from different tissues of mice housed under SPF vs. GF conditions was created (Figure 4.22). The cluster dendrogram demonstrated that in almost all cases, the three samples of each group were the closest to each other. For example, the SPF blood samples (SPF_12B, SPF_11B and SFP_13B) were the most similar and were at the same time very different to the same tissue from mice housed under different hygiene conditions, i.e. in this case the blood samples from GF mice (GF_17B, GF_21B and GF_22B). One outlier was a lymph sample from an SPF mouse (SPF_13L) that was more similar to the GF samples than to the other SPF lymph samples. In the spleen samples, the housing condition seemed to have a minor impact on the gene expression as five out of six spleen samples were a group of very similar samples, whereas besides these, the highest split divided the samples in two branches according to the housing conditions of the mice (GF vs. SPF).

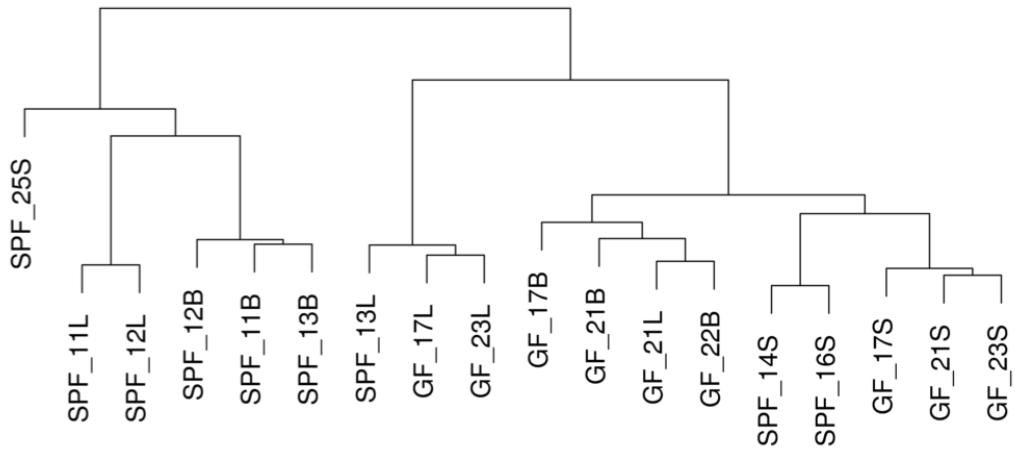

Figure 4.22: Cluster dendrogram based on transcriptomes of MOG-specific T cells.

For getting a better insight into the impact of gut microbiota in the stimulation of MOG-specific T cells in the small intestine, the transcriptomes of T_{MOG} cells from the efferent mesenteric lymph of mice with and without microbiota were compared. Differential gene expression DEG analysis using DEseq2 algorithm identified 14241 non-differentially regulated genes, 18 upregulated and 116 downregulated genes in lymph from SPF vs. lymph from GF mice.

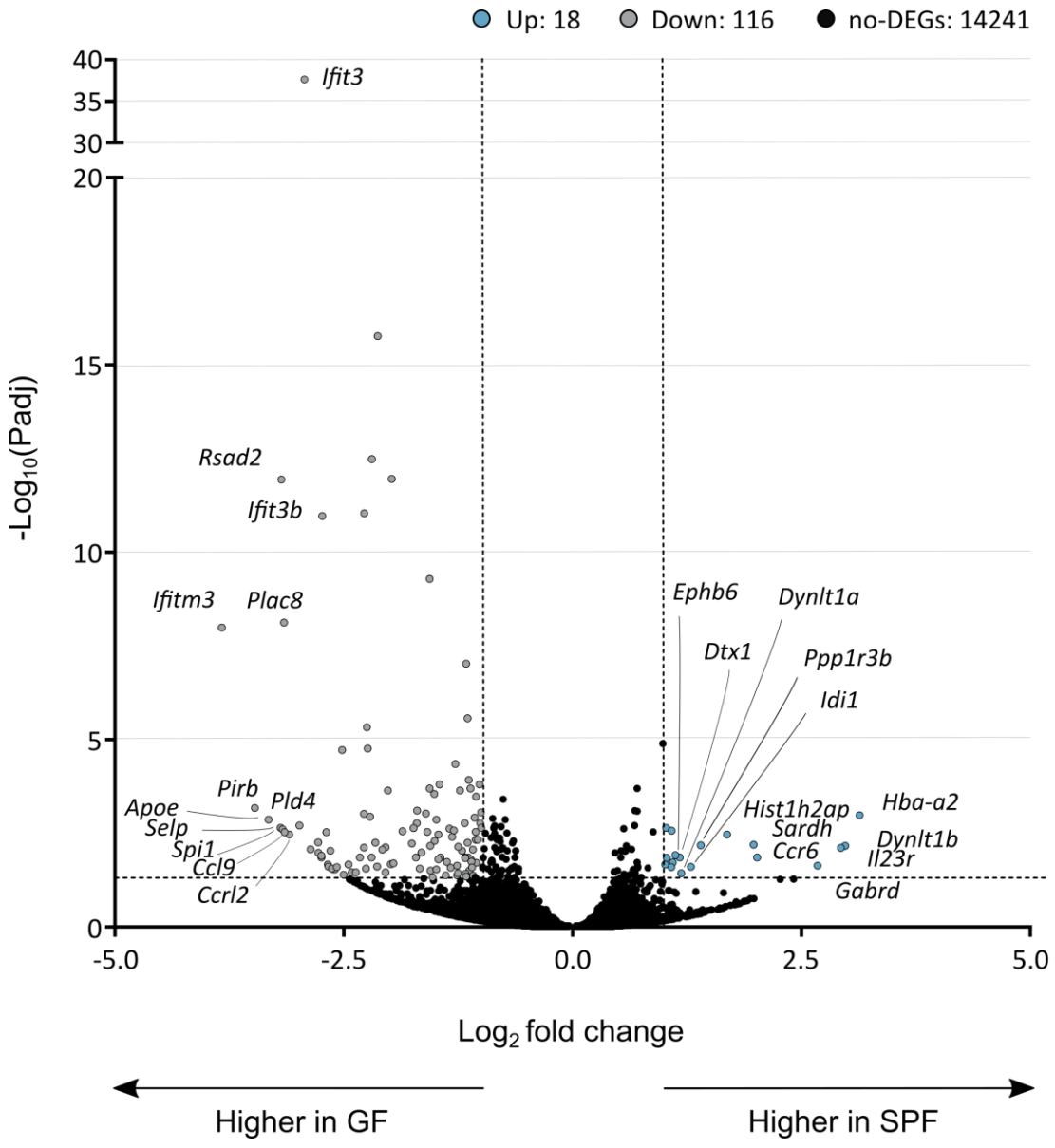

Figure 4.23: Volcano plot of DEGs from the transcriptomes of MOG-specific CD4⁺ T cells from the lymph of SPF vs. GF mice. The vertical dotted lines indicate the fold change cut-off of 2, and the horizontal dotted line shows the adjusted P-value cut-off of 0.05.

Genes being upregulated in the lymph of SPF mice included the Th17 markers *Il23r* and *Ccr6* as well as the erythropoietin-producing hepatocyte (Eph) kinase *Ephb6.* Further significantly upregulated genes in lymph from SPF vs. GF mice included *Gabrd*, *Dynlt1b*,

Hba-a2, *Hist1h2ap*, *Sardh*, *Dtx1*, *Acadsb*, *Tmem181a*, *Idi1*, *Gsn*, *Ckb*, *Ppp1r3b*, *Hist1h1e* and *Zfp386* (Figure 4.23, Supplementary Table 2). The top upregulated genes in the lymph of GF mice were *Ifitm3*, *Pirb*, *Cfp*, *Pld4, Apoe*, *Rsad2, Selp*, *Plac8*, *Spi1*, *Ccl9*, *Ccrl2*, *Ifit3*, *Ifi204*, *Fcgr3, Csf1, Tyrobp, Ifit3b*, *Mx1*, *Lrg1, and Ly6c* (Figure 4.23, Supplementary Table 3).

As this comparison did not yield in an obvious pattern of microbiota-induced gene expression of $CD4^+$ T cells exiting the intestine, DEGs from SPF Lymph vs. SPF spleen were combined with DEGs from lymph of SPF vs. GF mice. This approach allowed to not only identify genes that were upregulated uniquely in the lymph of SPF mice as compared to two other tissues but also to assign less importance to p-values and instead focus on expression values only, as p-values can be misleading with a sample size of three per group.

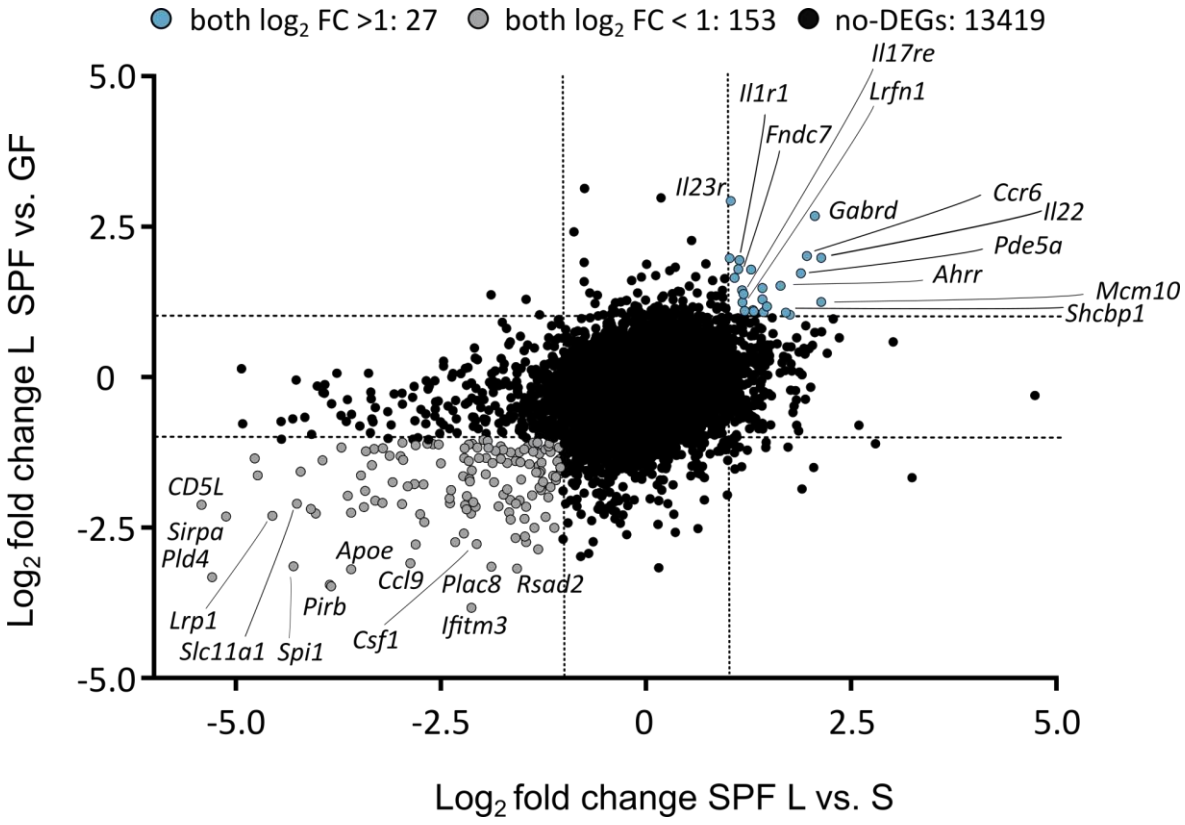

Figure 4.24: Scatterplot of DEGs from SPF lymph vs. spleen plotted against the DEGs from lymph SPF vs. GF. Dotted lines indicate the fold change cut-off of 2.

Hence, to identify genes that were uniquely upregulated in the lymph of mice housed under SPF conditions, the log2 fold changes of SPF Lymph vs. spleen were plotted against the log2 fold changes of the lymph from SPF vs. GF mice (Figure 4.24). This

scatterplot revealed genes that were expressed at higher levels in the lymph of SPF mice as compared to the spleen of SPF mice and at the same time as compared to the lymph of GF mice. The scatterplot identified genes as differentially expressed when the absolute value of the $\log_2$ fold change was >1. 27 genes were found to be upregulated in the lymph of mice housed under SPF conditions: *Mcm10*, *Il22*, *Gabrd*, *Ccr6*, *Pde5a*, *Atp8a2*, *Shcbp1*, *Ahrr*, *Ube2c*, *Trcg1*, *Pcdhga2*, *Apol1*, *Scl6a20b*, *Gga2*, *Rrm2*, *Csgalnact1*, *Nuf2*, *Tmtc1*, *Troap*, *Lrfn1*, *Il17re*, *Il1r1*, *Fndc7*, *Cdk1*, *Il23r*, *Lrfn1, Sardh,* and *Dock1* (Figure 4.24, Supplementary Table 3). Of those, six genes are associated with Th17 cells: *Il22*, *Ccr6, Ahrr, Il17re, Il1r1, and Il23r. Furthermore, Il1r* and *Ccr6* are known to be involved in leukocyte migration. *Fndc7* and *Lrfn1* encode fibronectins and other genes of this set are known to be involved in migration or proliferation: *Shcbp1* and *Gabrd* (Figure 4.24, Supplementary Table 4). Genes that were the most downregulated in $CD4^+$ T cells from the lymph of SPF mice included *Cd5l*, *Pld4*, *Sirpa*, *Adgre4*, *Itgad*, *Lrp1*, *Egr2*, *Spi1*, *Slc11a1*, *Fcgr4*, *Ptgs1*, *Ctsh*, *Pilra*, *Cfp*, *Pirb*, *Hmox1*, *Dnase1l3*, *Apoe*, *Cd68*, *Zeb2*, *Fcna*, *Cd83*, *Mpeg1*, *Dok3* and *Ly6d* (Figure 4.24, Supplementary Table 5).

4.3.2 Transfer of $CD4^+$ T cells from the mesenteric lymph

The subsequent question of this study was whether the calcium stimulation in the small intestine also gave rise to functional differences. As described above, T cells efferent from the small intestine were isolated by cannulating the efferent mesenteric lymph. In this part of the study, the $CD4^+$ T cells were isolated, stained with a fluorescent dye (CTV or CTR) and re-transferred into recipient mice.

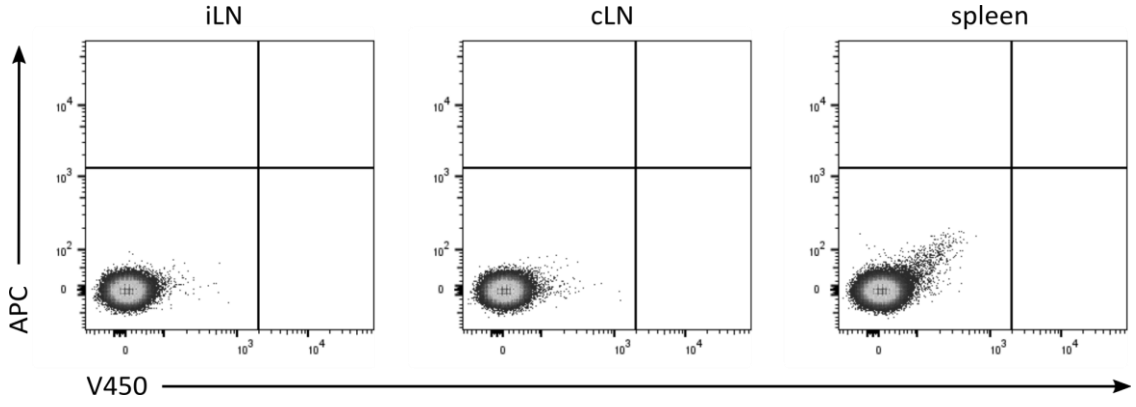

Figure 4.25: Negative controls of target organs in immunized mice without T cell transfer. FACS analysis of lymphocytes isolated from iLN, cLN and spleen of mice immunized with OVA/CFA on day 2 p.i.. Cells were pre-gated on lymphocytes.

As internal control, the same amount of $CD4^+$ T cells was isolated from the spleen, stained with a different fluorophore and co-transferred into the recipient. Afterwards, the labelled T cells were quantified in different peripheral organs. These experiments aimed to identify functional differences in cells that had been stimulated in the gut to those that had not. In order to mimic a target organ, the recipients had been immunized with OVA/CFA on the day before transfer of OVA-specific T cells from lymphatic fluid and spleen. As the OVA/CFA emulsion was injected subcutaneously, the skin-draining iLNs constituted the primary site antigen-uptake and -presentation.

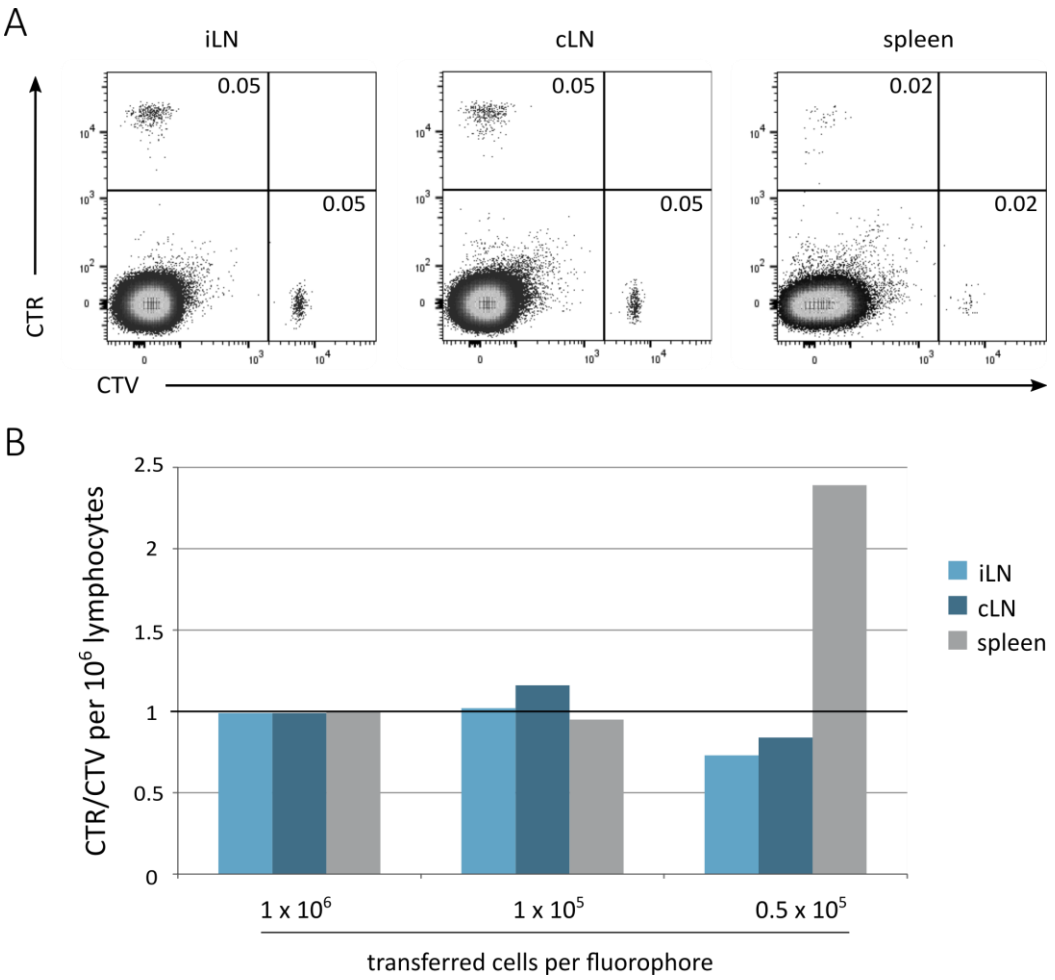

Figure 4.26: Recovery of transferred of CTR- and CTV- labelled splenocytes from target organs. (A) Exemplary FACS plots from iLNs, cLNs and spleens from a mouse that had received 10 $x10^5$ cells per fluorophore. Cells were pre-gated on lymphocytes. (B) Ratio of CTR- to CTV-positive cells in different organs and from different amounts. Line at 1 indicates equal amounts of both cell populations.

As controls, cervical LNs (cLNs) and spleens were also harvested. Figure 4.25 provides data from flow cytometric analysis of the three organs that have been isolated from immunized mice to prove the absence of signal in the APC and V450 channels

constituting the detection channels for the cell trace dyes CTR and CTV, respectively, when no stained cells had been transferred. Lymphatic cannulation constitutes a challenging technique and thus, the amount of $CD4^+$ T cells that could be isolated from the efferent mesenteric lymph constituted the limiting factor for this project. Hence, the first aim was to identify the minimum number of cells that needed to be transferred to the recipient to facilitate a reasonable recovery rate from target organs. Therefore, equal amounts of $CD4^+$ T cells from the spleen of a wt mouse were stained each with one of the dyes (CTR or CTV). Subsequently, both CTR- and CTV-labelled cells were co-transferred into recipient mice in varying amounts: one mouse received 0.5×10^5, another 1×10^5 and a third 1×10^6 cells per dye. One day after transfer, iLNs, cLNs and spleens of recipient mice were harvested, smashed and subjected to flow cytometric analysis to quantify the transferred cells. Figure 4.26A depicts exemplary FACS plots of the mouse that had received 1×10^6 CTV- and CTR-positive cells each. In all three organs, the labelled cells appeared as distinct populations and, most importantly, in very similar amounts. Figure 4.26B provides an overview of the results shown as ratios of CTR to CTV in the different target organs and the different recipients. In the mouse that had received 1×10^6 cells of each dye, the numbers were the most consistent with ratios of 0.99 in the LNs and a ratio of 1 in the spleen. In the condition with the second highest amount of cells, the ratio varied slightly from 0.95 (spleen) to 1.16 (cLN) but was at 1 in the iLNs. When only 0.5×10^5 cells of each fluorophore were transferred, ratios diverged significantly from the expected ratio of 1 (0.73 in iLNs, 0.84 in cLNs and 2.39 in spleens). Hence, the threshold for the transfer studies with cells from the mesenteric lymphatic fluid was set to 1×10^5 cells (Figure 4.26B).

The mesenteric lymphatic fluid of OTII mice was drawn. On average, lymphatic cannulation yielded in 199 µl lymph per mouse containing a total of 1.2×10^5 $CD4^+$ T cells on average. Spleens were isolated as well, which on average comprised 20 % $CD4^+$ T cells. In order to assure a cell number of more than 1×10^5 cells, lymphatic fluid from up to four mice was pooled. As number of $CD4^+$ T cells from the lymphatic fluid constituted the limiting factor, amounts of $CD4^+$ T cells from the spleen were adjusted to the yield of the lymphatic fluid. The number of transferred cells varied from 1.05×10^5 to 1.9×10^5 per each lymph and spleen, respectively. Prior to transfer, the

ratio of CTV^+ to CTR^+ cells in the injection mix was assessed by flow cytometry (Figure 4.27A). 24 h after transfer, the recipients were sacrificed and their spleens, iLNs and cLNs were harvested, smashed and subjected to FACS analysis to quantify CTR- and CTV-positive T cells. In all three organs, transferred $CD4^+$ T cells from lymph were more abundant than the spleen-derived T cells (Figure 4.27B).

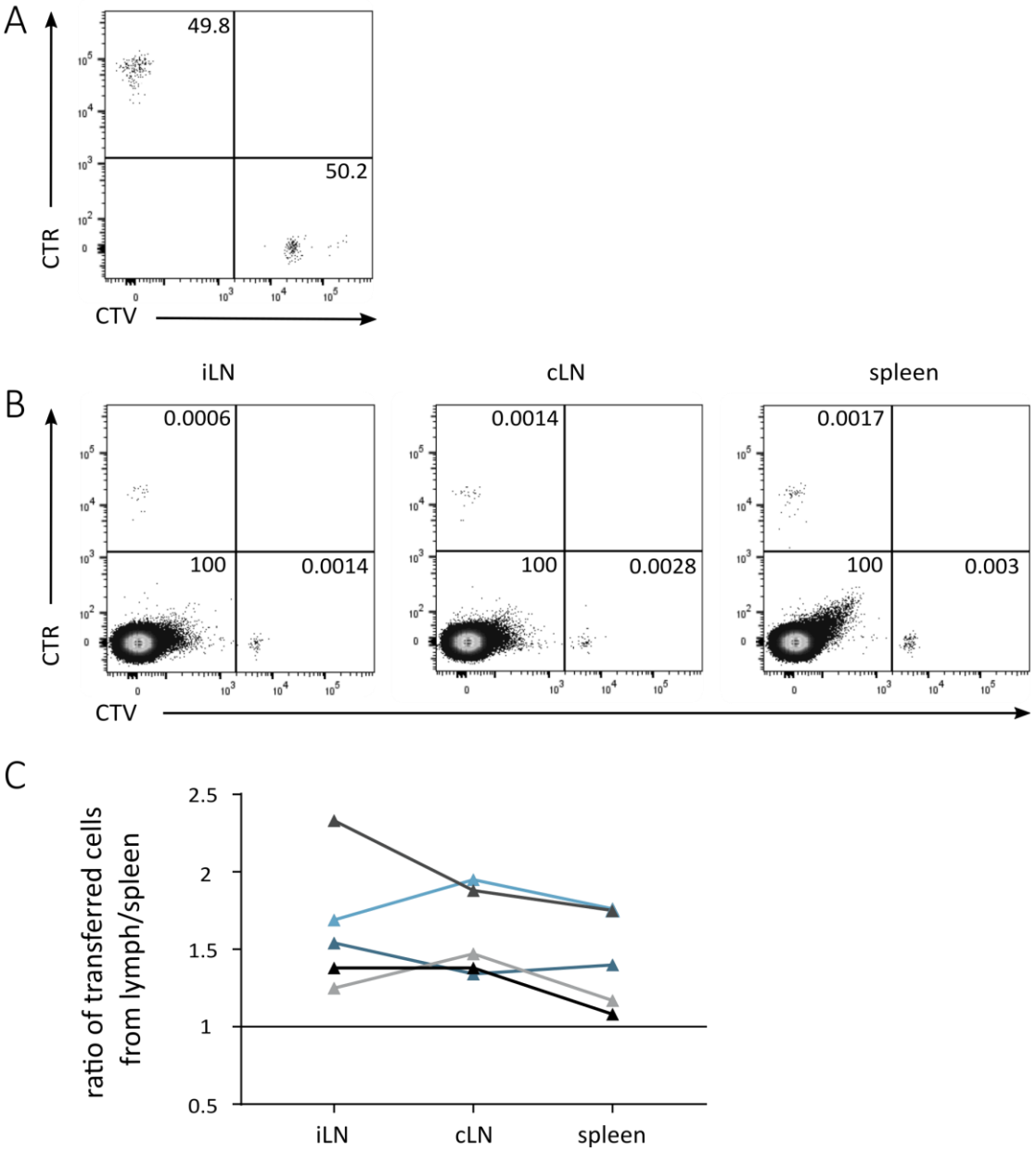

Figure 4.27: Transfer of $CD4^+$ T cells from lymph and spleen to immunized recipient mice. (A) Representative FACS plot showing T cells prior to injection. In this example, CTR^+ cells originate from the spleen, CTV^+ cells from the mesenteric lymph. (B) Analysis of the transferred cells in target organs. Cells were pre-gated on lymphocytes. CTR^+ cells originate from the spleen, CTV^+ cells from the mesenteric lymph. (C) Ratio of recovered T cells from lymph vs. from spleen in different target organs. Results from five independent experiments are shown.

This observation held true for all experiments as the amount of recovered cells was always higher for the ones from the lymphatic fluid as compared to the spleen. To suspend differences induced by the fluorophores, the two cell populations were stained with CTV and CTR, respectively, in an alternating manner among the five independent experiments.

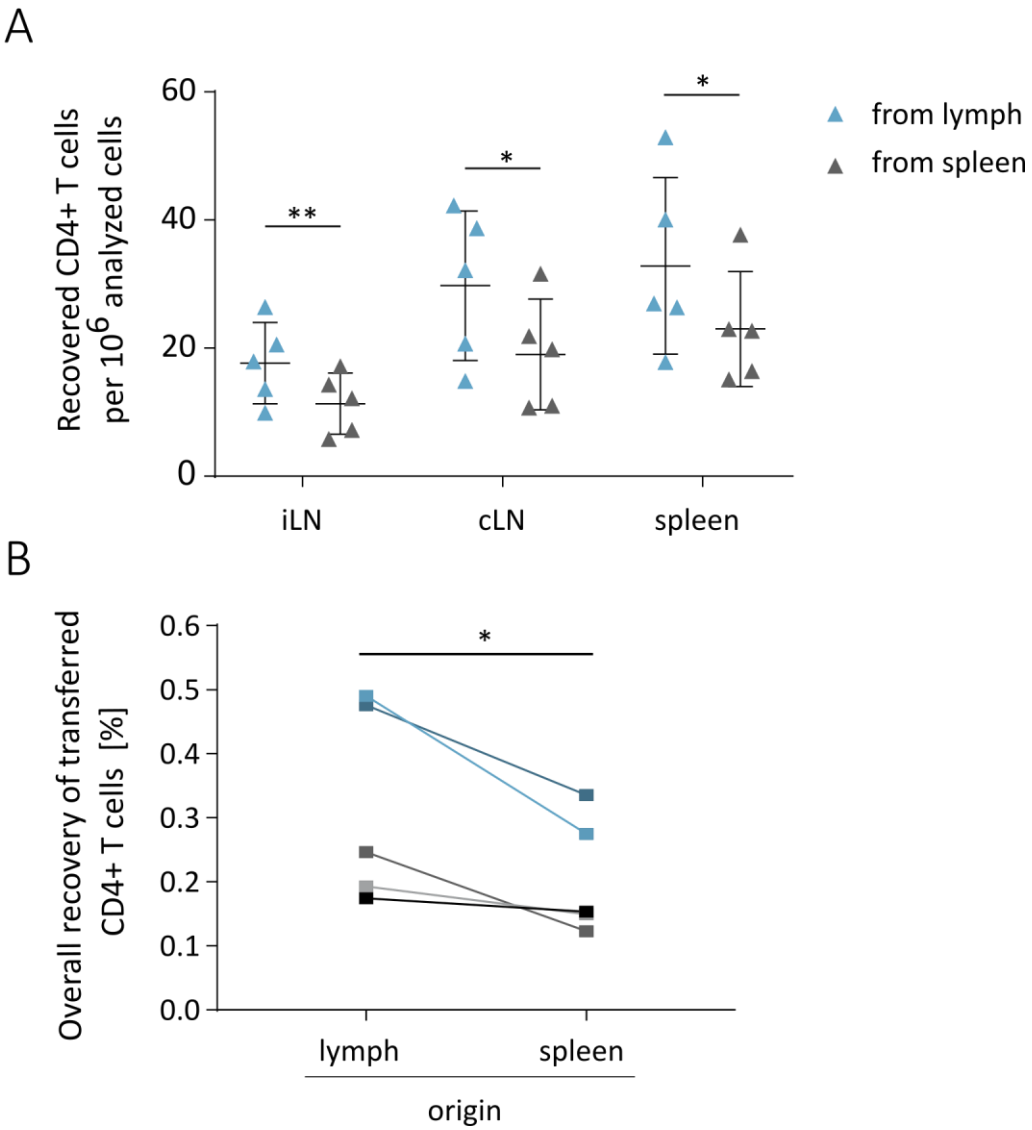

Figure 4.28: Recovered cells from target organs. (A) Numbers of retrieved $CD4^+$ T cells from both origins (lymph vs. spleen) from iLNs, cLNs and spleens of recipient mice per 1 x 10^6 analyzed lymphocytes. Cells were pre-gated on lymphocytes. (B) Recovery rate of retrieved $CD4^+$ T cells as percentage of initially transferred cells compared between different origins. Data represent five independent experiments (*<0.05, **<0.01, paired Student's t-test).

All calculated ratios were above 1: 1.64 ± 0.42 in the iLNs, 1.60 ± 0.29 in the cLNs, and the lowest in the spleen with an average of 1.43 ± 0.31 (Figure 4.27C). As shown before, the cells from the lymph always appeared in higher numbers as compared to

the ones from the spleen. In absolute numbers, most cells of both origins were detected in the recipients' spleen (mean (from lymph) = 32.84 ± 13.8, mean (from spleen) = 23.0 ± 8.9), second-highest in the cLNs (mean (from lymph) = 29.8 ± 11.7, mean (from spleen) = 19.0 ± 8.7) and the least in the iLN (mean (from lymph) = 17.7 ± 6.4, mean (from spleen)=11.3 ±4.8).

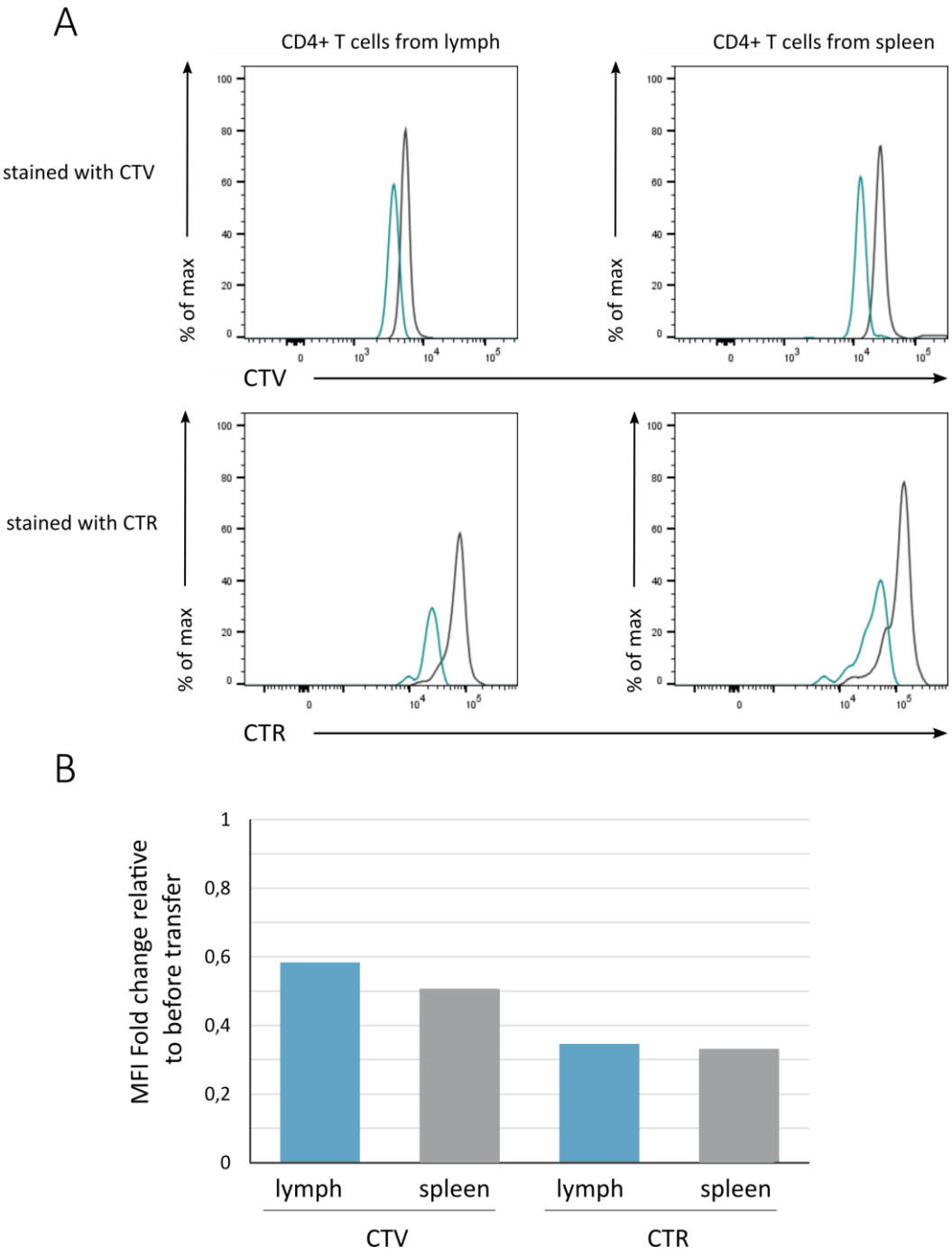

Figure 4.29: Proliferation CD4⁺ T cells. (A) FACS analysis of fluorescence intensities of CD4⁺ T cells from lymph vs. spleen before transfer (grey curve) and after retrieval (blue curve) of CTR/CTV-stained cells from recipient mice. (B) Fold change of MFI of retrieved cells relative to MFI before injection (n=1).

The difference between the two origins was the most pronounced in the iLNs (Figure 4.28A). When looking at the cumulative numbers of recovered cells in all three examined organs, cells from the lymphatic fluid were always retrieved in significantly higher numbers than T cells from the spleen although equal amounts have been transferred initially (Figure 4.29B). As the numbers of $CD4^+$ T cells from the lymph were higher in all organs not only in the iLNs that mimicked the target organ, the suspicion forced itself that the cells from the mesenteric lymph might not migrate better but proliferate more.

The dyes used in this study could also be used for proliferation studies. Hence, the median fluorescence intensities of CTV and CTR were examined before and after injection with cells from the lymphatic fluid vs. from the spleen (Figure 4.29A). The median fluorescence intensities decreased in all four conditions (staining of lymph or spleen with either CTV or CTR, respectively). The fold changes from before to after transfer between the two dyes differed (average fold change (CTV)=0.54, average fold change (CTR) = 0.34). However, the organ origin of the $CD4^+$ T cells had only little impact on the fold change in each dye (CTV: 0.58 (lymph) vs. 0.51 (spleen), CTR: 0.35 (lymph) and 0.33 (spleen) (Figure 4.29B). Hence, these data do not provide evidence of a higher proliferative activity in $CD4^+$ T cells from the efferent mesenteric lymph vs. from the spleen.

4.4 Intravital imaging of the impact of different adhesion molecules on T cell crawling at the Blood-Brain Barrier of Lewis rats

The infiltration of autoreactive T cells into the CNS induces pathogenesis in EAE. For CNS infiltration, T cells need to pass the BBB. In this set of experiments, the tEAE model in Lewis rats was used, because it harbors very stable infiltration time kinetics, i.e. the beginning infiltration of T cells into the CNS happens consistently at the same time point.

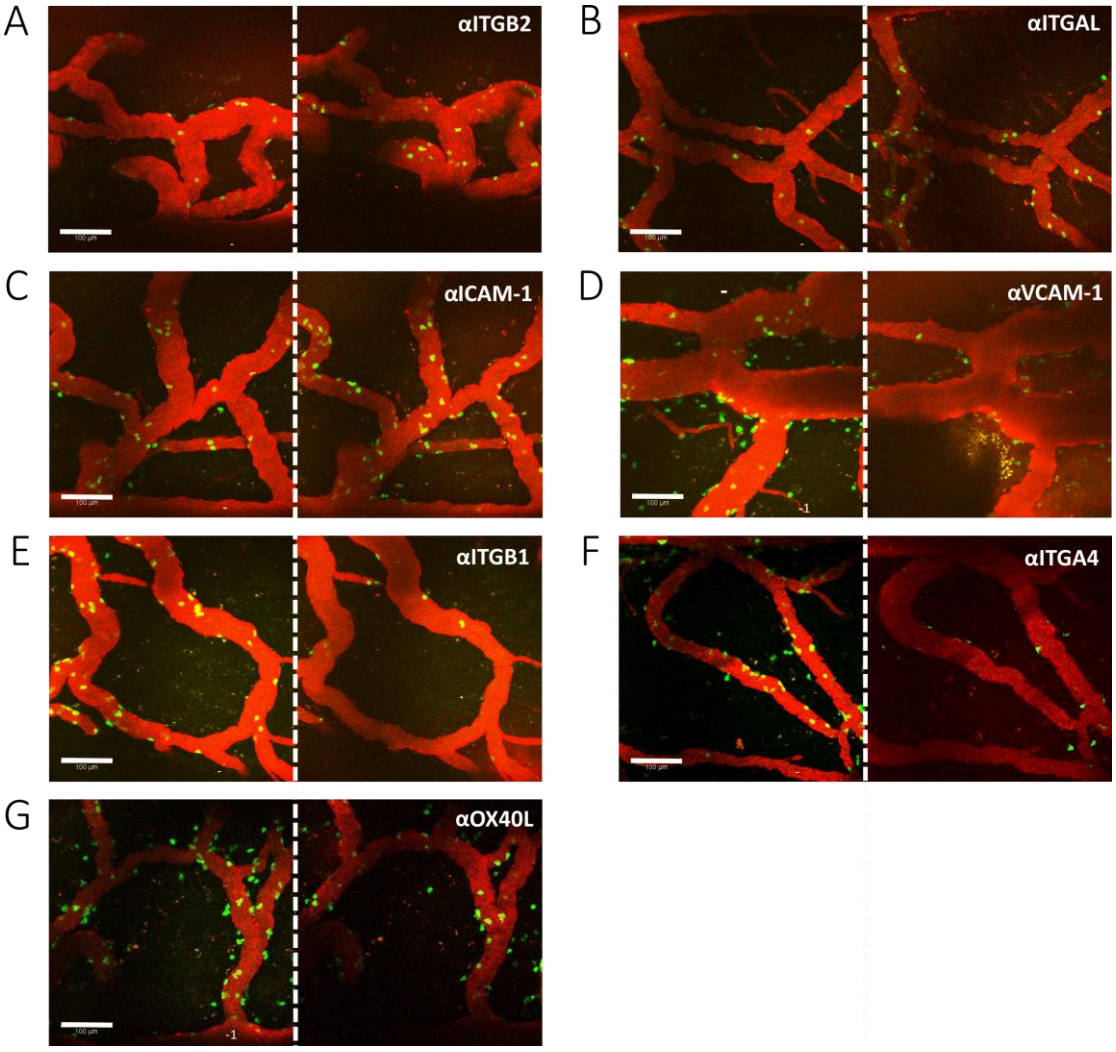

Figure 4.30: Two-photon imaging of $T_{MBP\text{-}GFP}$ cells at the BBB. Representative snapshots from intravital microscopy showing T cells (green) crawling along the leptomeningeal blood vessel wall. Images were taken before (left) and after Injection of 0.5 mg specific blocking antibodies (right). Blood vessels have been rendered visible by i.v. injection of 100 µg Texas red-conjugated dextran (70 kDa). Scale bar 100 µm.

T cell extravasation into the CNS starts in the prodromal phase on day 2 p.t. at the leptomeningeal blood vessels. Upon encountering cell adhesion molecules (CAMs),

T cells can crawl along the intraluminal endothelial surface of the blood vessels and subsequently extravasate. Natalizumab, a blocking antibody against integrin α4 (ITGA4/CD49d) is already being successfully used in the treatment of MS and serves as a positive control. This part of the study addressed the identification of further key adhesion molecules for encephalitogenic T cells to infiltrate the CNS using intravital two-photon imaging in Lewis rats. The molecules evaluated in this study were VLA-4, a heterodimer formed by ITGA4 and ITGB1 (CD29), its ligand VCAM-1 (CD106), LFA-1, whichs Is formed by ITGAL (CD11a) and ITGB2 (CD18), its ligand ICAM-1 (CD54) and OX40L (CD252).

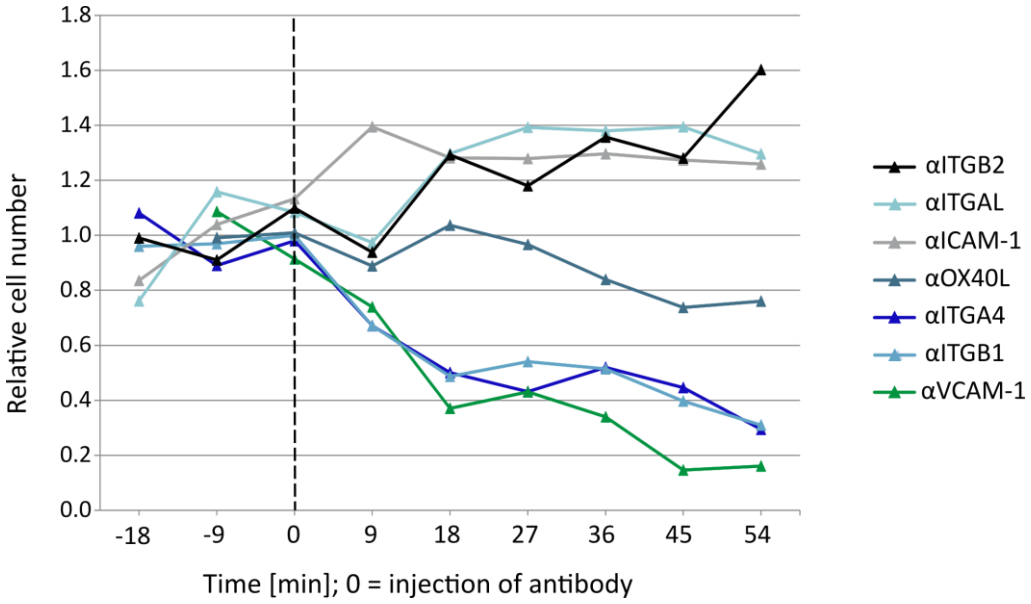

Figure 4.31: Numbers of $T_{MBP\text{-}GFP}$ cells before and after i.v. injection of blocking antibodies detected by intravital two-photon imaging. Amounts are normalized to the average cell number before antibody injection. Data is shown as mean, n=3 per group.

During intravital imaging, different blocking antibodies against known integrins and their respective adhesion molecules were injected i.v. and numbers of crawling $T_{MBP\text{-}GFP}$ cells were assessed starting from 20 minutes before until at least 54 minutes after application of blocking antibodies. The blocking antibodies had varying capacities to block T cells from crawling at the BBB (Figure 4.30, Figure 4.31). Antibodies against components of the LFA-1 (ITGAL/ITGB2)/ICAM-1 complex had no impact on the number of crawling cells. This is indicated by the representative images from two-photon microscopy (Figure 4.30A, B, C) and by the quantification, which revealed that in the groups treated with anti-ITGAL, anti-ITGB2 and anti-ICAM-1, the cell numbers did not decrease but rather increase over time (Figure 4.31). When blocking ITGB1 or

ITGA4, the integrins that bind to VCAM-1, or blocking VCAM-1 directly, the outcome changed dramatically as crawling T cells vanished almost completely (Figure 4.30D, E, F). The quantification in Figure 4.31 confirmed that not only in the positive control using anti-ITGA4 antibodies but also when blocking of VCAM-1 and ITGB1, numbers of crawling T cells started to decrease directly after i.v. application of blocking antibodies. Relative cell numbers were reduced to below 20 % of numbers detected prior to antibody application. An intermediate effect was observed when blocking OX40L, which is expressed on endothelial cells. Here, the amount of crawling cells decreased by approximately 25 % after blocking antibody injection (Figure 4.30G, Figure 4.31).

In order to prove the binding of the blocking antibodies to their target antigens, spleens of rats were isolated after imaging and T cells or endothelial cells were exposed to staining with secondary antibodies to identify the blocking antibodies on cell surfaces. Primary antibodies against VCAM-1 and OX40L - that had been injected while imaging - bound successfully to their surface antigens: there was no difference between stainings with primary and secondary antibody (positive control) as compared to staining with secondary antibody only. After imaging T cells at the BBB with injection of blocking antibodies against ICAM-1, the FACS staining revealed that *in vivo*, there was no complete saturation with the primary antibody on endothelial cells. In the positive control, i.e. in the ITGA4-antibody condition, a complete saturation of ITGA4 with *in vivo* injected antibody was achieved. The same pattern was observed with the blocking of other T-cell surface antigens, ITGAL and ITGB2. Solely blocking of ITGB1 was not found to be complete on T cells after imaging although the effect of anti-ITGB1 antibodies on crawling T cells had been pronounced (Figure 4.32).

Therefore, the question raised whether the incomplete saturation of antigen was due to a too little dosage or due to an increased turnover rate. To address this question, flow cytometry stainings with primary and secondary or only secondary antibody after intravital imaging were performed. To control for a dosage effect, ITGB1 was blocked with two different doses, 0.5 mg or 1 mg per animal. The flow cytometric analysis revealed that the saturation of ITGB1 was at least partially depending on the amount of blocking antibody: transfer of 1 mg increased the staining intensity as compared to application of 0.5 mg but still did not mediate complete saturation which is seen in the positive control (primary and secondary antibody) (Figure 4.33A).

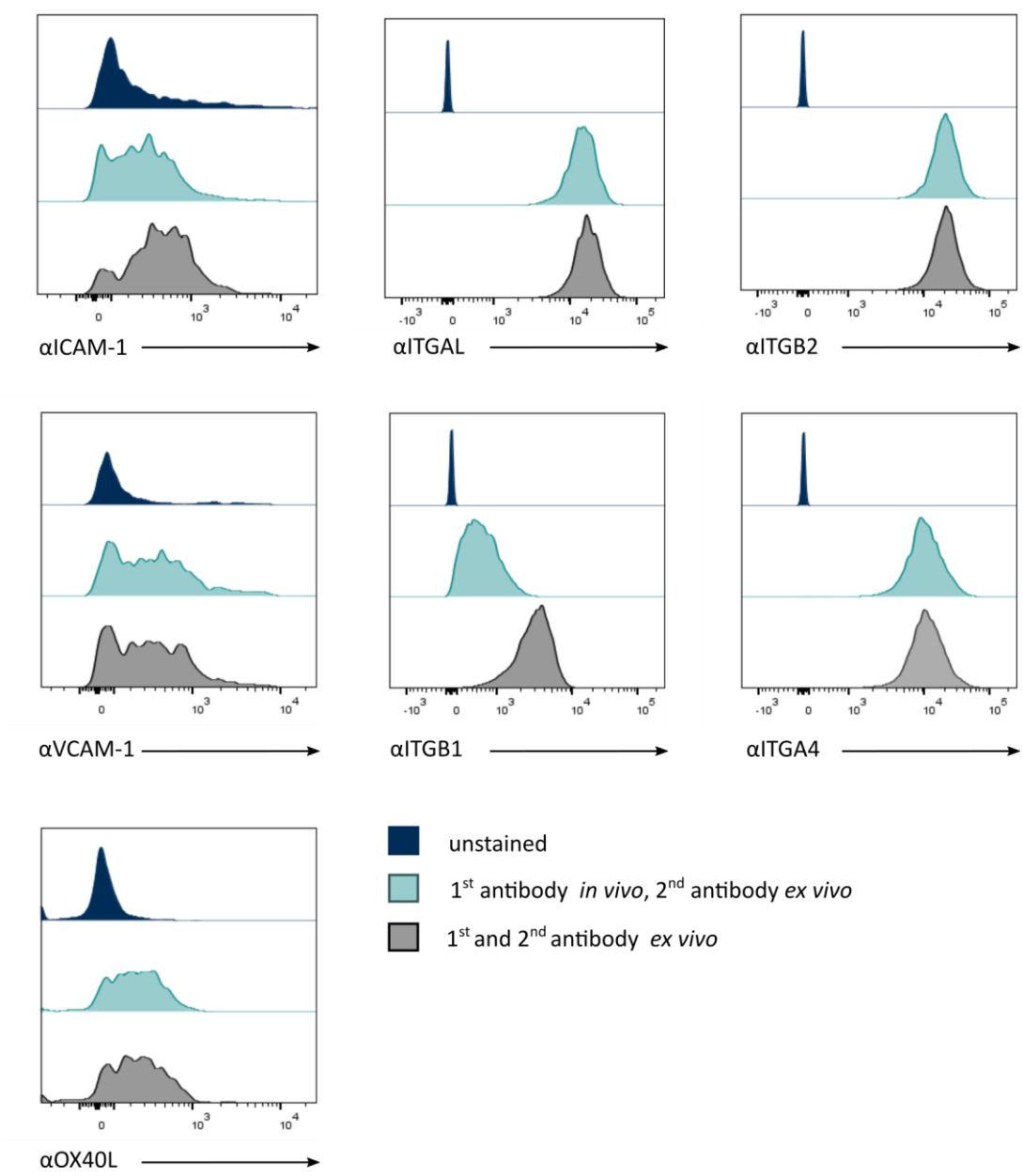

Figure 4.32: Representative FACS histograms of endothelial cells or lymphocytes isolated from spleens of Lewis rats after imaging. Primary antibodies were applied either *in vivo* (light blue) or *ex vivo* (grey) to measure antibody saturation. Depending on the respective antigen expression site, cells were pre-gated for endothelial cells or lymphocytes.

The quantification of crawling cells at the BBB revealed that a double dose of anti-ITGB1 antibody did not dramatically affect the numbers of crawling cells, as those had already been low in the 0.5 mg condition. Cell numbers were reduced by 71 % when injecting 0.5 mg of anti-ITGB1 antibody and decreased by 83 % when using 1 mg of blocking antibody (Figure 4.33C). Notably, in one experiment with the single dose of antibody, a similar reduction as in the double dose was achieved. Furthermore, the

staining after imaging still revealed an incomplete blocking, i.e. the turnover rate of this integrin or antibody could also be higher.

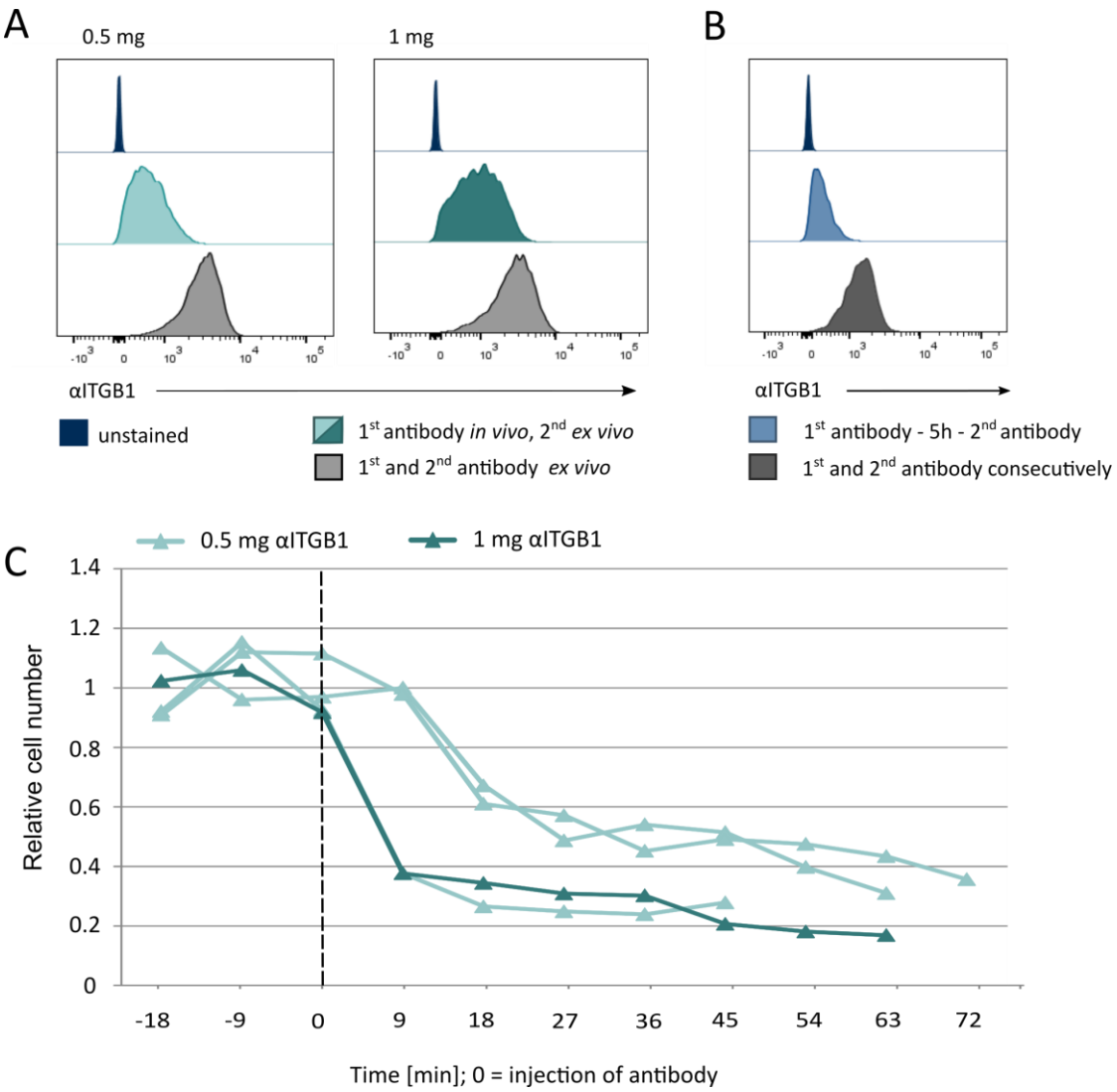

Figure 4.33: Blocking of ITGB1 on T cells. (A) Representative FACS histograms of lymphocytes isolated from spleens of Lewis rats after i.v. injection of 0.5 mg (left, already shown in Figure 4.32)) or 1 mg (right) of anti-ITGB1 antibody during intravital imaging. The *ex vivo* T cells were analyzed without additional staining (unstained), with staining with 1° and 2° antibodies or only with 2° antibody. (B) Staining of cultured T cells with a primary anti-ITGB1 antibody either 5h (blue) or directly before (gray) staining with fluorescently labelled secondary antibody. (C) Relative numbers of $T_{MBP\text{-}GFP}$ cells before and after i.v. injection of 0.5 (already shown as mean of three in Figure 4.31) or 1 mg anti-ITGB1 antibody detected by intravital two-photon imaging.

To test this hypothesis, cultured T cells were stained with anti-ITGB1 antibody 5 h before and directly before staining with secondary antibody, respectively, and were then subjected to FACS analysis. Indeed, after 5 h of delay, the antibody signal was decreased as compared to the staining directly before analysis (Figure 4.33B).

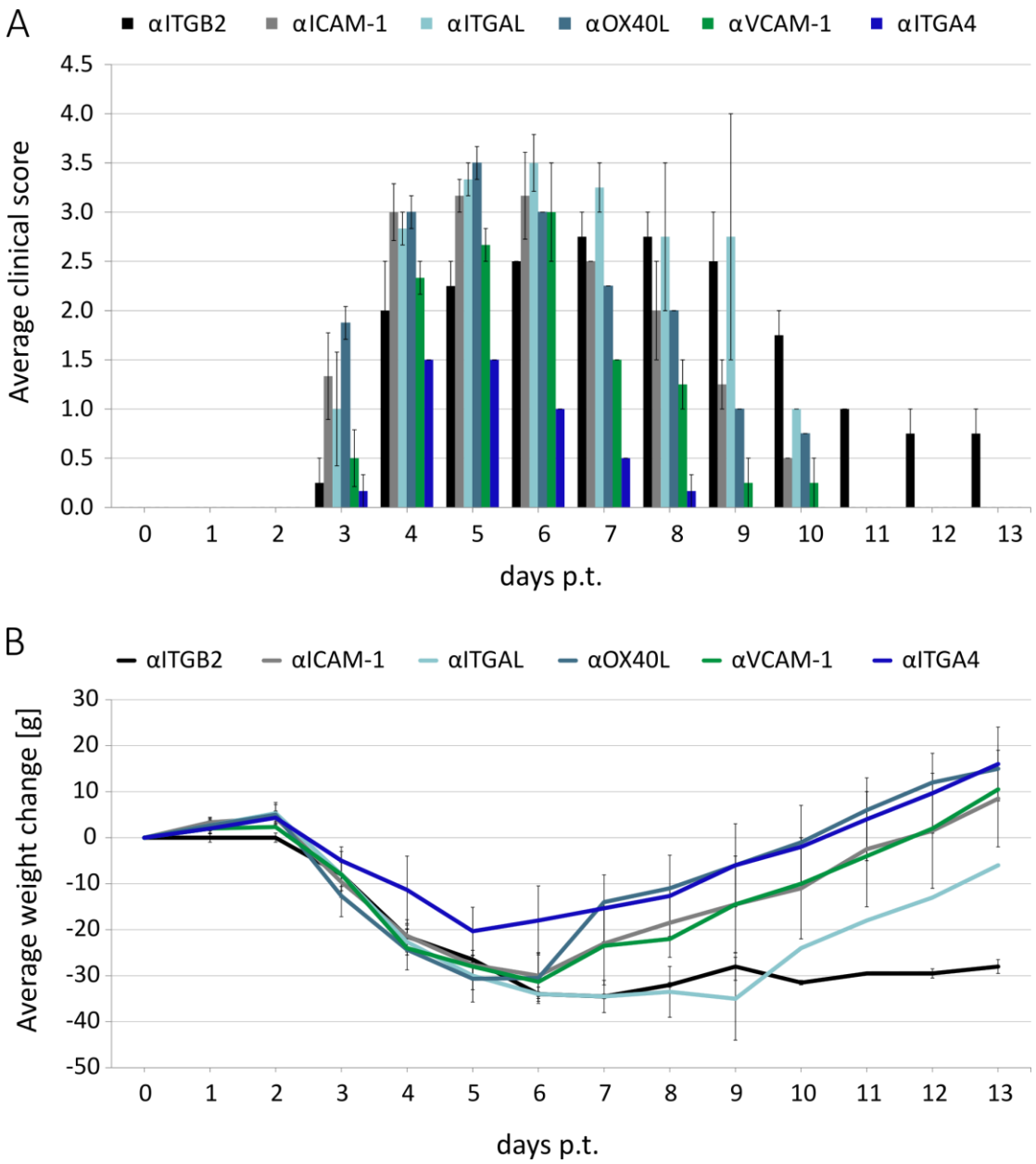

Figure 4.34: Effect of anti-integrin/anti-CAM antibody treatment on clinical EAE. 48h p.t. of $T_{MBP\text{-}GFP}$ T cells, Lewis rats were treated with i.v. infusion of different blocking antibodies. (A) Bars indicate average clinical scores starting on the day of T cell transfer (B) Body weight changes in relation to day 0 p.t. n=3 per group, data shown as mean ± SEM.

Hence, the low abundance of anti-ITGB1 staining after imaging could be due to both an incomplete saturation but mainly due to a high turnover rate of this blocking antibody or its respective ligand, ITGB1. Therefore, this antibody was excluded from further analysis.

Subsequently, the obvious suspicion was that T cells could not infiltrate the CNS when their crawling at the endothelial wall was abolished and thus the course of EAE would be attenuated. To investigate the ameliorating effect of blocking antibodies on the

course of EAE, tEAE was induced in Lewis rats whereby the animals were treated with 0.5 mg of specific blocking antibodies injected 2 days p.t, i.e. in the prodromal phase of EAE. Treatment with blocking antibodies against members of the ICAM-1/LFA-1 had no effect on the clinical course of tEAE in Lewis rats. Also blocking of OX40L did not ameliorate EAE although the antibody had been shown to mildly affect T cell crawling in the imaging experiments. The positive control treatment with anti-ITGA4 indeed had a pronounced effect on EAE and decreased the maximum clinical score from 3.5 in the most diseased animals to a maximum score of 1.5 on days 4 and 5 p.t. (Figure 4.34). In addition, the weight loss was the least in this control condition (Figure 4.34B). Given that treatment with VCAM-1 prevented T cells from crawling at the BBB, a beneficial effect on clinical EAE scores had been anticipated. However, the ameliorating impact on EAE was very mild and not as pronounced as in the ITGA4 antibody condition: the maximum clinical scores were 3 on day 6 p.t. along with pronounced loss of body weight.

5 Discussion

5.1 Encephalitogenic T cells get stimulated in the ileal LP

The present study addressed the stimulation of encephalitogenic T cells in the GALT as potential scenario for peripheral priming prior to onset of EAE. The intestine-related parts of this study were conducted using mice as model organisms taking advantage of the availability of different TCR transgenic mice. To assess T cell stimulation, we made use of intravital two-photon microscopy combined with a calcium indicator that enables the visualization of changes in intracellular calcium levels in real time. Given that calcium is an essential second messenger for pathways induced by signals from the surrounding environment, it is a useful parameter to assess T cell stimulation/ activation. T cells were isolated from donor mice for culture and transduced with the calcium sensor Twitch-2B prior to transfer into recipient mice. The results of the present study indicate that MOG-specific T cells exhibited increased calcium levels as compared to polyclonal T cells in the ileal LP. Noteworthy, the encephalitogenic T cells spiked more often and their spikes lasted longer. As described before, calcium signals exert different effects on the T cells depending on their duration. When persisting for longer than two minutes, high-calcium signaling is associated with T cell activation e.g. by stimuli that cross-link the TCR such as cognate antigen (Kyratsous et al., 2017). MOG-specific T cells exhibited a pronounced amount of those long-lasting calcium signals with an increased duration of up to 20 minutes, whereas those long-lasting calcium signals were almost absent in polyclonal T cells. In a previous study, we have shown that those long-term calcium spikes are antigen-dependent as they were abolished by blocking MHCII molecules on APCs and in turn, they were increased dramatically after application of exogenous antigen (Kyratsous et al., 2017). The calcium signals in the latter study were acquired in MBP-specific T cells in the CNS of Lewis rats and lasted up to more than one hour in the presence of cognate antigen. Presumably, also in the present setup, high-calcium spikes were lasting longer but the individual movies usually lasted 20 minutes, therefore the length of calcium signaling is probably underestimated. The present imaging data suggests that in the ileal LP, MOG-specific T cells encounter antigen. This assumption is strengthened by preliminary experiments showing that the application of an MHCII blocking antibody eradicated

those long-term spikes in the ileal LP (unpublished data). Short-lasting signals were present in both polyclonal and MOG-specific T cells. These short calcium spikes (shorter than 2 min) are neither induced by antigen nor followed by NFAT translocation, but, at least partially, by chemokine receptor signaling (Kyratsous et al., 2017). However, it has been shown before that also short-term calcium spikes can influence T cell behavior, e.g. in the spleen of Lewis rats, where encephalitogenic T cells exhibit solely short-lasting spikes and upregulate chemokine receptors and further surface markers that indicate their migratory phenotype (Flügel et al., 2001; Revy et al., 2001; Kyratsous et al., 2017). Long-term spikes were not solely identified in MOG- but also in OVA-specific T cells in the ileal LP, though to a lesser extent (15 % vs. 20 % of T_{MOG} cells). In LCMV-specific T cells however, the amount of cells exhibiting long-lasting calcium spikes was as low as in polyclonal cells (5 %). These comparisons led to the conclusion that those long-lasting spikes are not caused solely by the high affinity of the engineered TCRs but must also depend on the availability of cognate antigen. Given that LCMV constitutes a prevalent human pathogen that is transmitted primarily by rodents and can cause neurological pathologies in humans, animal facilities routinely test for the presence of the virus in their colonies. The Core Facility Animal Models of the Biomedical Center, where the mice used in this study were kept, publishes quarterly health monitoring reports. According to the latest report, no LCMV-positive animals were discovered at least in the last 18 months (as from third quarter of 2020). Hence, the LCMV-specific T cells in this study were not able to find their cognate antigen which is in line with the absence of long-term calcium spikes in those cells.

In contrast, we found increased long-term calcium signaling in OVA-specific T cells. As ovalbumin constitutes a major component of chicken egg white, it might be a minor component of the mouse chow, but this is hard to ascertain. However, by oral application of OVA protein and a subsequent but time-limited increase in the long-term high-calcium signaling, this study provided a positive control of antigen-dependent signaling in the ileal LP. This data provides evidence that orally applied antigen is capable of inducing T cell stimulation in the ileal LP when applied in large amounts. Although, as the applied amount (4 mg) was unnaturally high and is unlikely

to be equally abundant in mouse chow, it is more likely that both MOG- and OVA-T cell stimulation are caused by different source of antigen.

For the T_{MOG} cells, we have a strong hint that their stimulation is microbiota-dependent as this has been tested in one preliminary experiment in our lab. In the absence of microbiota, MOG-specific T cells do not exhibit long-term spikes and the calcium levels are even lower than in polyclonal T cells in SPF mice (Figure 5.1, Figure 4.4) (unpublished data). For a better comparison, the calcium levels from the MOG-specific T cells in the ileal LP of a GF mouse are shown together with the calcium levels of MOG-specific T cells in the ileal LP of SPF mice recorded in the present study in Figure 5.1.

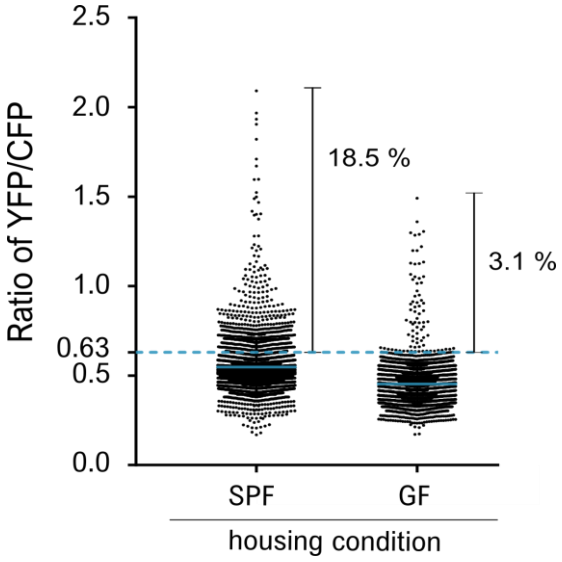

Figure 5.1: Calcium signaling of Twitch-2B$^+$ T_{MOG} cells in the ileal LP of C57BL/6J mice housed under SPF vs. GF conditions. The dotted line indicates the ratio threshold of YFP/CFP=0.63. Each dot represents a calcium ratio at a single time point in a particular cell. n(SPF)=5, conducted in this study, n(GF)=1 (unpublished).

As discussed in chapter 1.3.2, molecular mimicry of autoantigens is a frequently proposed mechanism for the microbiota-induced activation of autoreactive T cells (Westall, 2006; Harkiolaki et al., 2009; Chen et al., 2016). Given that it is unlikely that the mouse chow contains sufficient amounts of OVA and as it has been shown that stimulation of MOG-specific T cells is depending on the presence of microbiota, the stimulating factors are most likely to be microbiota(-derived). Molecular mimicry of gut microbiota or their metabolites constitutes a plausible mechanism for the stimulation of MOG- and OVA-specific T cells observed in the present study.

One limitation of the intravital imaging applied in this study is the obligation to stimulate T cells prior to transfer. Due to the fact that the retrovirus used for transduction with the calcium sensor Twitch-2B only infects proliferating cells, the *in vitro* activation step cannot be skipped. Therefore, all T cells that can be visualized are not naïve but antigen-experienced T cells. This could be circumvented by the introduction of a Twitch-2B transgenic mouse. In 2012, scientists succeeded in generating a transgenic mouse with widespread functional expression of the GECI TN-XXL, an ancestor of Twitch-2B, using the ubiquitous CAG promoter (Direnberger et al., 2012). However, for unknown reasons, calcium sensor expression was spared in cell lineages of the hematopoietic system, i.e. $CD4^+$ T cells did not express TN-XXL. Despite great efforts, all following attempts of generating a Twitch-transgenic mouse failed as well in different steps of the process.

5.2 GALT-located T cell stimulation induces expression of Th17 markers

In order to investigate whether the observed stimulation of encephalitogenic T cells in the ileal LP induced transcriptional or functional changes in T cells, we aimed to isolate and characterize cells after they had been stimulated in the gut. To this end, we made use of the lymphatic system whose purpose is to return lymphocytes to the blood circulation after tissue penetration. To collect lymphocytes from the small intestine, a suitable method is to cannulate the intestinal lymph trunk as it bears advantages for lymph isolation by being big enough to be cannulated and relatively easy to access.

The volumes and cell concentrations achieved by lymphatic cannulation varied significantly among mouse lines and housing conditions with wt mice housed under SPF conditions exhibiting the highest lymphatic flow rate and cell numbers. As GF mice do not harbor pathogens and microbial antigens in their intestines, it is an intuitive finding that in those mice without microbiota, lower immune cell counts and lower volumes of mesenteric lymphatic fluid were isolated. These results are in line with previous descriptions of germ-free mice having lower lymphocyte counts in their intestine (Umesaki et al., 1993) and even reduced amounts of intestinal lymphatic vessels (Moghadamrad et al., 2015).

After lymphatic cannulation, $CD4^+$ T cells from different mouse lines housed under different hygiene conditions were subjected to transcriptome analysis to identify

differential gene expression depending on TCR-specificity and microbiota status. NGS was performed by the sequencing service BGI and yielded in very high amounts of reads (50 million per sample). In accordance with the findings from the intravital imaging, polyclonal T cells from mice housed under SPF vs. housed under GF conditions exhibited no DEGs related to immune functions, i.e. in the absence of long-term calcium spiking in T cells in the ileal LP, the microbiota status has no influence gene expression of polyclonal T cells.

In contrast, the results from the transcriptome analysis of encephalitogenic $CD4^+$ T cells revealed that they differed according to the housing conditions: MOG-specific T cells from mice housed under SPF conditions expressed different genes as the respective cells from mice housed under GF conditions. This indicates that microbiota-stimulated T cells expressed different genes. Unexpectedly, there was no unidirectional shift of genes related to the immune system towards the SPF mice, as in both conditions, genes that are commonly associated with host defense against pathogens were found to be upregulated. Also in the GF condition, T cells upregulated genes involved e.g. in the innate immune system such as *Ifit3* or *Ccl9*. There is no overt explanation for this. However, also the MOG-specific T cells from the SPF mice upregulated genes associated with the immune system, e.g. *Il23r* or *Ccr6*. When comparing DEGs as identified by a fold change of more than 2 and an adjusted p-value of less than 0.05 in $CD4^+$ T_{MOG} cells from lymph of SPF vs. GF mice, no overt pattern was observed. Hence, another approach was taken: instead of focusing on p-values which may be too restrictive with small group sizes of just three samples, it is reasonable to just look at relative differences in expression levels. In order to identify genes that were upregulated uniquely in the gut in the presence of microbiota but were not induced in organs other than the gut, fold changes of DEGs from lymph SPF vs. GF were plotted against fold changes of DEGs from SPF lymph vs. spleen (Figure 4.24). This way of displaying the data revealed microbiota-induced and organ-specific regulation at the same time. The most striking finding in this set of genes was a high abundance of Th17 markers being upregulated in the lymph of SPF mice: $CD4^+$ T cells from the lymph of mice housed under conventional conditions expressed *Il22*, *Ccr6, Ahrr, Il17re, Il1r1,* and *Il23r* with a fold change of more than 2 as compared to $CD4^+$

T cells from both spleen from the same mice and lymph from mice housed under GF conditions.

The microbiota-dependent induction of Th17 cells in the murine gut has been described previously (Ivanov et al., 2008; Gaboriau-Routhiau et al., 2009; Ivanov et al., 2009; Berer et al., 2011). Yet, the underlying mechanisms of microbiome dependent control of Th17 induction are largely unclear. For the first time, this study provides *in situ* footage of T cell stimulation by microbiota associated with a downstream increase in Th17 cells. Considerably, the source of analyzed $CD4^+$ T cells, i.e. the efferent mesenteric lymph, does not only contain lymphocytes from the ileum where T cell stimulation has been shown, but also encompasses cells from the whole intestinal tract of the mouse. Preliminary imaging data from our lab indicates that T cells get stimulated neither in the colon nor in Peyer's patches (unpublished data). These findings are corroborated by an increasing body of evidence showing that the ileal LP is the site of action for the induction of Th17 cells (Esplugues et al., 2011; Farkas et al., 2015). Also in MS patients, a microbiota-dependent abundance of Th17 cells in the gut has been pinned down to the small intestine by analyzing small intestine biopsies (Cosorich et al., 2017). To prove that the stimulation seen in the intravital imaging experiments definitely induces Th17 cells, further studies will focus on T cells directly isolated from the ileal LP right after imaging of their stimulation. Alternatively, the use of a calcium sensor that retains its activated state for an extended period after activation might help to link the T cell stimulation in the ileal LP directly to the downstream effects.

The observation that Th17 cells are induced in the ileal LP was connected to the high abundance of SFB, a bacterial strain that has been shown to be sufficient to induce Th17 cells and thus promote autoimmunity (Ivanov et al., 2009; Lee et al., 2011). Yang et al. (2014) discovered that most Th17 cells, but not other T cell subsets, recognized mainly SFB-derived antigens, which highlights the importance of microbial antigens in effector T cell induction (Yang et al., 2014). More recently, scientists showed that after active immunization with MOG peptide, MOG-specific Th17 cells were observed in the small intestine of mice and that those cells were induced by a strain of *Lactobacillus reuteri* (Miyauchi et al., 2020). Although our model bears some differences as e.g. it

mimics T cell stimulation in a pre-EAE setting, we also see that Th17 induction is restricted to MOG-specific T cells over polyclonal T cells.

Also under homeostatic conditions, Th17 cells are induced by microbiota in the small intestine (Wang et al., 2009). For example, LP DCs from C57BL/6J mice supplied from Charles River Laboratories bearing SFB are more efficient in Th17 cell induction than DCs from equivalent mice from The Jackson Laboratory (Denning et al., 2011). Hence, their differential microbiota status explains differential Th17 abundance among mouse providers. Th17 cells have a contrasting role in immunity. They have been shown to be potent inducers of autoimmunity in different diseases (Korn et al., 2009; Yasuda et al., 2019) but at the same time, Th17 cells are involved in mounting protective responses against extracellular pathogens (Hernández-Santos and Gaffen, 2012) and in maintenance of mucosal barrier functions (Blaschitz and Raffatellu, 2010). The mechanistic details underlying the regulation of their pathogenic potential remain largely elusive. Recently, scientists have identified several regulators of Th17 pathogenicity. One of them is CD5-like (CD5l), which has been shown to be associated with non-pathogenic Th17 cells (Gaublomme et al., 2015; Wang et al., 2015). *Cd5l* is one of the most regulated genes found in the transcriptome data acquired in this study with a strong downregulation in the $CD4^+$ T cells from the lymph of SPF mice as compared to $CD4^+$ T cells from both the spleen of SPF mice and lymph of GF mice. Furthermore, *Il23r* belongs to the top upregulated genes in the MOG-specific $CD4^+$ T cells from SPF lymph in this study. *Il23r* has been intensively studied and identified to be a crucial determinant for pathogenicity of Th17 cells (Cua et al., 2003; Meyer zu Horste et al., 2016). Hence, the present data indicates that the Th17 cells induced in the ileal LP have a pathogenic phenotype.

To sum up, the transcriptome analysis of $CD4^+$ T cells isolated from the mesenteric lymph indicates that microbiota induce the differentiation of T cells into pathogenic, antigen-specific Th17 cells. Of note, those findings are based on RNA analysis which does not necessarily reflect protein expression. Thus, to confirm these observations, Th17 markers will be quantified on a protein level in future experiments.

5.3 Stimulation in the GALT alters T cell behavior

Besides analyzing their transcriptomes, we also functionally characterized T cells that underwent stimulation in the intestine. For this approach, we also used antigen-specific $CD4^+$ T cells isolated from the efferent mesenteric lymphatic fluid. Due to limited availability of 2D2 mice, OTII mice were used in this part of the project. As OVA-specific T cells exhibited similarly increased calcium levels and hence stimulation in the ileal LP according to our imaging data, we considered them as suitable surrogates for MOG-specific T cells.

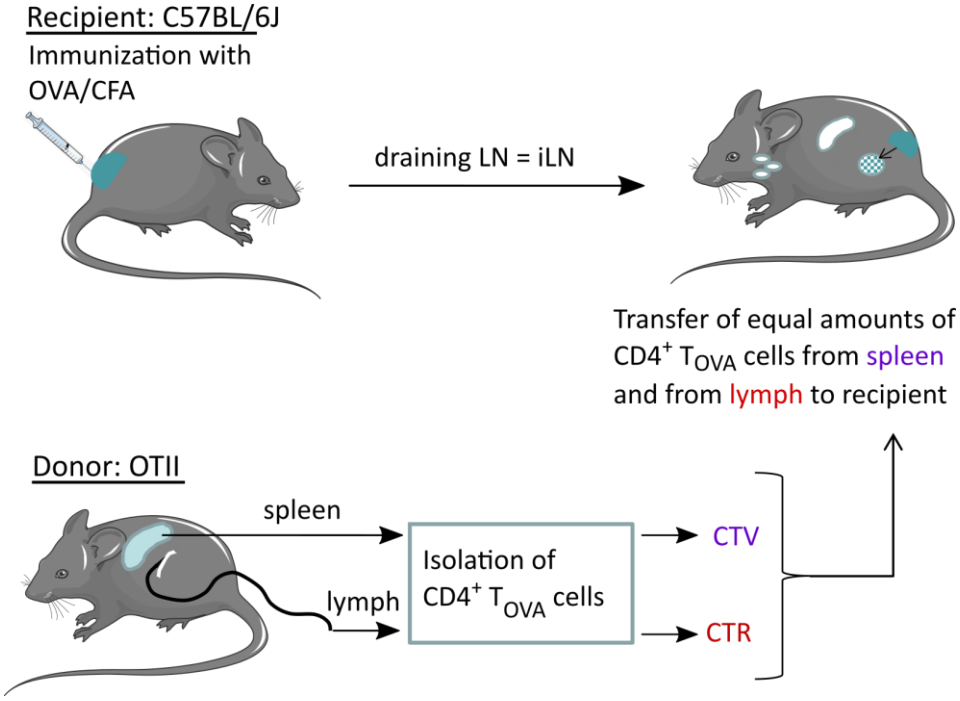

Figure 5.2: Schematic overview of $CD4^+$ T cell transfer assays into immunized recipient mice. The mouse schematic used in this figure was provided by Servier Medical art (https://smart.servier.com/). Servier Medical Art by Servier is licensed under a Creative Commons Attribution 3.0 Unported License.

Figure 5.2 provides a schematic overview of the experimental setup. In order to assess the migrating behavior of gut-stimulated $CD4^+$ T cells as compared to $CD4^+$ T cells without stimulation in the gut, we co-transferred equal amounts of $CD4^+$ T cells from the mesenteric lymph and from the spleen into the same recipient mouse. To distinguish the cells, they were labelled with two different fluorescent dyes, CTV and CTR, respectively, prior to transfer. By interchanging the dyes among the two populations, potential fluorophore-induced differences were ruled out. On the day before transfer, the recipient mice had been immunized with OVA/CFA s.c. into the

lower back. Hence the draining iLNs constituted a “target organ” for the transferred OVA-specific T cells used in the study. In addition to the iLNs, spleens and cLNs were isolated from the recipient mice 1 d.p.t. of labelled cells and all organs were subjected to flow cytometric analysis to quantify the respective numbers of the two transferred cell populations.

The results from this set of experiments showed that in all experiments, more $CD4^+$ T_{OVA} cells from the lymph (referred to as L cells hereafter) as compared to $CD4^+$ T cells from the spleen (referred to as S cells hereafter) were detected in all three analyzed organs. Notably, the ratio of L cells to S cells was the highest in the iLNs, although in absolute numbers (normalized to 1×10^6 total cells), most transferred cells migrated to the cLNs. These findings indicate that the generation of a target organ by immunization has not been successful. Most likely, the immunization with OVA/CFA should be performed earlier than on the day before cell transfer. This will be addressed in future experiments. However, the results elegantly demonstrate that L cells appear in higher numbers as compared to S cells despite equal numbers transferred indicating that stimulation in the gut induces altered T cell behavior. There are several possible reasons for this enhanced amount of lymph-derived T cells in the examined organs. The higher abundance of L cells over S cells in the recipient may be either due to an increased proliferation rate in L cells, due to a better survival of gut-stimulated L cells or due to an enhanced migration efficiency of L cells that had been stimulated in the gut.

To determine whether L cells proliferate better, we assessed the cell division by dye dilution, which was measured using flow cytometry. The data indicated that the dyes were diluted to similar extents in both cell populations, i.e. the proliferation rates appeared to be very similar. We conclude that there is no enhanced proliferative activity in gut-stimulated $CD4^+$ T cells.

As the first possibility was ruled out, another explanation was an enhanced survival rate of L cells due to microbiota-induced downregulation of pro-apoptotic genes. To address this question, we checked the transcriptome data and probed for respective gene expression. Gene Ontology (GO) analysis had been performed by the sequencing service BGI. In order to identify genes related to apoptosis, expression of genes

associated to the GO Terms “negative regulation of apoptotic process” (GO:0043066) and “positive regulation of apoptotic process” (GO:0043065), according to the Gene Ontology Consortium, was analyzed. Indeed, there were genes associated with positive and negative regulation of apoptosis. However, there was no unidirectional pattern detectable: In the MOG-specific $CD4^+$ T cells from SPF lymph vs. SPF spleen (corresponding to L and S cells of the transfer assay setup, respectively) we found DEGs up- as well as downregulated associated with both positive and negative regulation of apoptotic processes. Hence, there is no clear positive or negative influence of ileal stimulation on apoptotic processes in T cells. These findings do not allow for the conclusion that in the lymphatic fluid of SPF mice, $CD4^+$ T cells express more genes that negatively regulate apoptotic processes or downregulated genes that might act in favor of apoptosis.

The last hypothesis for the increased frequency of L over S cells in the recipient organs was that $CD4^+$ T cells that got stimulated in the gut to migrate more efficiently by upregulating of migration-related genes. In general, Th17 cells are considered to expose an enhanced capacity to migrate to sites of inflammation, hence the microbiota-induced stimulation and the subsequent differentiation to Th17 cells in the gut may account for the increased migration efficiency observed in the T cell transfer experiments of this study. *Il1r1* constitutes a Th17-associated gene that is upregulated in the $CD4^+$ T cells in the lymph of SPF mice. Il1R1 KO T cells have been discovered to be less efficient in migrating to the sites of inflammation in EAE (Chung et al., 2009) most likely mainly due to a diminished Th17 differentiation. The most prominent, Th17-restricted migration marker found in the transcriptome data was *Ccr6*, which is significantly upregulated in the lymph of SPF mice over lymph of GF mice and spleen of SPF mice. CCR6 is known to mediate Th17 cell migration to the site of inflammation and has been implicated in the pathogenesis of various autoimmune and inflammatory diseases such as Psoriasis (Hedrick et al., 2010) or Crohn’s disease (Marafini et al., 2017). Most intriguingly, CCR6 has been shown to be crucial for the initiation of EAE by mediating the migration of Th17 cells into the CNS (Reboldi et al., 2009).

Besides their Th17 phenotype, the transcriptome analysis revealed that the $CD4^+$ T cells from the mesenteric lymph of SPF mice upregulated genes that have been associated with migration, e.g. *Dock1*, a member of the dedicator of cytokinesis

(DOCK) family of proteins (Kunimura et al., 2019). Other DEGs found in the transcriptome data indicated a more activated phenotype of T cell, which might correlate with T cell migration capacities. Among them, two genes, *Lrfn1* and *Fndc7*, constitute domains of fibronectin, which have been shown to be expressed in activated T cells (Wagner et al., 2000).

To decipher the driving molecules for the migratory phenotype of $CD4^+$ T cells stimulated in the gut, future experiments will address their identification on a protein level and assess their importance for the tissue homing e.g. by application of blocking antibodies or by genetic modification.

5.4 In active EAE, T cell priming also takes place in the mesenteric lymph nodes

The LN imaging performed in this study focused on elucidating whether antigen spreads to other than the directly draining lymph nodes after immunization. In the active EAE model that we were using, the skin draining LNs constitute the draining LNs as the emulsion was injected subcutaneously into the lower back. Calcium imaging in the iLNs of MOG-immunized mice on d13 p.i. served as a positive control and revealed extensive calcium signaling in MOG-specific T cells. The levels of calcium signaling in this condition were comparable to the signaling in OVA-specific T cells in the ileal LP after oral gavage with ovalbumin. This correlation is in line with the proven presence of antigen in both conditions. The interesting finding in this set of experiments was the strong stimulation of MOG-specific T cells in the mLNs of immunized mice. Hence, these results indicate that antigen indeed spread to the mLNs and primed T cells there which was visualized by the two-photon microscopy in real-time.

As controls, mice were immunized with PBS/CFA. In this condition, i.e. in the absence of antigen, we still observed pronounced calcium signaling in the draining iLNs in contrast to mLNs, where calcium levels were significantly reduced in the absence of MOG in the immunization emulsion. These controversial findings in the different LNs in the absence of antigen lead to the conclusion, that the CFA must exert some effect on the T cells in the draining iLNs but does not reach out to the distant mLNs.

5.5 Differential requirement of integrins and their ligands for crawling at the BBB

The last part of this study focused on another critical step in the journey of encephalitogenic T cells, namely the step of infiltration into the CNS across the BBB. The infiltration of lymphocytes into the CNS is rigorously controlled under homeostatic conditions, as the BBB constitutes a tight border restricting the movement of soluble mediators and cells. However, under inflammatory conditions, endothelial cells of brain and spinal cord microvessels upregulate adhesion molecules like integrin ligands to allow T cell transmigration (Engelhardt and Ransohoff, 2012). Blocking of integrins and their ligands is a powerful tool to abolish T cell extravasation into the CNS and thus to decrease the relapse rate in MS: As mentioned before, the blocking antibody against ITGA4 is already being successfully used in the therapy of relapsing-remitting MS (Polman et al., 2006). However, ITGA4 is not the only integrin that is involved in T cell crawling. More importantly, the blocking of ITGA4 also affects the migration capacities of other immune cells resulting in general immune suppression. Therefore, we applied our intravital two-photon microscopy setup to identify the involvement of different cell adhesion molecules in T cell crawling and CNS infiltration, which might serve as therapeutic targets.

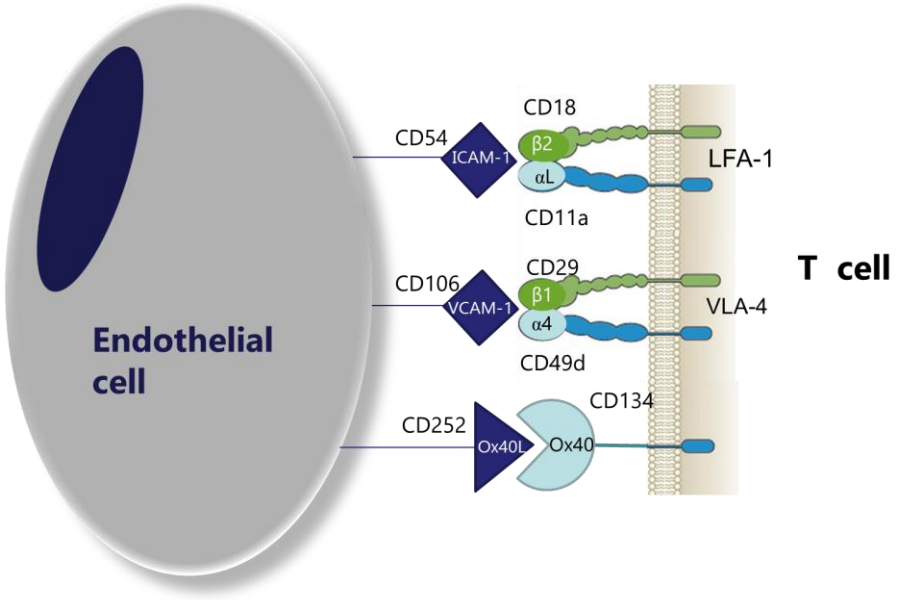

Figure 5.3: Schematic overview of adhesion molecules at the BBB.

For this approach, we made use of the tEAE model in the Lewis rat whose major advantage is that the time kinetic of T cell behavior is highly predictable. This was especially crucial in this setup as we imaged T cells before infiltration, i.e. before EAE was fully developed. Figure 5.3 summarizes the different complexes involved in T cell adhesion to the BBB: The intravital imaging data suggests that blocking the three components of the ICAM-1/LFA-1 complex does not affect T cell crawling. In all three conditions, the numbers of T cells at the BBB did not decrease after application of respective blocking antibodies. These findings were in line with the EAE scores after injection of blocking antibodies. Neither anti-ICAM-1, nor anti-ITGAL or anti-ITGB2 antibodies ameliorated the clinical course of rat tEAE. An intermediate effect was observed in the microscopy following injection of an anti-OX40L antibody, which was not reflected in the clinical data. This might be explained by compensatory mechanisms of the other cell adhesion molecule/integrin complexes.

The intravital imaging data reveals that all three components of the VCAM-1/VLA-4 complex are important in the crawling of T cells. The application of blocking antibodies against components of this complex, i.e. anti-VCAM-1, anti-ITGA4 and anti-ITGB1, significantly reduced the numbers of crawling T cells at the BBB. However, the FACS stainings after imaging revealed that the anti-ITGB1 antibody or the ITGB1 molecule itself, respectively, has a fast turnover time. Therefore, the antibody only achieves incomplete saturation on T cells, so that there was little hope to see a clinical benefit. Since the *in vivo* treatment requires huge amounts of antibody, anti-integrin β1 was excluded from the clinical course evaluation. VCAM-1 however was a quite promising candidate in the imaging data and the FACS staining revealed good saturation of the antibody after hours of incubation. Unfortunately, this effect was not mirrored by the clinical courses of animals that had received this blocking antibody prior to onset of tEAE, where only a minor decrease in EAE scores was observed. This suggests the presence of compensatory mechanisms by other integrins. A probable control would be to combine different blocking antibodies in order to block potential compensatory mechanisms. In addition, fibronectin can substitute VCAM-1 as ligand for VLA-4.

To sum up, the best candidate remains the blocking antibody against ITGA4, which gave the best results in all experiments. It caused a significant reduction in crawling T cells according to the two-photon microscopy, full saturation and no detectable

turnover in the flow cytometric analysis as well as great reduction of clinical scores in animals treated with the blocking antibody in the prodromal phase of EAE. Hence, this experiment did not reveal a better or equally qualified candidate for therapeutic applications than the one already in use.

6 CONCLUSION

By performing intravital two-photon microscopy, this study elegantly visualized *in situ* and real-time T cell stimulation in the ileal LP. With the application of downstream transcriptome analyses, we demonstrated that the microbiota-dependent stimulation in the small intestine induces antigen-specific Th17 cells with a pathogenic phenotype. Ultimately, by transferring gut-stimulated T cells into recipient mice, we managed to add a functional component to the observed stimulation in the ileal LP. $CD4^+$ T cells that underwent stimulation in the ileal LP migrate more efficiently to lymphoid organs *in vivo*.

In the last part of the study, we applied the intravital two-photon microscopy at another crucial step during EAE initiation, i.e. at the BBB where T cells infiltrate the CNS. This enabled visualization of the mechanism of antibodies blocking the entry of encephalitogenic T cells into the CNS. This study confirmed that blocking ITGA4 has the most pronounced therapeutic effect.

The findings of the present study add to the mechanistic understanding of peripheral priming of encephalitogenic T cells preceding CNS inflammation, which remains one of the least deciphered processes in the pathogenesis of CNS autoimmunity.

REFERENCES

Abromson-Leeman, S., Bronson, R., Luo, Y., Berman, M., Leeman, R., Leeman, J., and Dorf, M. (2004). T-cell properties determine disease site, clinical presentation, and cellular pathology of experimental autoimmune encephalomyelitis. The American journal of pathology *165*, 1519-1533.

Baecher-Allan, C., Kaskow, B.J., and Weiner, H.L. (2018). Multiple Sclerosis: Mechanisms and Immunotherapy. Neuron *97*, 742-768.

Barnden, M.J., Allison, J., Heath, W.R., and Carbone, F.R. (1998). Defective TCR expression in transgenic mice constructed using cDNA-based alpha- and beta-chain genes under the control of heterologous regulatory elements. Immunology and cell biology *76*, 34-40.

Bartholomäus, I., Kawakami, N., Odoardi, F., Schläger, C., Miljkovic, D., Ellwart, J.W., Klinkert, W.E., Flügel-Koch, C., Issekutz, T.B., Wekerle, H.*, et al.* (2009). Effector T cell interactions with meningeal vascular structures in nascent autoimmune CNS lesions. Nature *462*, 94-98.

Beecham, A.H., Patsopoulos, N.A., Xifara, D.K., Davis, M.F., Kemppinen, A., Cotsapas, C., Shah, T.S., Spencer, C., Booth, D., Goris, A.*, et al.* (2013). Analysis of immune-related loci identifies 48 new susceptibility variants for multiple sclerosis. Nature genetics *45*, 1353-1360.

Ben-Nun, A., Wekerle, H., and Cohen, I.R. (1981). The rapid isolation of clonable antigen-specific T lymphocyte lines capable of mediating autoimmune encephalomyelitis. European journal of immunology *11*, 195-199.

Benakis, C., Brea, D., Caballero, S., Faraco, G., Moore, J., Murphy, M., Sita, G., Racchumi, G., Ling, L., Pamer, E.G.*, et al.* (2016). Commensal microbiota affects ischemic stroke outcome by regulating intestinal γδ T cells. Nature medicine *22*, 516-523.

Benoit, J.N., Zawieja, D.C., Goodman, A.H., and Granger, H.J. (1989). Characterization of intact mesenteric lymphatic pump and its responsiveness to acute edemagenic stress. The American journal of physiology *257*, H2059-2069.

Berer, K., Gerdes, L.A., Cekanaviciute, E., Jia, X., Xiao, L., Xia, Z., Liu, C., Klotz, L., Stauffer, U., Baranzini, S.E.*, et al.* (2017). Gut microbiota from multiple sclerosis patients enables spontaneous autoimmune encephalomyelitis in mice. Proceedings of the National Academy of Sciences of the United States of America *114*, 10719-10724.

Berer, K., Mues, M., Koutrolos, M., Rasbi, Z.A., Boziki, M., Johner, C., Wekerle, H., and Krishnamoorthy, G. (2011). Commensal microbiota and myelin autoantigen cooperate to trigger autoimmune demyelination. Nature *479*, 538-541.

Berger, T., Rubner, P., Schautzer, F., Egg, R., Ulmer, H., Mayringer, I., Dilitz, E., Deisenhammer, F., and Reindl, M. (2003). Antimyelin antibodies as a predictor of clinically definite multiple sclerosis after a first demyelinating event. N Engl J Med *349*, 139-145.

Bernard, C.C., and Carnegie, P.R. (1975). Experimental autoimmune encephalomyelitis in mice: immunologic response to mouse spinal cord and myelin basic proteins. Journal of immunology (Baltimore, Md : 1950) *114*, 1537-1540.

Bettelli, E. (2007). Building Different Mouse Models for Human MS. Annals of the New York Academy of Sciences *1103*, 11-18.

Bettelli, E., Baeten, D., Jäger, A., Sobel, R.A., and Kuchroo, V.K. (2006). Myelin oligodendrocyte glycoprotein-specific T and B cells cooperate to induce a Devic-like disease in mice. The Journal of clinical investigation *116*, 2393-2402.

Bettelli, E., Pagany, M., Weiner, H.L., Linington, C., Sobel, R.A., and Kuchroo, V.K. (2003). Myelin oligodendrocyte glycoprotein-specific T cell receptor transgenic mice develop spontaneous autoimmune optic neuritis. The Journal of experimental medicine *197*, 1073-1081.

Bettelli, E., Sullivan, B., Szabo, S.J., Sobel, R.A., Glimcher, L.H., and Kuchroo, V.K. (2004). Loss of T-bet, but not STAT1, prevents the development of experimental autoimmune encephalomyelitis. The Journal of experimental medicine *200*, 79-87.

Bielekova, B., Sung, M.H., Kadom, N., Simon, R., McFarland, H., and Martin, R. (2004). Expansion and functional relevance of high-avidity myelin-specific CD4+ T cells in multiple sclerosis. J Immunol *172*, 3893-3904.

Bittner, S., Afzali, A.M., Wiendl, H., and Meuth, S.G. (2014). Myelin oligodendrocyte glycoprotein (MOG35-55) induced experimental autoimmune encephalomyelitis (EAE) in C57BL/6 mice. Journal of visualized experiments : JoVE.

Blaschitz, C., and Raffatellu, M. (2010). Th17 cytokines and the gut mucosal barrier. Journal of clinical immunology *30*, 196-203.

Bradley, C.P., Teng, F., Felix, K.M., Sano, T., Naskar, D., Block, K.E., Huang, H., Knox, K.S., Littman, D.R., and Wu, H.J. (2017). Segmented Filamentous Bacteria Provoke Lung Autoimmunity by Inducing Gut-Lung Axis Th17 Cells Expressing Dual TCRs. Cell host & microbe *22*, 697-704.e694.

Breslin, J.W. (2014). Mechanical forces and lymphatic transport. Microvasc Res *96*, 46-54.

Campbell, B., Vogel, P.J., Fisher, E., and Lorenz, R. (1973). Myelin basic protein administration in multiple sclerosis. Archives of neurology *29*, 10-15.

Capecchi, M.R. (1989). Altering the genome by homologous recombination. Science *244*, 1288-1292.

Cekanaviciute, E., Yoo, B.B., Runia, T.F., Debelius, J.W., Singh, S., Nelson, C.A., Kanner, R., Bencosme, Y., Lee, Y.K., Hauser, S.L*., et al.* (2017). Gut bacteria from multiple sclerosis patients modulate human T cells and exacerbate symptoms in mouse models. Proceedings of the National Academy of Sciences of the United States of America *114*, 10713-10718.

Charcot, J.-M., Charcot, J., Charcot, J., and Charcot, M. (1868). Histologie de la sclerose en plaques.

Chen, J., Chia, N., Kalari, K.R., Yao, J.Z., Novotna, M., Paz Soldan, M.M., Luckey, D.H., Marietta, E.V., Jeraldo, P.R., Chen, X*., et al.* (2016). Multiple sclerosis patients have a distinct gut microbiota compared to healthy controls. Scientific reports *6*, 28484.

Chung, Y., Chang, S.H., Martinez, G.J., Yang, X.O., Nurieva, R., Kang, H.S., Ma, L., Watowich, S.S., Jetten, A.M., Tian, Q*., et al.* (2009). Critical regulation of early Th17 cell differentiation by interleukin-1 signaling. Immunity *30*, 576-587.

Cifarelli, V., and Eichmann, A. (2019). The Intestinal Lymphatic System: Functions and Metabolic Implications. Cellular and molecular gastroenterology and hepatology *7*, 503-513.

Coles, A.J., Twyman, C.L., Arnold, D.L., Cohen, J.A., Confavreux, C., Fox, E.J., Hartung, H.-P., Havrdova, E., Selmaj, K.W., and Weiner, H.L. (2012). Alemtuzumab for patients with relapsing multiple sclerosis after disease-modifying therapy: a randomised controlled phase 3 trial. The lancet *380*, 1829-1839.

Coles, A.J., Wing, M.G., Molyneux, P., Paolillo, A., Davie, C.M., Hale, G., Miller, D., Waldmann, H., and Compston, A. (1999). Monoclonal antibody treatment exposes three mechanisms underlying the clinical course of multiple sclerosis. Annals of neurology *46*, 296-304.

Constantinescu, C.S., Farooqi, N., O'Brien, K., and Gran, B. (2011). Experimental autoimmune encephalomyelitis (EAE) as a model for multiple sclerosis (MS). British journal of pharmacology *164*, 1079-1106.

Cosorich, I., Dalla-Costa, G., Sorini, C., Ferrarese, R., Messina, M.J., Dolpady, J., Radice, E., Mariani, A., Testoni, P.A., Canducci, F*., et al.* (2017). High frequency of intestinal Th17 cells correlates with microbiota alterations and disease activity in multiple sclerosis. Sci Adv *3*, e1700492.

Crabtree, G.R., and Clipstone, N.A. (1994). Signal transmission between the plasma membrane and nucleus of T lymphocytes. Annual review of biochemistry *63*, 1045-1083.

Croxford, A.L., Kurschus, F.C., and Waisman, A. (2011). Mouse models for multiple sclerosis: Historical facts and future implications. Biochimica et Biophysica Acta (BBA) - Molecular Basis of Disease *1812*, 177-183.

Croxford, J.L., and Miyake, S. (2015). Immunoregulation of multiple sclerosis by gut environmental factors. Clinical and Experimental Neuroimmunology *6*, 362-369.

Cua, D.J., Sherlock, J., Chen, Y., Murphy, C.A., Joyce, B., Seymour, B., Lucian, L., To, W., Kwan, S., Churakova, T*., et al.* (2003). Interleukin-23 rather than interleukin-12 is the critical cytokine for autoimmune inflammation of the brain. Nature *421*, 744-748.

Delon, J., Bercovici, N., Raposo, G., Liblau, R., and Trautmann, A. (1998). Antigen-dependent and -independent Ca2+ responses triggered in T cells by dendritic cells compared with B cells. The Journal of experimental medicine *188*, 1473-1484.

Denning, T.L., Norris, B.A., Medina-Contreras, O., Manicassamy, S., Geem, D., Madan, R., Karp, C.L., and Pulendran, B. (2011). Functional specializations of intestinal dendritic cell and macrophage subsets that control Th17 and regulatory T cell responses are dependent on the T cell/APC ratio, source of mouse strain, and regional localization. J Immunol *187*, 733-747.

Direnberger, S., Mues, M., Micale, V., Wotjak, C.T., Dietzel, S., Schubert, M., Scharr, A., Hassan, S., Wahl-Schott, C., Biel, M*., et al.* (2012). Biocompatibility of a genetically encoded calcium indicator in a transgenic mouse model. Nature Communications *3*, 1031.

Dobson, R., and Giovannoni, G. (2019). Multiple sclerosis - a review. European journal of neurology *26*, 27-40.

Dolmetsch, R.E., Lewis, R.S., Goodnow, C.C., and Healy, J.I. (1997). Differential activation of transcription factors induced by Ca2+ response amplitude and duration. Nature *386*, 855-858.

Dolmetsch, R.E., Xu, K., and Lewis, R.S. (1998). Calcium oscillations increase the efficiency and specificity of gene expression. Nature *392*, 933-936.

Druzd, D., Matveeva, O., Ince, L., Harrison, U., He, W., Schmal, C., Herzel, H., Tsang, A.H., Kawakami, N., Leliavski, A*., et al.* (2017). Lymphocyte Circadian Clocks Control Lymph Node Trafficking and Adaptive Immune Responses. Immunity *46*, 120-132.

Du, C., and Sriram, S. (2002). Increased Severity of Experimental Allergic Encephalomyelitis in lyn^{−/−} Mice in the Absence of Elevated Proinflammatory Cytokine Response in the Central Nervous System. The Journal of Immunology *168*, 3105-3112.

Engelhardt, B., and Ransohoff, R.M. (2005). The ins and outs of T-lymphocyte trafficking to the CNS: anatomical sites and molecular mechanisms. Trends in immunology *26*, 485-495.

Engelhardt, B., and Ransohoff, R.M. (2012). Capture, crawl, cross: the T cell code to breach the blood–brain barriers. Trends in Immunology *33*, 579-589.

Esplugues, E., Huber, S., Gagliani, N., Hauser, A.E., Town, T., Wan, Y.Y., O'Connor, W., Jr., Rongvaux, A., Van Rooijen, N., Haberman, A.M*., et al.* (2011). Control of TH17 cells occurs in the small intestine. Nature *475*, 514-518.

Eugster, H.P., Frei, K., Bachmann, R., Bluethmann, H., Lassmann, H., and Fontana, A. (1999). Severity of symptoms and demyelination in MOG-induced EAE depends on TNFR1. European journal of immunology *29*, 626-632.

Fabriek, B.O., Van Haastert, E.S., Galea, I., Polfliet, M.M., Döpp, E.D., Van Den Heuvel, M.M., Van Den Berg, T.K., De Groot, C.J., Van Der Valk, P., and Dijkstra, C.D. (2005). CD163-positive perivascular macrophages in the human CNS express molecules for antigen recognition and presentation. Glia *51*, 297-305.

Farkas, A.M., Panea, C., Goto, Y., Nakato, G., Galan-Diez, M., Narushima, S., Honda, K., and Ivanov, I.I. (2015). Induction of Th17 cells by segmented filamentous bacteria in the murine intestine. Journal of Immunological Methods *421*, 104-111.

Feske, S. (2007). Calcium signalling in lymphocyte activation and disease. Nature reviews Immunology *7*, 690-702.

Filippi, M., Rocca, M.A., Pagani, E., Iannucci, G., Sormani, M.P., Fazekas, F., Ropele, S., Hommes, O.R., and Comi, G. (2004). European study on intravenous immunoglobulin in multiple sclerosis: results of magnetization transfer magnetic resonance imaging analysis. Archives of neurology *61*, 1409-1412.

Filippi, M., Rovaris, M., Rice, G.P., Sormani, M.P., Iannucci, G., Giacomotti, L., and Comi, G. (2000). The effect of cladribine on T(1) 'black hole' changes in progressive MS. Journal of the neurological sciences *176*, 42-44.

Finegold, S.M. (2011). State of the art; microbiology in health and disease. Intestinal bacterial flora in autism. Anaerobe *17*, 367-368.

Flügel, A., Berkowicz, T., Ritter, T., Labeur, M., Jenne, D.E., Li, Z., Ellwart, J.W., Willem, M., Lassmann, H., and Wekerle, H. (2001). Migratory activity and functional changes of green fluorescent effector cells before and during experimental autoimmune encephalomyelitis. Immunity *14*, 547-560.

Flügel, A., Odoardi, F., Nosov, M., and Kawakami, N. (2007). Autoaggressive effector T cells in the course of experimental autoimmune encephalomyelitis visualized in the light of two-photon microscopy. Journal of neuroimmunology *191*, 86-97.

Fracchia, K.M., Pai, C.Y., and Walsh, C.M. (2013). Modulation of T Cell Metabolism and Function through Calcium Signaling. Frontiers in immunology *4*, 324.

Freund, J., and McDermott, K. (1942). Sensitization to horse serum by means of adjuvants. Proceedings of the society for experimental biology and medicine *49*, 548-553.

Fujinami, R., and Oldstone, M. (1985). Amino acid homology between the encephalitogenic site of myelin basic protein and virus: mechanism for autoimmunity. Science *230*, 1043-1045.

Fujinami, R.S., Oldstone, M.B., Wroblewska, Z., Frankel, M.E., and Koprowski, H. (1983). Molecular mimicry in virus infection: crossreaction of measles virus phosphoprotein or of herpes simplex virus protein with human intermediate filaments. Proceedings of the National Academy of Sciences of the United States of America *80*, 2346-2350.

Fujinami, R.S., von Herrath, M.G., Christen, U., and Whitton, J.L. (2006). Molecular mimicry, bystander activation, or viral persistence: infections and autoimmune disease. Clinical microbiology reviews *19*, 80-94.

Gaboriau-Routhiau, V., Rakotobe, S., Lécuyer, E., Mulder, I., Lan, A., Bridonneau, C., Rochet, V., Pisi, A., De Paepe, M., Brandi, G.*, et al.* (2009). The key role of segmented filamentous bacteria in the coordinated maturation of gut helper T cell responses. Immunity *31*, 677-689.

Gaublomme, J.T., Yosef, N., Lee, Y., Gertner, R.S., Yang, L.V., Wu, C., Pandolfi, P.P., Mak, T., Satija, R., Shalek, A.K.*, et al.* (2015). Single-Cell Genomics Unveils Critical Regulators of Th17 Cell Pathogenicity. Cell *163*, 1400-1412.

GBD (2017). Global, regional, and national burden of neurological disorders during 1990-2015: a systematic analysis for the Global Burden of Disease Study 2015. The Lancet Neurology *16*, 877-897.

Gold, R., Linington, C., and Lassmann, H. (2006). Understanding pathogenesis and therapy of multiple sclerosis via animal models: 70 years of merits and culprits in experimental autoimmune encephalomyelitis research. Brain : a journal of neurology *129*, 1953-1971.

Goverman, J. (2009). Autoimmune T cell responses in the central nervous system. Nature reviews Immunology *9*, 393-407.

Goverman, J., Woods, A., Larson, L., Weiner, L.P., Hood, L., and Zaller, D.M. (1993). Transgenic mice that express a myelin basic protein-specific T cell receptor develop spontaneous autoimmunity. Cell *72*, 551-560.

Gregory, A.P., Dendrou, C.A., Attfield, K.E., Haghikia, A., Xifara, D.K., Butter, F., Poschmann, G., Kaur, G., Lambert, L., Leach, O.A.*, et al.* (2012). TNF receptor 1 genetic risk mirrors outcome of anti-TNF therapy in multiple sclerosis. Nature *488*, 508-511.

Greter, M., Heppner, F.L., Lemos, M.P., Odermatt, B.M., Goebels, N., Laufer, T., Noelle, R.J., and Becher, B. (2005). Dendritic cells permit immune invasion of the CNS in an animal model of multiple sclerosis. Nature medicine *11*, 328-334.

Harkiolaki, M., Holmes, S.L., Svendsen, P., Gregersen, J.W., Jensen, L.T., McMahon, R., Friese, M.A., van Boxel, G., Etzensperger, R., Tzartos, J.S*., et al.* (2009). T cell-mediated autoimmune disease due to low-affinity crossreactivity to common microbial peptides. Immunity *30*, 348-357.

Hedrick, M.N., Lonsdorf, A.S., Hwang, S.T., and Farber, J.M. (2010). CCR6 as a possible therapeutic target in psoriasis. Expert opinion on therapeutic targets *14*, 911-922.

Heissmeyer, V., and Rao, A. (2004). E3 ligases in T cell anergy--turning immune responses into tolerance. Science's STKE : signal transduction knowledge environment *2004*, pe29.

Hernández-Santos, N., and Gaffen, S.L. (2012). Th17 cells in immunity to Candida albicans. Cell host & microbe *11*, 425-435.

Herz, J., Zipp, F., and Siffrin, V. (2010). Neurodegeneration in autoimmune CNS inflammation. Experimental Neurology *225*, 9-17.

Hill, D.A., and Artis, D. (2010). Intestinal bacteria and the regulation of immune cell homeostasis. Annual review of immunology *28*, 623-667.

Hogan, P.G., Lewis, R.S., and Rao, A. (2010). Molecular basis of calcium signaling in lymphocytes: STIM and ORAI. Annual review of immunology *28*, 491-533.

Horai, R., Zárate-Bladés, C.R., Dillenburg-Pilla, P., Chen, J., Kielczewski, J.L., Silver, P.B., Jittayasothorn, Y., Chan, C.C., Yamane, H., Honda, K*., et al.* (2015). Microbiota-Dependent Activation of an Autoreactive T Cell Receptor Provokes Autoimmunity in an Immunologically Privileged Site. Immunity *43*, 343-353.

Hsiao, Elaine Y., McBride, Sara W., Hsien, S., Sharon, G., Hyde, Embriette R., McCue, T., Codelli, Julian A., Chow, J., Reisman, Sarah E., Petrosino, Joseph F*., et al.* (2013). Microbiota Modulate Behavioral and Physiological Abnormalities Associated with Neurodevelopmental Disorders. Cell *155*, 1451-1463.

Ivanov, II, Frutos Rde, L., Manel, N., Yoshinaga, K., Rifkin, D.B., Sartor, R.B., Finlay, B.B., and Littman, D.R. (2008). Specific microbiota direct the differentiation of IL-17-producing T-helper cells in the mucosa of the small intestine. Cell host & microbe *4*, 337-349.

Ivanov, I.I., Atarashi, K., Manel, N., Brodie, E.L., Shima, T., Karaoz, U., Wei, D., Goldfarb, K.C., Santee, C.A., Lynch, S.V*., et al.* (2009). Induction of Intestinal Th17 Cells by Segmented Filamentous Bacteria. Cell *139*, 485-498.

Jangi, S., Gandhi, R., Cox, L.M., Li, N., von Glehn, F., Yan, R., Patel, B., Mazzola, M.A., Liu, S., Glanz, B.L*., et al.* (2016). Alterations of the human gut microbiome in multiple sclerosis. Nature communications *7*, 12015.

Joseph, N., Reicher, B., and Barda-Saad, M. (2014). The calcium feedback loop and T cell activation: how cytoskeleton networks control intracellular calcium flux. Biochimica et biophysica acta *1838*, 557-568.

Kabat, E.A., Wolf, A., and Bezer, A.E. (1947). The rapid production of acute disseminated encephalomyelitis in rhesus monkeys by injection of heterologous and homologous brain tissue with adjuvants. Journal of experimental medicine *85*, 117-130.

Karni, A., Bakimer-Kleiner, R., Abramsky, O., and Ben-Nun, A. (1999). Elevated levels of antibody to myelin oligodendrocyte glycoprotein is not specific for patients with multiple sclerosis. Archives of neurology *56*, 311-315.

Kawakami, N., Bartholomäus, I., Pesic, M., and Mues, M. (2012). An autoimmunity odyssey: how autoreactive T cells infiltrate into the CNS. Immunological reviews *248*, 140-155.

Kawakami, N., Lassmann, S., Li, Z., Odoardi, F., Ritter, T., Ziemssen, T., Klinkert, W.E., Ellwart, J.W., Bradl, M., Krivacic, K*., et al.* (2004). The activation status of neuroantigen-specific T cells in the target organ determines the clinical outcome of autoimmune encephalomyelitis. J Exp Med *199*, 185-197.

Kebir, H., Kreymborg, K., Ifergan, I., Dodelet-Devillers, A., Cayrol, R., Bernard, M., Giuliani, F., Arbour, N., Becher, B., and Prat, A. (2007). Human TH17 lymphocytes promote blood-brain barrier disruption and central nervous system inflammation. Nature medicine *13*, 1173-1175.

Kerlero de Rosbo, N., Hoffman, M., Mendel, I., Yust, I., Kaye, J., Bakimer, R., Flechter, S., Abramsky, O., Milo, R., Karni, A*., et al.* (1997). Predominance of the autoimmune response to myelin oligodendrocyte glycoprotein (MOG) in multiple sclerosis: reactivity to the extracellular domain of MOG is directed against three main regions. European journal of immunology *27*, 3059-3069.

Kibler, R.F., Fritz, R.B., Chou, F., Jen Chou, C.H., Peacocke, N.Y., Brown, N.M., and McFarlin, D.E. (1977). Immune response of Lewis rats to peptide C1 (residues 68-88) of guinea pig and rat myelin basic proteins. The Journal of experimental medicine *146*, 1323-1331.

Kim, D., Paggi, J.M., Park, C., Bennett, C., and Salzberg, S.L. (2019). Graph-based genome alignment and genotyping with HISAT2 and HISAT-genotype. Nature Biotechnology *37*, 907-915.

Kivisäkk, P., Imitola, J., Rasmussen, S., Elyaman, W., Zhu, B., Ransohoff, R.M., and Khoury, S.J. (2009). Localizing central nervous system immune surveillance: meningeal antigen-presenting cells activate T cells during experimental autoimmune encephalomyelitis. Annals of neurology *65*, 457-469.

Koritschoner, R., and Schweinburg, F. (1925). Induktion von Paralyse und Rückenmarksentzündung durch Immunisierung von Kaninchen mit menschlichem Rückenmarksgewebe. Z Immunitätsf Exp Therapie *42*, 217-283.

Korn, T., Bettelli, E., Oukka, M., and Kuchroo, V.K. (2009). IL-17 and Th17 Cells. Annu Rev Immunol *27*, 485-517.

Körner, H., Riminton, D.S., Strickland, D.H., Lemckert, F.A., Pollard, J.D., and Sedgwick, J.D. (1997). Critical points of tumor necrosis factor action in central nervous system autoimmune inflammation defined by gene targeting. The Journal of experimental medicine *186*, 1585-1590.

Krishnamoorthy, G., Lassmann, H., Wekerle, H., and Holz, A. (2006). Spontaneous opticospinal encephalomyelitis in a double-transgenic mouse model of autoimmune T cell/B cell cooperation. The Journal of clinical investigation *116*, 2385-2392.

Krishnamoorthy, G., and Wekerle, H. (2009). EAE: An immunologist's magic eye. European journal of immunology *39*, 2031-2035.

Kuchroo, V.K., Martin, C.A., Greer, J.M., Ju, S.T., Sobel, R.A., and Dorf, M.E. (1993). Cytokines and adhesion molecules contribute to the ability of myelin proteolipid protein-specific T cell clones to mediate experimental allergic encephalomyelitis. Journal of immunology (Baltimore, Md : 1950) *151*, 4371-4382.

Kunimura, K., Uruno, T., and Fukui, Y. (2019). DOCK family proteins: key players in immune surveillance mechanisms. International Immunology *32*, 5-15.

Kyratsous, N.I., Bauer, I.J., Zhang, G., Pesic, M., Bartholomäus, I., Mues, M., Fang, P., Wörner, M., Everts, S., Ellwart, J.W.*, et al.* (2017). Visualizing context-dependent calcium signaling in encephalitogenic T cells in vivo by two-photon microscopy. Proceedings of the National Academy of Sciences of the United States of America *114*, E6381-e6389.

Lando, Z., Teitelbaum, D., and Arnon, R. (1979). Genetic control of susceptibility to experimental allergic encephalomyelitis in mice. Immunogenetics *9*, 435-442.

Lanzillo, R., Bonavita, S., Quarantelli, M., Vacca, G., Lus, G., Amato, L., Carotenuto, A., Tedeschi, G., Orefice, G., and Brescia Morra, V. (2013). Natalizumab is effective in multiple sclerosis patients switching from other disease modifying therapies in clinical practice. Neurological sciences : official journal of the Italian Neurological Society and of the Italian Society of Clinical Neurophysiology *34*, 521-528.

Lassmann, H., Brück, W., and Lucchinetti, C.F. (2007). The immunopathology of multiple sclerosis: an overview. Brain pathology (Zurich, Switzerland) *17*, 210-218.

Lee, Y.K., Menezes, J.S., Umesaki, Y., and Mazmanian, S.K. (2011). Proinflammatory T-cell responses to gut microbiota promote experimental autoimmune encephalomyelitis. Proceedings of the National Academy of Sciences *108*, 4615.

Lehmann, P.V., Sercarz, E.E., Forsthuber, T., Dayan, C.M., and Gammon, G. (1993). Determinant spreading and the dynamics of the autoimmune T-cell repertoire. Immunology today *14*, 203-208.

Levine, S., and Sowinski, R. (1973). Experimental allergic encephalomyelitis in inbred and outbred mice. Journal of immunology (Baltimore, Md : 1950) *110*, 139-143.

Lewis, R.S. (2001). Calcium Signaling Mechanisms in T Lymphocytes. Annual review of immunology *19*, 497-521.

Lewis, R.S., and Cahalan, M.D. (1988). The plasticity of ion channels: parallels between the nervous and immune systems. Trends Neurosci *11*, 214-218.

Li, W., Llopis, J., Whitney, M., Zlokarnik, G., and Tsien, R.Y. (1998). Cell-permeant caged InsP3 ester shows that Ca2+ spike frequency can optimize gene expression. Nature *392*, 936-941.

Liblau, R., Tournier-Lasserve, E., Maciazek, J., Dumas, G., Siffert, O., Hashim, G., and Bach, M.A. (1991). T cell response to myelin basic protein epitopes in multiple sclerosis patients and healthy subjects. European journal of immunology *21*, 1391-1395.

Linnington, C., Webb, M., and Woodhams, P.L. (1984). A novel myelin-associated glycoprotein defined by a mouse monoclonal antibody. Journal of neuroimmunology *6*, 387-396.

Litzenburger, T., Fässler, R., Bauer, J., Lassmann, H., Linington, C., Wekerle, H., and Iglesias, A. (1998). B lymphocytes producing demyelinating autoantibodies: development and function in gene-targeted transgenic mice. The Journal of experimental medicine *188*, 169-180.

Lodygin, D., Hermann, M., Schweingruber, N., Flügel-Koch, C., Watanabe, T., Schlosser, C., Merlini, A., Körner, H., Chang, H.-F., Fischer, H.J*., et al.* (2019). β-Synuclein-reactive T cells induce autoimmune CNS grey matter degeneration. Nature *566*, 503-508.

Love, M.I., Huber, W., and Anders, S. (2014). Moderated estimation of fold change and dispersion for RNA-seq data with DESeq2. Genome Biology *15*, 550.

Lublin, F.D., and Reingold, S.C. (1996). Defining the clinical course of multiple sclerosis: results of an international survey. National Multiple Sclerosis Society (USA) Advisory Committee on Clinical Trials of New Agents in Multiple Sclerosis. Neurology *46*, 907-911.

Lublin, F.D., Reingold, S.C., Cohen, J.A., Cutter, G.R., Sørensen, P.S., Thompson, A.J., Wolinsky, J.S., Balcer, L.J., Banwell, B., Barkhof, F*., et al.* (2014). Defining the clinical course of multiple sclerosis: the 2013 revisions. Neurology *83*, 278-286.

Lundmark, F., Duvefelt, K., Iacobaeus, E., Kockum, I., Wallström, E., Khademi, M., Oturai, A., Ryder, L.P., Saarela, J., Harbo, H.F*., et al.* (2007). Variation in interleukin 7 receptor alpha chain (IL7R) influences risk of multiple sclerosis. Nature genetics *39*, 1108-1113.

Macian, F. (2005). NFAT proteins: key regulators of T-cell development and function. Nature reviews Immunology *5*, 472-484.

Maier, L.M., Lowe, C.E., Cooper, J., Downes, K., Anderson, D.E., Severson, C., Clark, P.M., Healy, B., Walker, N., Aubin, C*., et al.* (2009). IL2RA genetic heterogeneity in multiple sclerosis and type 1 diabetes susceptibility and soluble interleukin-2 receptor production. PLoS genetics *5*, e1000322.

Malipiero, U., Frei, K., Spanaus, K.S., Agresti, C., Lassmann, H., Hahne, M., Tschopp, J., Eugster, H.P., and Fontana, A. (1997). Myelin oligodendrocyte glycoprotein-induced autoimmune encephalomyelitis is chronic/relapsing in perforin knockout mice, but monophasic in Fas- and Fas ligand-deficient lpr and gld mice. European journal of immunology *27*, 3151-3160.

Mangalam, A., Shahi, S.K., Luckey, D., Karau, M., Marietta, E., Luo, N., Choung, R.S., Ju, J., Sompallae, R., Gibson-Corley, K*., et al.* (2017). Human Gut-Derived Commensal Bacteria Suppress CNS Inflammatory and Demyelinating Disease. Cell reports *20*, 1269-1277.

Marafini, I., Monteleone, I., Dinallo, V., Di Fusco, D., De Simone, V., Laudisi, F., Fantini, M.C., Di Sabatino, A., Pallone, F., and Monteleone, G. (2017). CCL20 Is Negatively Regulated by TGF-β1 in Intestinal Epithelial Cells and Reduced in Crohn's Disease Patients With a Successful Response to Mongersen, a Smad7 Antisense Oligonucleotide. Journal of Crohn's & colitis *11*, 603-609.

Maynard, C.L., Harrington, L.E., Janowski, K.M., Oliver, J.R., Zindl, C.L., Rudensky, A.Y., and Weaver, C.T. (2007). Regulatory T cells expressing interleukin 10 develop from Foxp3+ and Foxp3- precursor cells in the absence of interleukin 10. Nature immunology *8*, 931-941.

McCoy, L., Tsunoda, I., and Fujinami, R.S. (2006). Multiple sclerosis and virus induced immune responses: Autoimmunity can be primed by molecular mimicry and augmented by bystander activation. Autoimmunity *39*, 9-19.

Mendel, I., Kerlero de Rosbo, N., and Ben-Nun, A. (1995). A myelin oligodendrocyte glycoprotein peptide induces typical chronic experimental autoimmune encephalomyelitis in H-2b mice: fine specificity and T cell receptor V beta expression of encephalitogenic T cells. European journal of immunology *25*, 1951-1959.

Meyer zu Horste, G., Wu, C., Wang, C., Cong, L., Pawlak, M., Lee, Y., Elyaman, W., Xiao, S., Regev, A., and Kuchroo, V.K. (2016). RBPJ Controls Development of Pathogenic Th17 Cells by Regulating IL-23 Receptor Expression. Cell reports *16*, 392-404.

Miller, S.D., Vanderlugt, C.L., Begolka, W.S., Pao, W., Yauch, R.L., Neville, K.L., Katz-Levy, Y., Carrizosa, A., and Kim, B.S. (1997). Persistent infection with Theiler's virus leads to CNS autoimmunity via epitope spreading. Nature medicine *3*, 1133-1136.

Miyake, S., Kim, S., Suda, W., Oshima, K., Nakamura, M., Matsuoka, T., Chihara, N., Tomita, A., Sato, W., Kim, S.W*., et al.* (2015). Dysbiosis in the Gut Microbiota of Patients with Multiple Sclerosis, with a Striking Depletion of Species Belonging to Clostridia XIVa and IV Clusters. PloS one *10*, e0137429.

Miyauchi, E., Kim, S.-W., Suda, W., Kawasumi, M., Onawa, S., Taguchi-Atarashi, N., Morita, H., Taylor, T.D., Hattori, M., and Ohno, H. (2020). Gut microorganisms act together to exacerbate inflammation in spinal cords. Nature *585*, 102-106.

Miyawaki, A., Llopis, J., Heim, R., McCaffery, J.M., Adams, J.A., Ikura, M., and Tsien, R.Y. (1997). Fluorescent indicators for Ca2+based on green fluorescent proteins and calmodulin. Nature *388*, 882-887.

Moghadamrad, S., McCoy, K.D., Geuking, M.B., Sägesser, H., Kirundi, J., Macpherson, A.J., and De Gottardi, A. (2015). Attenuated portal hypertension in germ-free mice: Function of bacterial flora on the development of mesenteric lymphatic and blood vessels. Hepatology *61*, 1685-1695.

Molyneux, P.D., Kappos, L., Polman, C., Pozzilli, C., Barkhof, F., Filippi, M., Yousry, T., Hahn, D., Wagner, K., Ghazi, M*., et al.* (2000). The effect of interferon beta-1b treatment on MRI measures of cerebral atrophy in secondary progressive multiple sclerosis. European Study Group on Interferon beta-1b in secondary progressive multiple sclerosis. Brain : a journal of neurology *123 (Pt 11)*, 2256-2263.

Mowat, A.M., and Agace, W.W. (2014). Regional specialization within the intestinal immune system. Nature reviews Immunology *14*, 667-685.

Mues, M., Bartholomäus, I., Thestrup, T., Griesbeck, O., Wekerle, H., Kawakami, N., and Krishnamoorthy, G. (2013). Real-time in vivo analysis of T cell activation in the central nervous system using a genetically encoded calcium indicator. Nature medicine *19*, 778-783.

Munch, M., Riisom, K., Christensen, T., Møller-Larsen, A., and Haahr, S. (1998). The significance of Epstein-Barr virus seropositivity in multiple sclerosis patients? Acta neurologica Scandinavica *97*, 171-174.

Munoz, J.J., Bernard, C.C., and Mackay, I.R. (1984). Elicitation of experimental allergic encephalomyelitis (EAE) in mice with the aid of pertussigen. Cellular immunology *83*, 92-100.

Murfee, W.L., Rappleye, J.W., Ceballos, M., and Schmid-Schönbein, G.W. (2007). Discontinuous expression of endothelial cell adhesion molecules along initial lymphatic vessels in mesentery: the primary valve structure. Lymphatic research and biology *5*, 81-89.

Murphy, K., Travers, P., and Walport, M. (2012). Janeway's immunobiology, 8th edn New York. NY: Garland Science[Google Scholar].

Ochoa-Repáraz, J., Mielcarz, D.W., Ditrio, L.E., Burroughs, A.R., Begum-Haque, S., Dasgupta, S., Kasper, D.L., and Kasper, L.H. (2010). Central nervous system demyelinating disease protection by the human commensal Bacteroides fragilis depends on polysaccharide A expression. J Immunol *185*, 4101-4108.

Ochoa-Repáraz, J., Mielcarz, D.W., Ditrio, L.E., Burroughs, A.R., Foureau, D.M., Haque-Begum, S., and Kasper, L.H. (2009). Role of Gut Commensal Microflora in the Development of Experimental Autoimmune Encephalomyelitis. The Journal of Immunology *183*, 6041.

Ota, K., Matsui, M., Milford, E.L., Mackin, G.A., Weiner, H.L., and Hafler, D.A. (1990). T-cell recognition of an immunodominant myelin basic protein epitope in multiple sclerosis. Nature *346*, 183-187.

Oxenius, A., Bachmann, M.F., Zinkernagel, R.M., and Hengartner, H. (1998). Virus-specific MHC-class II-restricted TCR-transgenic mice: effects on humoral and cellular immune responses after viral infection. Eur J Immunol *28*, 390-400.

Pau, D., Al Zubidi, N., Yalamanchili, S., Plant, G.T., and Lee, A.G. (2011). Optic neuritis. Eye (London, England) *25*, 833-842.

Pesic, M., Bartholomaus, I., Kyratsous, N.I., Heissmeyer, V., Wekerle, H., and Kawakami, N. (2013). 2-photon imaging of phagocyte-mediated T cell activation in the CNS. J Clin Invest *123*, 1192-1201.

Pette, M., Fujita, K., Kitze, B., Whitaker, J.N., Albert, E., Kappos, L., and Wekerle, H. (1990). Myelin basic protein-specific T lymphocyte lines from MS patients and healthy individuals. Neurology *40*, 1770-1776.

Piccio, L., Rossi, B., Scarpini, E., Laudanna, C., Giagulli, C., Issekutz, A.C., Vestweber, D., Butcher, E.C., and Constantin, G. (2002). Molecular mechanisms involved in lymphocyte recruitment in inflamed brain microvessels: critical roles for P-selectin glycoprotein ligand-1 and heterotrimeric G(i)-linked receptors. Journal of immunology (Baltimore, Md : 1950) *168*, 1940-1949.

Pittock, S.J., Reindl, M., Achenbach, S., Berger, T., Bruck, W., Konig, F., Morales, Y., Lassmann, H., Bryant, S., Moore, S.B.*, et al.* (2007). Myelin oligodendrocyte glycoprotein antibodies in pathologically proven multiple sclerosis: frequency, stability and clinicopathologic correlations. Multiple sclerosis (Houndmills, Basingstoke, England) *13*, 7-16.

Pöllinger, B., Krishnamoorthy, G., Berer, K., Lassmann, H., Bösl, M.R., Dunn, R., Domingues, H.S., Holz, A., Kurschus, F.C., and Wekerle, H. (2009). Spontaneous relapsing-remitting EAE in the SJL/J mouse: MOG-reactive transgenic T cells recruit endogenous MOG-specific B cells. J Exp Med *206*, 1303-1316.

Polman, C.H., O'Connor, P.W., Havrdova, E., Hutchinson, M., Kappos, L., Miller, D.H., Phillips, J.T., Lublin, F.D., Giovannoni, G., Wajgt, A.*, et al.* (2006). A randomized, placebo-controlled trial of natalizumab for relapsing multiple sclerosis. N Engl J Med *354*, 899-910.

Quintana, A., Griesemer, D., Schwarz, E.C., and Hoth, M. (2005). Calcium-dependent activation of T-lymphocytes. Pflügers Archiv *450*, 1-12.

Raddassi, K., Kent, S.C., Yang, J., Bourcier, K., Bradshaw, E.M., Seyfert-Margolis, V., Nepom, G.T., Kwok, W.W., and Hafler, D.A. (2011). Increased frequencies of myelin oligodendrocyte glycoprotein/MHC class II-binding CD4 cells in patients with multiple sclerosis. Journal of immunology (Baltimore, Md : 1950) *187*, 1039-1046.

Reboldi, A., Coisne, C., Baumjohann, D., Benvenuto, F., Bottinelli, D., Lira, S., Uccelli, A., Lanzavecchia, A., Engelhardt, B., and Sallusto, F. (2009). C-C chemokine receptor 6-regulated entry of TH-17 cells into the CNS through the choroid plexus is required for the initiation of EAE. Nature immunology *10*, 514-523.

Reich, D.S., Lucchinetti, C.F., and Calabresi, P.A. (2018). Multiple Sclerosis. N Engl J Med *378*, 169-180.

Revy, P., Sospedra, M., Barbour, B., and Trautmann, A. (2001). Functional antigen-independent synapses formed between T cells and dendritic cells. Nature immunology *2*, 925-931.

Rivers, T.M., Sprunt, D., and Berry, G. (1933). Observations on attempts to produce acute disseminated encephalomyelitis in monkeys. Journal of Experimental Medicine *58*, 39-53.

Round, J.L., and Mazmanian, S.K. (2009). The gut microbiota shapes intestinal immune responses during health and disease. Nature reviews Immunology *9*, 313-323.

Sartor, R.B. (2015). Optimal sampling of the intestinal microbiota for research. Nature Reviews Gastroenterology & Hepatology *12*, 253-254.

Sathaliyawala, T., Kubota, M., Yudanin, N., Turner, D., Camp, P., Thome, J.J., Bickham, K.L., Lerner, H., Goldstein, M., Sykes, M.*, et al.* (2013). Distribution and compartmentalization of human circulating and tissue-resident memory T cell subsets. Immunity *38*, 187-197.

Sawcer, S., Hellenthal, G., Pirinen, M., Spencer, C.C., Patsopoulos, N.A., Moutsianas, L., Dilthey, A., Su, Z., Freeman, C., Hunt, S.E.*, et al.* (2011). Genetic risk and a primary role for cell-mediated immune mechanisms in multiple sclerosis. Nature *476*, 214-219.

Scheperjans, F., Aho, V., Pereira, P.A., Koskinen, K., Paulin, L., Pekkonen, E., Haapaniemi, E., Kaakkola, S., Eerola-Rautio, J., Pohja, M.*, et al.* (2015). Gut microbiota are related to Parkinson's disease and clinical phenotype. Movement disorders : official journal of the Movement Disorder Society *30*, 350-358.

Schmid-Schönbein, G.W. (1990). Microlymphatics and lymph flow. Physiological reviews *70*, 987-1028.

Secher, T., Kassem, S., Benamar, M., Bernard, I., Boury, M., Barreau, F., Oswald, E., and Saoudi, A. (2017). Oral Administration of the Probiotic Strain Escherichia coli Nissle 1917 Reduces Susceptibility to Neuroinflammation and Repairs Experimental Autoimmune Encephalomyelitis-Induced Intestinal Barrier Dysfunction. Frontiers in immunology *8*, 1096.

Sharief, M.K., and Thompson, E.J. (1993). Correlation of interleukin-2 and soluble interleukin-2 receptor with clinical activity of multiple sclerosis. Journal of neurology, neurosurgery, and psychiatry *56*, 169-174.

Smolders, J., Menheere, P., Kessels, A., Damoiseaux, J., and Hupperts, R. (2008). Association of vitamin D metabolite levels with relapse rate and disability in multiple sclerosis. Multiple sclerosis (Houndmills, Basingstoke, England) *14*, 1220-1224.

Sospedra, M., and Martin, R. (2005). Immunology of multiple sclerosis. Annual review of immunology *23*, 683-747.

Spadaro, M., Winklmeier, S., Beltrán, E., Macrini, C., Höftberger, R., Schuh, E., Thaler, F.S., Gerdes, L.A., Laurent, S., Gerhards, R.*, et al.* (2018). Pathogenicity of human antibodies against myelin oligodendrocyte glycoprotein. Ann Neurol *84*, 315-328.

Stromnes, I.M., and Goverman, J.M. (2006). Active induction of experimental allergic encephalomyelitis. Nature protocols *1*, 1810-1819.

Strunk, T., Bubel, S., Mascher, B., Schlenke, P., Kirchner, H., and Wandinger, K.P. (2000). Increased numbers of CCR5+ interferon-gamma- and tumor necrosis factor-alpha-secreting T lymphocytes in multiple sclerosis patients. Annals of neurology *47*, 269-273.

Stys, P.K., Zamponi, G.W., van Minnen, J., and Geurts, J.J. (2012). Will the real multiple sclerosis please stand up? Nature reviews Neuroscience *13*, 507-514.

Sun, J., Link, H., Olsson, T., Xiao, B.G., Andersson, G., Ekre, H.P., Linington, C., and Diener, P. (1991a). T and B cell responses to myelin-oligodendrocyte glycoprotein in multiple sclerosis. Journal of immunology (Baltimore, Md : 1950) *146*, 1490-1495.

Sun, J.B., Olsson, T., Wang, W.Z., Xiao, B.G., Kostulas, V., Fredrikson, S., Ekre, H.P., and Link, H. (1991b). Autoreactive T and B cells responding to myelin proteolipid protein in multiple sclerosis and controls. European journal of immunology *21*, 1461-1468.

Teitelbaum, D., Meshorer, A., Hirshfeld, T., Arnon, R., and Sela, M. (1971). Suppression of experimental allergic encephalomyelitis by a synthetic polypeptide. European journal of immunology *1*, 242-248.

Thestrup, T., Litzlbauer, J., Bartholomäus, I., Mues, M., Russo, L., Dana, H., Kovalchuk, Y., Liang, Y., Kalamakis, G., Laukat, Y.*, et al.* (2014). Optimized ratiometric calcium sensors for functional in vivo imaging of neurons and T lymphocytes. Nature methods *11*, 175-182.

Thompson, A.J., Banwell, B.L., Barkhof, F., Carroll, W.M., Coetzee, T., Comi, G., Correale, J., Fazekas, F., Filippi, M., Freedman, M.S.*, et al.* (2018). Diagnosis of multiple sclerosis: 2017 revisions of the McDonald criteria. The Lancet Neurology *17*, 162-173.

Tilney, N.L. (1971). Patterns of lymphatic drainage in the adult laboratory rat. Journal of anatomy *109*, 369-383.

Tran, E.H., Prince, E.N., and Owens, T. (2000). IFN-γ Shapes Immune Invasion of the Central Nervous System Via Regulation of Chemokines. The Journal of Immunology *164*, 2759-2768.

Trebak, M., and Kinet, J.-P. (2019). Calcium signalling in T cells. Nature Reviews Immunology *19*, 154-169.

Umesaki, Y., Setoyama, H., Matsumoto, S., and Okada, Y. (1993). Expansion of alpha beta T-cell receptor-bearing intestinal intraepithelial lymphocytes after microbial colonization in germ-free mice and its independence from thymus. Immunology *79*, 32-37.

Van den Broeck, W., Derore, A., and Simoens, P. (2006). Anatomy and nomenclature of murine lymph nodes: Descriptive study and nomenclatory standardization in BALB/cAnNCrl mice. Journal of Immunological Methods *312*, 12-19.

Vanderlugt, C.J., and Miller, S.D. (1996). Epitope spreading. Current opinion in immunology *8*, 831-836.

Vanderlugt, C.L., and Miller, S.D. (2002). Epitope spreading in immune-mediated diseases: implications for immunotherapy. Nature reviews Immunology *2*, 85-95.

Vandevyver, C., Mertens, N., van den Elsen, P., Medaer, R., Raus, J., and Zhang, J. (1995). Clonal expansion of myelin basic protein-reactive T cells in patients with multiple sclerosis: restricted T cell receptor V gene rearrangements and CDR3 sequence. Eur J Immunol *25*, 958-968.

Vogt, N.M., Kerby, R.L., Dill-McFarland, K.A., Harding, S.J., Merluzzi, A.P., Johnson, S.C., Carlsson, C.M., Asthana, S., Zetterberg, H., Blennow, K.*, et al.* (2017). Gut microbiome alterations in Alzheimer's disease. Scientific reports *7*, 13537.

Wagner, C., Bürger, A., Radsak, M., Blum, S., Hug, F., and Hänsch, G.M. (2000). Fibronectin synthesis by activated T lymphocytes: up-regulation of a surface-associated isoform with signalling function. Immunology *99*, 532-539.

Walker, L.S., and Abbas, A.K. (2002). The enemy within: keeping self-reactive T cells at bay in the periphery. Nature reviews Immunology *2*, 11-19.

Wang, C., Kang, S.G., Lee, J., Sun, Z., and Kim, C.H. (2009). The roles of CCR6 in migration of Th17 cells and regulation of effector T-cell balance in the gut. Mucosal immunology *2*, 173-183.

Wang, C., Yosef, N., Gaublomme, J., Wu, C., Lee, Y., Clish, C.B., Kaminski, J., Xiao, S., Meyer Zu Horste, G., Pawlak, M.*, et al.* (2015). CD5L/AIM Regulates Lipid Biosynthesis and Restrains Th17 Cell Pathogenicity. Cell *163*, 1413-1427.

Weiner, H.L. (2004). Multiple Sclerosis Is an Inflammatory T-Cell–Mediated Autoimmune Disease. Archives of neurology *61*, 1613-1615.

Weinshenker, B.G., Bass, B., Rice, G.P., Noseworthy, J., Carriere, W., Baskerville, J., and Ebers, G.C. (1989). The natural history of multiple sclerosis: a geographically based study. I. Clinical course and disability. Brain : a journal of neurology *112 (Pt 1)*, 133-146.

Weissert, R., Wallström, E., Storch, M.K., Stefferl, A., Lorentzen, J., Lassmann, H., Linington, C., and Olsson, T. (1998). MHC haplotype-dependent regulation of MOG-induced EAE in rats. The Journal of clinical investigation *102*, 1265-1273.

Wekerle, H., Kojima, K., Lannes-Vieira, J., Lassmann, H., and Linington, C. (1994). Animal models. Annals of neurology *36 Suppl*, S47-53.

Wekerle, H., Linington, C., Lassmann, H., and Meyermann, R. (1986). Cellular immune reactivity within the CNS. Trends in Neurosciences *9*, 271-277.

Westall, F.C. (2006). Molecular Mimicry Revisited: Gut Bacteria and Multiple Sclerosis. Journal of Clinical Microbiology *44*, 2099-2104.

Wiesel, P.H., Norton, C., Glickman, S., and Kamm, M.A. (2001). Pathophysiology and management of bowel dysfunction in multiple sclerosis. European journal of gastroenterology & hepatology *13*, 441-448.

Willer, C.J., Dyment, D.A., Risch, N.J., Sadovnick, A.D., and Ebers, G.C. (2003). Twin concordance and sibling recurrence rates in multiple sclerosis. Proceedings of the National Academy of Sciences of the United States of America *100*, 12877-12882.

Wucherpfennig, K.W., and Strominger, J.L. (1995). Molecular mimicry in T cell-mediated autoimmunity: viral peptides activate human T cell clones specific for myelin basic protein. Cell *80*, 695-705.

Yamashita, M., Ukibe, K., Matsubara, Y., Hosoya, T., Sakai, F., Kon, S., Arima, Y., Murakami, M., Nakagawa, H., and Miyazaki, T. (2017). Lactobacillus helveticus SBT2171 Attenuates Experimental Autoimmune Encephalomyelitis in Mice. Frontiers in microbiology *8*, 2596.

Yang, Y., Torchinsky, M.B., Gobert, M., Xiong, H., Xu, M., Linehan, J.L., Alonzo, F., Ng, C., Chen, A., Lin, X.*, et al.* (2014). Focused specificity of intestinal TH17 cells towards commensal bacterial antigens. Nature *510*, 152-156.

Yasuda, K., Takeuchi, Y., and Hirota, K. (2019). The pathogenicity of Th17 cells in autoimmune diseases. Seminars in immunopathology *41*, 283-297.

Yasukawa, M., Yakushijin, Y., Hasegawa, H., Miyake, M., Hitsumoto, Y., Kimura, S., Takeuchi, N., and Fujita, S. (1993). Expression of perforin and membrane-bound lymphotoxin (tumor necrosis factor-beta) in virus-specific CD4+ human cytotoxic T-cell clones. Blood *81*, 1527-1534.

Yednock, T.A., Cannon, C., Fritz, L.C., Sanchez-Madrid, F., Steinman, L., and Karin, N. (1992). Prevention of experimental autoimmune encephalomyelitis by antibodies against alpha 4 beta 1 integrin. Nature *356*, 63-66.

Yokote, H., Miyake, S., Croxford, J.L., Oki, S., Mizusawa, H., and Yamamura, T. (2008). NKT cell-dependent amelioration of a mouse model of multiple sclerosis by altering gut flora. The American journal of pathology *173*, 1714-1723.

Zeitz, M., Schieferdecker, H.L., Ullrich, R., Jahn, H.U., James, S.P., and Riecken, E.O. (1991). Phenotype and function of lamina propria T lymphocytes. Immunologic research *10*, 199-206.

Zhang, J., Markovic-Plese, S., Lacet, B., Raus, J., Weiner, H.L., and Hafler, D.A. (1994). Increased frequency of interleukin 2-responsive T cells specific for myelin basic protein and proteolipid protein in peripheral blood and cerebrospinal fluid of patients with multiple sclerosis. The Journal of experimental medicine *179*, 973-984.

SUPPLEMENT

Supplementary Table 1: Polyclonal $CD4^+$ T cells from lymph SPF vs. GF mice, differentially expressed downregulated genes.

Gene Symbol	log10 (expression(SPF)	log10 (expression(GF)	log2FoldChange	adjusted p-value
Churc1	3.706	3.143	-1.869	0.034
H2-Ab1	3.550	2.479	-3.557	0.038
Hba-a1	3.603	1.410	-7.286	0.000
Hba-a2	3.450	1.545	-6.326	0.000
Hbb-bs	3.259	1.404	-6.162	0.000
Ssr1	4.227	3.518	-2.357	0.000

Supplementary Table 2: MOG-specific $CD4^+$ T cells from lymph of GF vs. SPF mice; differentially expressed upregulated genes.

Gene Symbol	Log_2FoldChange	Adjusted p-value	$-LOG_{10}$(padj)
Hba-a2	3.137	0.001	2.984
Ckb	1.022	0.002	2.647
Tmem181a	1.082	0.003	2.572
Hist1h2ap	1.690	0.003	2.469
Sardh	1.979	0.006	2.197
Ppp1r3b	1.401	0.007	2.181
Dynlt1b	2.981	0.007	2.162
Il23r	2.932	0.008	2.113
Ephb6	1.125	0.012	1.915
Dtx1	1.173	0.014	1.858
Ccr6	2.017	0.014	1.855
Gsn	1.029	0.014	1.850
Acadsb	1.096	0.019	1.720
Zfp386	1.014	0.022	1.667
Gabrd	2.678	0.023	1.639
Idi1	1.292	0.025	1.608
Hist1h1e	1.080	0.025	1.596
Dynlt1a	1.189	0.037	1.435

Supplementary Table 3: MOG-specific $CD4^+$ T cells from lymph of GF vs. SPF mice; differentially expressed downregulated genes.

Gene Symbol	Log_2FoldChange	Adjusted p-value	$-LOG_{10}$(padj)
Ifitm3	-3.831	0.000	7.992
Pirb	-3.472	0.001	3.175
Cfp	-3.450	0.000	4.913
Pld4	-3.322	0.001	2.864
Apoe	-3.192	0.002	2.647

Rsad2	-3.180	0.000	11.943
Selp	-3.167	0.002	2.607
Plac8	-3.151	0.000	8.123
Spi1	-3.145	0.003	2.530
Ccl9	-3.094	0.003	2.469
Ccrl2	-2.982	0.002	2.712
Ifit3	-2.929	0.000	37.649
Ifi204	-2.862	0.008	2.076
Fcgr3	-2.779	0.006	2.256
Csf1	-2.775	0.010	1.982
Tyrobp	-2.744	0.013	1.898
5430427O19Rik	-2.742	0.014	1.854
Ifit3b	-2.735	0.000	10.966
Mx1	-2.690	0.003	2.528
Gas2l1	-2.674	0.022	1.665
Lrg1	-2.669	0.024	1.615
Ly6c2	-2.645	0.009	2.032
Pmp22	-2.628	0.028	1.560
Clec4d	-2.619	0.028	1.553
Cxcl2	-2.612	0.029	1.544
Fcer1g	-2.596	0.029	1.534
Prg4	-2.576	0.025	1.596
Tspan9	-2.517	0.000	4.721
Samd3	-2.502	0.040	1.394
Slc7a8	-2.501	0.040	1.394
Rnf128	-2.446	0.022	1.667
Lyl1	-2.412	0.035	1.460
Xylb	-2.367	0.035	1.460
Ifitm2	-2.322	0.014	1.852
Deptor	-2.280	0.008	2.118
Coro2a	-2.279	0.001	3.018
Oas1a	-2.276	0.000	11.035
Cd68	-2.254	0.028	1.559
Ms4a4c	-2.246	0.000	5.327
Oas2	-2.236	0.000	4.765
Plxdc2	-2.213	0.001	2.939
Icosl	-2.196	0.014	1.854
Ifit1	-2.191	0.000	12.485
Cd86	-2.154	0.006	2.249
Ptafr	-2.135	0.024	1.613
Oasl2	-2.127	0.000	15.769
Slpi	-2.077	0.009	2.061
Degs2	-2.044	0.008	2.125
Ebi3	-2.043	0.035	1.462
Unc5a	-2.018	0.000	3.641
Mx2	-1.985	0.021	1.674

Usp18	-1.975	0.000	11.953
Plk2	-1.956	0.020	1.697
Rgs1	-1.857	0.003	2.553
Gpr34	-1.757	0.006	2.232
Gm4070	-1.737	0.002	2.642
Trib1	-1.710	0.014	1.854
Brpf3	-1.701	0.002	2.770
Ar	-1.698	0.001	3.108
Shisa7	-1.670	0.027	1.562
Ttn	-1.650	0.010	1.985
Col11a2	-1.602	0.001	3.030
Mink1	-1.586	0.003	2.538
Irf7	-1.562	0.000	9.289
Dennd6b	-1.561	0.000	3.701
Rnf19b	-1.555	0.007	2.162
Adgrg5	-1.552	0.031	1.505
Neb	-1.528	0.047	1.327
Oasl1	-1.509	0.000	3.553
Cep250	-1.508	0.005	2.297
Fkbp5	-1.488	0.001	2.868
Slc36a1	-1.487	0.029	1.538
Hipk2	-1.467	0.003	2.469
Rxra	-1.464	0.016	1.809
Isg15	-1.451	0.000	3.806
Ikzf2	-1.444	0.014	1.854
H2-Q8	-1.384	0.042	1.378
Cst7	-1.372	0.018	1.738
Cmpk2	-1.344	0.002	2.626
Git1	-1.331	0.026	1.586
Egr1	-1.314	0.004	2.407
Mprip	-1.297	0.003	2.574
Phf11c	-1.282	0.000	4.353
Dbndd2	-1.261	0.042	1.378
Kmt2b	-1.260	0.023	1.639
Dennd5a	-1.250	0.037	1.433
Nfkbiz	-1.247	0.007	2.145
Erdr1	-1.228	0.000	3.641
Bcl2	-1.207	0.009	2.033
Atn1	-1.177	0.002	2.770
Ppp1r9b	-1.173	0.014	1.854
Synj2	-1.171	0.014	1.842
Dusp1	-1.168	0.038	1.416
Tnfaip3	-1.164	0.045	1.349
Ccdc53	-1.162	0.000	7.025
Ppp1r15a	-1.147	0.006	2.253
Rrbp1	-1.146	0.000	5.575

Larp1	-1.140	0.014	1.858
Ifi27l2a	-1.134	0.000	3.925
Ankrd11	-1.126	0.031	1.507
Oas3	-1.113	0.000	3.701
Ncor2	-1.112	0.016	1.799
Rnf144a	-1.104	0.018	1.745
Sap25	-1.098	0.026	1.588
Gigyf1	-1.089	0.009	2.062
Hexim1	-1.087	0.043	1.370
Rtp4	-1.069	0.001	2.918
Ppp3cc	-1.064	0.047	1.328
Tnrc6a	-1.058	0.005	2.326
Dhx58	-1.058	0.003	2.538
Gvin1	-1.055	0.000	3.480
Golgb1	-1.050	0.019	1.717
Tspyl2	-1.036	0.005	2.326
Xaf1	-1.015	0.000	3.806
Helz2	-1.008	0.002	2.770
Cd69	-1.001	0.001	3.058

Supplementary Table 4: MOG-specific $CD4^+$ T cells from lymph vs. spleen of SPF mice and MOG-specific CD4+ T cells from lymph of SPF vs. GF mice; upregulated in SPF lymph as compared to both GF lymph and SPF spleen.

Gene Symbol	log2FC(SPF L/S)	Padj (SPF L/S)	log2FC(L SPF/GF)	Padj (L SPF/GF)
Il23r	1.033	0.666	2.932	0.008
Gabrd	2.058	0.075	2.678	0.023
Ccr6	1.960	0.001	2.017	0.014
Il22	2.136	0.067	1.981	0.176
Sardh	1.019	0.518	1.979	0.006
Il1r1	1.139	0.585	1.943	0.174
Fndc7	1.123	0.620	1.798	0.246
Nuf2	1.283	0.471	1.788	0.211
Pde5a	1.889	0.139	1.726	0.264
Cdk1	1.076	0.340	1.651	0.123
Ahrr	1.639	0.235	1.519	0.344
Slc6a20b	1.417	0.251	1.479	0.365
Il17re	1.172	0.542	1.446	0.401
Troap	1.186	0.571	1.380	0.448
Pcdhga2	1.421	0.352	1.309	0.446
Apold1	1.417	0.356	1.292	0.457
Mcm10	2.137	0.062	1.248	0.531
Lrfn1	1.174	0.546	1.244	0.479
Ube2c	1.474	0.167	1.174	0.421
Csgalnact1	1.302	0.037	1.113	0.115
Tmtc1	1.204	0.553	1.102	0.618

Rrm2	1.311	0.085	1.094	0.341
Trcg1	1.434	0.364	1.084	0.620
Shcbp1	1.702	0.174	1.077	0.615
Gga2	1.333	0.008	1.056	0.105
Atp8a2	1.754	0.048	1.038	0.466
Dock1	1.004	0.646	1.007	0.594

Supplementary Table 5: MOG-specific $CD4^+$ T cells from lymph vs. spleen of SPF mice and MOG-specific $CD4^+$ T cells from Lymph of SPF vs. GF mice; downregulated in SPF lymph as compared to both GF lymph and SPF spleen.

Gene Symbol	log2FC(SPF L/S))	Padj (SPF L/S)	log2FC(L SPF/GF)	Padj (L SPF/GF)
Cd5l	-5.421	0.000	-2.123	0.123
Pld4	-5.290	0.000	-3.322	0.001
Sirpa	-5.120	0.000	-2.315	0.078
Adgre4	-4.772	0.000	-1.350	0.437
Itgad	-4.733	0.000	-1.629	0.305
Lrp1	-4.554	0.000	-2.301	0.081
Egr2	-4.445	0.000	-1.030	0.599
Spi1	-4.299	0.000	-3.145	0.003
Slc11a1	-4.256	0.000	-2.104	0.134
Fcgr4	-4.210	0.000	-1.568	0.334
Ptgs1	-4.088	0.000	-2.188	0.105
Ctsh	-4.024	0.000	-2.264	0.090
Pilra	-3.944	0.000	-1.379	0.453
Cfp	-3.856	0.000	-3.450	0.000
Pirb	-3.839	0.000	-3.472	0.001
Hmox1	-3.712	0.000	-1.170	0.535
Dnase1l3	-3.638	0.000	-1.971	0.178
Apoe	-3.593	0.000	-3.192	0.002
Cd68	-3.592	0.000	-2.254	0.028
Zeb2	-3.474	0.000	-1.633	0.305
Fcna	-3.438	0.000	-2.156	0.113
Cd83	-3.423	0.000	-1.890	0.078
Mpeg1	-3.414	0.000	-1.229	0.483
Dok3	-3.341	0.000	-1.464	0.396
Ly6d	-3.313	0.000	-1.196	0.517
Fam43a	-3.301	0.000	-2.049	0.149
Ly86	-3.213	0.000	-2.092	0.078
Spib	-3.208	0.000	-1.180	0.558
Pilrb1	-3.146	0.001	-1.016	0.617
Napsa	-3.127	0.000	-1.303	0.494
Mgst1	-3.088	0.001	-1.747	0.250
Egr1	-2.995	0.000	-1.314	0.004
Rnase6	-2.976	0.001	-2.109	0.109
Cd22	-2.970	0.000	-1.088	0.607

Nr4a1	-2.960	0.000	-1.373	0.436
Tbxas1	-2.904	0.003	-1.814	0.225
Ccl9	-2.873	0.002	-3.094	0.003
Lrrk2	-2.842	0.004	-1.029	0.584
Cd300ld	-2.823	0.004	-1.774	0.242
Siglecg	-2.810	0.004	-1.130	0.571
Fcgr3	-2.810	0.000	-2.779	0.006
Clec7a	-2.780	0.005	-1.005	0.592
Cd36	-2.752	0.006	-2.277	0.084
Cxcl10	-2.711	0.002	-1.785	0.253
Lyl1	-2.704	0.003	-2.412	0.035
Cd74	-2.666	0.003	-1.105	0.277
Fcer2a	-2.653	0.000	-1.035	0.589
Cd19	-2.599	0.002	-1.114	0.607
H2-Aa	-2.529	0.013	-1.119	0.404
H2-Eb1	-2.503	0.014	-1.433	0.265
Ifitm1	-2.395	0.027	-2.012	0.158
Csf2rb	-2.393	0.027	-2.099	0.130
Lyn	-2.375	0.028	-1.879	0.164
Tyrobp	-2.328	0.035	-2.744	0.013
Lyz2	-2.228	0.047	-1.642	0.294
Fcer1g	-2.219	0.048	-2.596	0.029
Lag3	-2.215	0.021	-1.345	0.449
Wfdc17	-2.212	0.052	-1.184	0.509
Gm21188	-2.207	0.053	-2.128	0.127
Plxnb2	-2.187	0.054	-2.197	0.105
Cybb	-2.183	0.009	-1.975	0.171
Vsig10	-2.162	0.061	-1.118	0.557
Wdfy4	-2.159	0.060	-1.394	0.399
Nav1	-2.150	0.045	-1.696	0.291
Sh3bgrl2	-2.147	0.055	-1.730	0.280
Cd163l1	-2.134	0.050	-2.266	0.088
Ifitm3	-2.127	0.068	-3.831	0.000
Irf5	-2.125	0.002	-1.551	0.105
Klra2	-2.120	0.067	-1.104	0.544
Slpi	-2.104	0.014	-2.077	0.009
Cd86	-2.078	0.014	-2.154	0.006
Csf1	-2.064	0.076	-2.775	0.010
Lima1	-2.057	0.082	-1.169	0.510
Slamf7	-2.037	0.032	-1.345	0.466
Fcgr2b	-1.983	0.085	-1.043	0.648
Pomgnt2	-1.956	0.038	-1.611	0.241
Cd302	-1.949	0.038	-1.343	0.340
Fn1	-1.934	0.120	-1.061	0.562
Tspan4	-1.924	0.086	-1.176	0.545
Plac8	-1.883	0.139	-3.151	0.000

Cpq	-1.871	0.043	-1.428	0.211
Pik3ap1	-1.855	0.132	-1.747	0.255
Tmem198	-1.836	0.158	-1.226	0.531
Cbfa2t3	-1.796	0.171	-2.143	0.121
Ncf2	-1.772	0.055	-1.148	0.492
Penk	-1.770	0.188	-1.354	0.466
Pygl	-1.742	0.198	-1.207	0.545
Hp	-1.739	0.188	-1.952	0.176
Plekha8	-1.694	0.215	-1.866	0.213
Hcar2	-1.694	0.204	-1.428	0.381
Ms4a4c	-1.668	0.000	-2.246	0.000
Ebi3	-1.656	0.081	-2.043	0.035
Xylb	-1.652	0.229	-2.367	0.035
Lpl	-1.651	0.251	-1.248	0.531
Gas2l1	-1.593	0.278	-2.674	0.022
Bhlhe41	-1.590	0.259	-1.392	0.398
Tgfbi	-1.588	0.251	-2.103	0.128
Rsad2	-1.574	0.038	-3.180	0.000
Fut7	-1.545	0.254	-1.251	0.505
Degs2	-1.542	0.086	-2.044	0.008
Cyp4f18	-1.531	0.317	-1.415	0.426
Ptgis	-1.523	0.289	-1.702	0.274
Ssh3	-1.486	0.138	-1.201	0.378
Ms4a8a	-1.480	0.316	-2.352	0.069
Ly6c2	-1.479	0.041	-2.645	0.009
5430427O19Rik	-1.464	0.369	-2.742	0.014
Plek	-1.464	0.152	-2.153	0.063
Anxa3	-1.462	0.324	-1.005	0.592
Cx3cr1	-1.443	0.359	-1.159	0.577
Vsig10l	-1.422	0.236	-1.444	0.347
Kcnk6	-1.387	0.426	-1.962	0.170
Rassf4	-1.377	0.380	-1.236	0.522
Oas1b	-1.373	0.081	-1.086	0.087
Csf2rb2	-1.371	0.440	-1.148	0.580
Slc7a8	-1.360	0.448	-2.501	0.040
Tmbim1	-1.339	0.316	-1.584	0.310
Tppp	-1.327	0.452	-1.086	0.623
Arpp21	-1.322	0.301	-1.247	0.516
Ifi204	-1.313	0.448	-2.862	0.008
Adssl1	-1.308	0.435	-1.530	0.334
F13a1	-1.304	0.451	-1.468	0.378
Camk1	-1.302	0.484	-1.275	0.493
Ralgds	-1.300	0.233	-1.590	0.107
Ppp1r37	-1.297	0.188	-1.835	0.055
Klrk1	-1.282	0.271	-1.563	0.284
Lilrb4a	-1.278	0.297	-1.875	0.126

Fam212a	-1.276	0.319	-1.421	0.246
Mnda	-1.261	0.521	-1.766	0.256
Zfp608	-1.254	0.520	-1.739	0.277
Gm13152	-1.227	0.475	-1.200	0.512
Ifitm2	-1.222	0.387	-2.322	0.014
Hsd3b7	-1.192	0.564	-1.995	0.130
Igip	-1.188	0.258	-1.147	0.435
Nr4a3	-1.178	0.316	-1.098	0.539
Mtus1	-1.166	0.513	-1.827	0.220
Ier3	-1.165	0.588	-1.244	0.489
Bst1	-1.132	0.533	-1.638	0.301
Pou2f2	-1.121	0.264	-1.015	0.385
Samd3	-1.116	0.631	-2.502	0.040
Serpina3g	-1.101	0.303	-1.655	0.081
Fam83g	-1.100	0.622	-1.711	0.247
Pde1b	-1.079	0.414	-1.397	0.103
Fam46a	-1.061	0.048	-1.168	0.107
Dnd1	-1.054	0.654	-1.610	0.305
Alox5ap	-1.052	0.615	-1.364	0.247
Trp53inp2	-1.046	0.458	-1.502	0.181
Entpd1	-1.038	0.524	-1.541	0.256
Ager	-1.014	0.639	-1.236	0.458
Yes1	-1.013	0.671	-1.889	0.209
Dqx1	-1.012	0.652	-1.383	0.345
Mx1	-1.010	0.646	-2.690	0.003
Naip6	-1.002	0.659	-1.354	0.461
Pltp	-1.002	0.591	-1.487	0.329

ACKNOWLEDGEMENTS

First, I want to express my deepest gratitude to PD Dr. Naoto Kawakami. Beyond being the best doctoral supervisor I could have imagined, you are an inspiring mentor in both scientific and personal aspects, an outstanding scientist and a great support, also regarding practical aspects in the lab, a pleasant companion and an excellent advisor in Japanese cuisine. I know receiving compliments makes you feel uncomfortable, so I say no more, but 'Thank you very much!'

I am very grateful for my colleagues who supported me scientifically and personally and became close friends on this exciting journey. Alina, Cate, Edu, Julia, Katrin, Lian, Michelle, Miriam, Ramona and Stephan: you filled the last years with happiness and I do not want to miss a single day with you! Christian, you must not be omitted here, as almost co-worker and faithful lunch friend.

I further appreciate former colleagues and friends who accompanied me on a part of the way: Nikos, Clara, MC, Max, Sabine and Ping.

I also owe a great debt of gratitude to Nikos for introducing me to intravital imaging, to Daniel for his support with the transcriptome data analysis, to Edu for his guidance in LCM and NGS, and to Hong for helping in providing the germ-free mice.

It is a pleasure to work in the friendly and supporting environment of the Institute of Clinical Neuroimmunology, being surrounded by inspiring and motivated scientists.

Furthermore, I was lucky enough to meet you, Stefan. Thank you for your constant patience and unconditional support, your valuable input and for the love and joy you bring to my life every day.

From the depth of my heart, I want to express my gratefulness to my beloved parents, Astrid and Herbert, and to my dear sister Lilli for their devoted support in every possible way. Your boundless love, help, patience and generosity allow me to pursue my dreams.

AFFIDAVIT

Eidesstattliche Versicherung

Bauer, Isabel Julia

Name, Vorname

Ich erkläre hiermit an Eides statt, dass ich die vorliegende Dissertation mit dem Titel:

"Visualization and Functional Characterization of CD4^{+} T Cell Stimulation in the Ileal Lamina Propria"

selbständig verfasst, mich außer der angegebenen keiner weiteren Hilfsmittel bedient und alle Erkenntnisse, die aus dem Schrifttum ganz oder annähernd übernommen sind, als solche kenntlich gemacht und nach ihrer Herkunft unter Bezeichnung der Fundstelle einzeln nachgewiesen habe.

Ich erkläre des Weiteren, dass die hier vorgelegte Dissertation nicht in gleicher oder in ähnlicher Form bei einer anderen Stelle zur Erlangung eines akademischen Grades eingereicht wurde.

Martinsried, 10. Oktober 2021 — Ort, Datum

Isabel Bauer — Unterschrift Doktorandin bzw. Doktorand